Characterization of different types of stonin1 positive cellular adhesions

Inaugural-Dissertation

to obtain the academic degree
Doctor rerum naturalium (Dr.rer.nat.)

submitted to the Department of Biology, Chemistry, Pharmacy
of Freie Universität Berlin

by

Fabian Lukas

from Berlin, Germany

2021

Period of doctorate studies:	Oktober 2016 to November 2021
Supervisor:	Prof. Dr. Tanja Maritzen and Prof. Dr. Volker Haucke
Institute:	Leibniz-Forschungsinstitut für Molekulare Pharmakologie (FMP), Berlin

1. Reviewer: Prof. Dr. Tanja Maritzen
2. Reviewer: Prof. Dr. Volker Haucke

Date of defense: 23.03.2022

Affidavit

I declare that my doctoral thesis at hand has been written independently and with no other sources and aids then quoted.

Berlin, 30.11.2021

Acknowledgements

First, I would like to thank my supervisor, Prof. Tanja Maritzen, for her kind and generous support and her belief in me, which enabled me to sharpen my scientific skills, to outgrow myself and to master new challenges. I am pleased to have the opportunity to be part of her newly founded research group in Kaiserslautern. Then I want to express my deep gratitude to Prof. Volker Haucke for giving me the possibility to work in his lab, his constant guidance and advice. I especially like to thank Dr. Martin Lehmann, who supported me in microscopy and opened new experimental possibilities for me. I owe special thanks to Tania Lopez-Hernandez and Dr. Domenico Azarnia Tehran for their advice and their kind support. Many thanks to Dr. Dmytro Puchkov, the head of the electron microscopy facility, and Dr. Claudia Matthaeus for their help in preparing membrane sheets and performing electron microscopy. I am also truly grateful to Dr. Ines Lahmann for providing and teaching me the culture of primary myoblasts. Thanks to Dr. Wen-Ting Lo for his advice regarding affinity purifications and help with the insect culture. Thanks to Dr. Alexander Wallroth and Philipp Koch for their help with everything concerning CRISPR. I would also like to thank all the technicians who helped me in the lab: Uwe Fink, Delia Löwe, Maria Mühlbauer and Silke Zillmann. Special thanks to Claudia Schmidt, who supported my work with her experimental expertise and for providing help whenever required. Special thanks also to Prof. Fan Lio and Dr. Eberhard Krause, the current and former head of the mass spectrometry facility at the FMP-Berlin, and his team, especially Heike Stephanowitz, for the mass spectrometry. I would like to thank everyone who has contributed to this work or supported me: Marietta Bergmann, Svenja Bolz, Gabrielle Capin, Michael Ebner, Paula Samsó Ferre, Marine Gil, Hannes Gonschoir, Manuel Hessenberger, Lennart Hoffmann, Wonyul Jang, Maria Jäpel, Natalie Kaempf, Philipp Koch, Gaga Kochlamazashvili, Michael Krauß, Marijn Kuijpers, Guan-Ting Liu, Albert Mackintosh, Marta Maglione, Charles Malek, Kristine Oevel, Christoph Ott, York Posor, Filiz Sila Rizalar, Giulia Russo, Christopher Schmied, Linda Sawade, Tolga Soykan, Dennis Vollweiter, Haibin Wang, Mirjana Weimershaus and Celina Wortmann. Finally, and most important, I am grateful for all the support, care and love I receive from my family and friends.

Abstract

Adhesion structures are critical for anchoring cells in their environment, as signaling platforms and for cell migration. In line with these diverse functionalities there are different types of cellular adhesions. In contrast to canonical focal adhesions (FAs), reticular adhesions (RAs), also known as clathrin plaques or flat clathrin lattices lack most classical adhesome proteins, but are enriched in endocytic proteins like clathrin.

In this PhD thesis, we used different microscopic techniques (live-cell confocal microscopy, stimulated emission depletion nanoscopy, transmission electron microscopy, correlative light and electron microscopy) combined with manipulation of substrates and loss of function approaches to unravel the role of stonin1 during endocytosis, adhesion and cell migration. We here identify stonin1, a close relative of the endocytic adaptor stonin2, as a protein that predominantly localizes to diverse reticular adhesion structures.
By using stonin1 as a bona fide marker for RAs, we found a much higher diversity of RAs than previously known. In particular, we found general RA structures that cannot be classified as clathrin plaques. These include retraction fibers that are formed not only during mitosis but also during migration, as well as large networks found in resting confluent cells. We furthermore discovered that stonin1 is critical for actin recruitment to RAs, suggesting a novel connection of RAs to the cytoskeleton.

Since the relationship between RAs and other types of integrin-mediated adhesions is still poorly understood, we further investigated whether connections between these structures exist. Here, we found that stonin1 containing adhesions can convert into clathrin plaques or FAs. This appears to be an entirely novel mechanism for the assembly of FAs: RAs do not only form at the sites of focal adhesion disassembly, but unexpectedly, can serve as a template for the generation of new focal adhesions.

Our observations provide new insights into the transformation and interconvertibility of cellular adhesions and highlight the diverse patterns of cellular adhesions in different environments.

Zusammmenfassung

Adhäsionsstrukturen sind entscheidend für die Verankerung von Zellen in ihrer Umgebung, als Signalplattformen und für die Zellmigration. Entsprechend dieser vielfältigen Funktionalitäten gibt es verschiedene Arten von zellulären Adhäsionen. Im Gegensatz zu den kanonischen fokalen Adhäsionen (FAs) fehlen in den retikulären Adhäsionen (RAs), die auch als Clathrin Plaques bezeichnet werden, die meisten klassischen Adhäsionsproteine, während sie mit endozytischen Proteinen wie Clathrin angereichert sind.

In dieser Doktorarbeit haben wir verschiedene mikroskopische Techniken (konfokale Mikroskopie an lebenden Zellen, Nanoskopie mit stimulierter Emissionsdepletion, Transmissionselektronenmikroskopie, korrelative Licht- und Elektronenmikroskopie) in Verbindung mit der Manipulation von Substraten eingesetzt, um die Rolle von Stonin1 bei Endozytose, Adhäsion und Zellmigration zu entschlüsseln. Wir haben hier Stonin1, einen engen Verwandten des endozytischen Adaptors Stonin2, als ein Protein identifiziert, das vorwiegend in verschiedenen retikulären Adhäsionsstrukturen lokalisiert ist.

Durch die Verwendung von Stonin1 als bona fide Marker für RAs fanden wir eine viel größere Vielfalt an RAs vor als bisher bekannt. Insbesondere fanden wir allgemeine RA Strukturen, die nicht als Clathrin Plaques klassifiziert werden können. Dazu gehören Retraktionsfasern, die nicht nur während der Mitose, sondern auch während der Migration gebildet werden, sowie große Adhäsionsnetzwerke, die in ruhenden konfluenten Zellen zu finden sind. Weiterhin entdeckten wir, dass Stonin1 für die Aktin-Rekrutierung in RAs entscheidend ist, was auf eine neuartige Verbindung von RAs mit dem Zytoskelett hindeutet.

Da über die Beziehung zwischen RAs und anderen Arten von Integrin vermittelten Adhäsionen noch wenig bekannt ist, haben wir weiter untersucht, ob Verbindungen zwischen diesen Strukturen bestehen. Dabei fanden wir heraus, dass Stonin1 enthaltende Adhäsionen sich in Clathrin Plaques oder FAs umwandeln können.

Durch diesen Prozess haben wir schließlich einen neuen Mechanismus für die Bildung von FAs gefunden: RAs bilden sich nicht nur an den Stellen von FAs, sondern können überraschenderweise auch als Vorlage für die Bildung neuer FAs dienen.

Diese spezifischen Beobachtungen geben neue Einblicke in die Umwandlung zellulärer Adhäsionen und verdeutlichen die unterschiedlichen Formen zellulärer Adhäsionen in verschiedenen Umgebungen.

Table of Contents

1. Introduction

1.1 Clathrin-mediated endocytosis

Cells need to take up hormones, proteins, and metabolites in a selective manner. Specific cell surface receptors bind these extracellular macromolecular ligands. The internalization of the cargo (both receptor and ligand) happens in a process called receptor-mediated endocytosis. This process leads to the inward budding of the plasma membrane that is finally pinched off, resulting in vesicles that are transported further into the cell, thereby regulating nutrient uptake, cell signaling and cell adhesion (Kaksonen and Roux, 2021).

Although multiple different endocytic pathways are described, clathrin-mediated endocytosis is considered as the major endocytic route for the internalization of surface proteins (Bitsikas et al., 2021). Recent studies, however, also describe clathrin-independent ultrafast endocytosis as a mechanism for the retrieval of synaptic proteins within hundreds of milliseconds (Soykan et al., 2021). In contrast, the duration of CME is much slower at nerve terminals with a time constant of approximately 15 s (Dittman and Ryan, 2021). In cell culture models the lifetime of endocytosis is highly heterogeneous, ranging from less than 20s to a few minutes (Lehmann et al., 2021).

1.1.1 The molecular mechanism of CME

The name-giver of the CME is the coat protein clathrin, a triskelion-shaped hexamer of three heavy (CHC) and three light chains (CLC) that can oligomerize into a lattice (Kirchhausen and Harrison, 1981). The lattice forms a complex scaffold layer underneath defined plasma membrane sites that directs the formation and stabilization of plasma membrane invaginations thereby driving the formation of clathrin-coated pits (CCPs).

However, clathrin itself is not able to interact with the membrane or the cargo (Hirst and Robinson, 1998). Instead, clathrin binds accessory proteins that bridge the interaction of the cargo with clathrin at the plasma membrane. The formation of clathrin-coated vesicles is a complex process involving over 50 proteins that are recruited in a highly coordinated manner (Kaksonen and Roux, 2021). The progression of CME is accompanied by the conversion of phosphoinositides that determine membrane identity and regulate the specific recruitment of adaptor proteins (Posor et al., 2015). CME can be classified into five distinct steps (Figure 1.1):

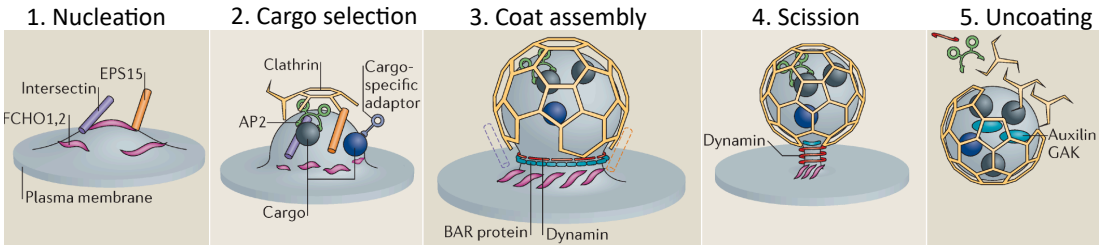

Figure 1.1: Clathrin mediated endocytosis. Schematic representation of the different steps of the CME. Illustrated are the steps involved in endocytosis with the key proteins: Nucleation, cargo selection, coat assembly, scission and uncoating. Modified from: McMahon and Boucrot 2011.

Endocytosis begins with the recruitment of FCHo1/2 proteins to phosphoinositol(4,5)-bisphosphate (PIP_2) at the plasma membrane. FCHo1/2 proteins have specific BAR domains that induce mild membrane curvature and initialize clathrin nucleation (Daumke et al., 2014). During the initial nucleation step of CME, the assembly polypeptide 2 (AP2) is recruited to PIP_2 to drive clathrin assembly (Collins et al., 2002). AP2 is a heterotetrameric complex consisting of four subunits. The small σ-subunit and the middle μ-subunit are responsible for cargo recognition, whereas the two large subunits, called α- and β-adaptin, are responsible for binding PIP_2 and clathrin, respectively (Kirchhausen and Harrison, 1981).

Cytosolic tails of transmembrane cargo molecules have specific recognition motifs that are recognized by AP2, which belong to two categories: The "tyrosine-based motif" YXXΦ as in the case of the transferrin receptor and the "dileucine motif" [DE]XXXL[LI] found for example in the epidermal growth factor receptor (Traub and Bonifacino, 2013).

Other alternative clathrin adaptors help to recruit specific cargos to clathrin, such as Dab2, Numb, and ARH, which can recognize specific NPXY recognition sites of the low-density lipoprotein receptor or ß integrin subunits (Traub, 2009). In addition to specific recognition motifs, ubiquitination also provides interaction sites for endocytic adaptors such as Eps15 and epsins (Traub and Bonifacino, 2013).

During the assembly of clathrin into polyhedral cages, BAR proteins help in the formation of CCPs. Amphiphysin, endophilin, and SNX9 play important roles in membrane bending and dynamin recruitment (Daumke et al., 2014).

The question of which exact role motor proteins and actin polymerization play in vesicle budding is still open. Actin regulatory proteins such as HIP1R, which binds directly to clathrin, or cortactin, which is recruited by dynamin, stimulate the actin nucleation activity of Arp2/3 and suggest that actin nucleation is involved in endocytosis (Kaksonen et al., 2006). However, only in the presence of increased plasma membrane tension (Boulant et al., 2011) or for large cargo proteins (Cureton et al., 2010) is actin polymerization required to facilitate membrane invagination and scission in mammalian cells.

CCPs are finally fissioned by the GTPase dynamin, resulting in a controlled release of vesicles into the cytosol (Sweitzer and Hinshaw, 1998). Finally, the clathrin scaffold is uncoated to allow vesicle fusion with endosomal compartments. Hsc70, together with its co-chaperone GAK or auxilin, help to disassemble the clathrin coat after vesicle formation (Ungewickell et al., 1995).

1.1.2 Stonin family members

Originally, the stoned locus of *Drosophila melanogaster* was identified in a screen for stress-sensitive behavioral mutants (Grigliatti et al., 1973). At higher temperatures, the "stoned" protein mutants exhibited severe neurological defects and were paralyzed, leading researchers to name them "stoned". The stoned gene is a dicistronic locus encoding stonedA and stonedB, which are specifically expressed in the brain of flies (Andrew et al., 1996). Stoned proteins regulate synaptic vesicle recycling and are required for proper sorting of synaptotagmin during endocytosis (Fergestad et al., 1999). This is mediated by the µ-homology domain of stonedB, which binds to synaptotagmin, a calcium sensor localized in synaptic vesicles (Gustavsson and Han, 2009). The regulatory role for synaptic vesicle retrieval was exclusively attributed to stonedB (Estes et al., 2003).

In mammals, there are two orthologs of stonedB: stonin1 and 2. Like stonedB, stonin2 plays an important role in the retrieval of synaptic vesicles (Martina et al., 2001). It acts as an endocytic adaptor for synaptotagmin1 and 2 and facilitates their uptake through clathrin-mediated endocytosis (Diril et al., 2006). All stonin proteins exhibit a comparable modular domain structure: An intrinsically disordered N-terminal region is followed by a stonin homology domain (SHD) and a µ-homology domain (µHD), which is homologous to the cargo-binding µ2 domain of AP2 (Figure 1.2). Stonin1 and 2 have conserved N-terminal WxxF motifs that have been shown to bind AP2 (Bergmann, 2017). 49 % of the amino acids are conserved in the stonin homology domain of human stonin1 and 2. However, a specific function for the SHD has not yet been identified. Stonin1 shows a different expression pattern than stonin2 with the highest expression in the lung and female reproductive organs, suggesting a distinct function of stonin1 (Feutlinske, 2014).
Stonin1 was found in a proteomic study when FA disassembly was selectively induced by blebbistatin-mediated inhibition of (Kuo et al., 2011). In line with this, stonin1 knockout fibroblasts have been shown to exhibit altered FA dynamics (Feutlinske et al., 2015).

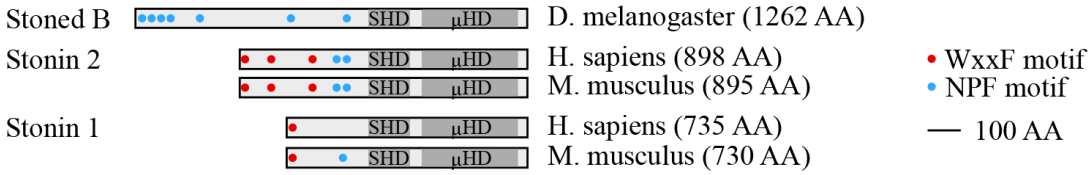

Figure 1.2: Domain structures of stonin family members. Stonin1 has an intrinsically disordered N-terminus, a central SHD, and a carboxy-terminal µHD domain. Most stonins harbor one or more EH domain-binding NPF motifs. All mammalian stonins contain WxxF motifs for AP2 binding. Modified from: Maritzen et al. 2010. *AA - amino acids, µHD - µ-homology domain, SHD - stonin homology domain*

Moreover, stonin1 is localized behind focal adhesions along with members of the endocytic machinery such as clathrin, AP2, dynamin, and intersectin (Feutlinske, 2014). In the following study, these clathrin-positive structures were identified as clathrin plaques, and stonin1 was shown to be selectively localized in these structures.

1.1.3 Clathrin plaques

Transmission electron microscopy (TEM) of metal replicates from unroofed cells revealed the structure of clathrin (Heuser, 1980). Using this experimental procedure, both curved and flat clathrin lattices (FCL) could be detected at the plasma membrane. Curved clathrin-coated structures (CCSs) exhibit polyhedral coats composed of hexagons and pentagons, while flat (CCSs) are mostly composed of hexagons (Figure 1.3). It was generally considered that the transformation from a flat to curved lattice would be energetically unfavorable, since it would require a dramatic reshaping of the flat hexagonal lattice to introduce pentagons in the right places. Therefore, a constant curvature model for the formation of CCPs was proposed, which envisages the assembly of CCSs as curved structures from the beginning (Kirchhausen, 2009). This contrasts with the constant area model, where clathrin assembles as a flat hexagonal lattice that later transforms into a coated invagination (Bucher et al., 2018a).

Although this question remains to be resolved, the diversity of clathrin-coated structures observed in cells suggests a further role for flat clathrin lattices beyond endocytosis. While CCPs are spherical, small, and homogeneous with a comparable length of about 100 to 150 nm, a second discrete population of polymerized clathrin was found only at ventral membrane surfaces that was planar, large, heterogeneous, and had a lifetime of more than 10 minutes (Grove et al., 2014). This second population was called clathrin plaques, and its function is still controversial. Plaque formation was found to be dependent on alternative splicing of the clathrin heavy chain gene (CLTC exon 31). The forced skipping of CLTC exon 31 in muscle cells changed the plasma membrane content from clathrin plaques to pits (Moulay et al., 2020).

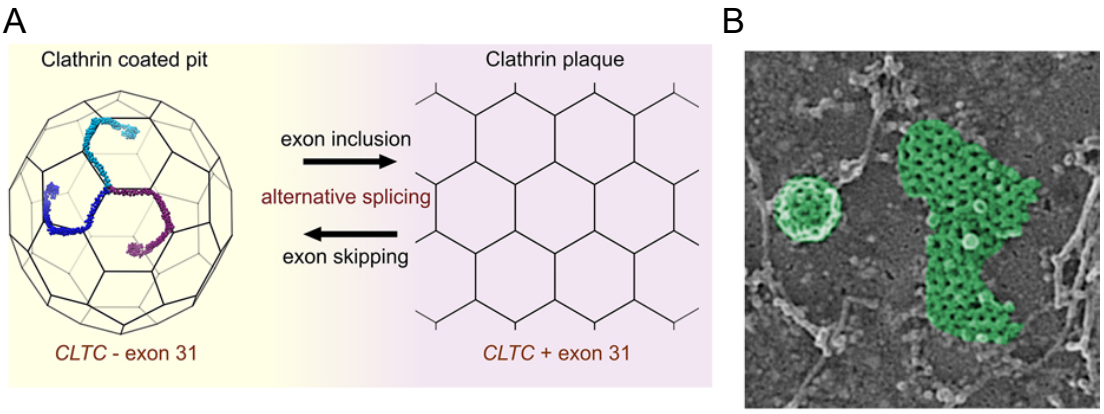

Figure 1.3: Clathrin plaques and endocytic pits. (A) Schematic representation of CCPs and clathrin plaques. Illustrated is the triskelion-shaped hexamer of clathrin and the soccer ball-shaped CCP (left). Exon inclusion of CHC stimulates flat plaque assembly (right). Source: Moulay et al. 2020.
(B) TEM image from metal replica of unroofed myoblasts showing an invaginated clathrin structure and a large clathrin plaque. Clathrin (green) is pseudo-colored. Source: Fabian Lukas. TEM performed by Dr. Claudia Matthaeus.

An actin-dependent mechanism for plaque disassembly was proposed. In this model, unlike CCPs, the clathrin lattices of plaques do not form a soccer ball-shaped CCP, but move inward from the cell surface as a flat clathrin lattice and rely on local remodeling of actin filaments. (Saffarian et al., 2009). Indeed, endocytosis of clathrin plaques has not yet been observed (Lock et al., 2019). However, flat clathrin lattices have been shown to be associated with curved, dome and pit shaped clathrin structures (Bucher et al., 2018a).

Clathrin plaques were therefore considered to be stable platforms for the recruitment of endocytic cargo and signaling (Grove et al., 2014). Several transmembrane receptors have been shown to be enriched in flat clathrin lattices (epidermal growth factor receptor (Grove et al., 2014), C-C chemokine receptor type 5 (Garay et al., 2015), LPA receptor 1 (Leyton-Puig et al., 2017), lipoprotein-related protein 6 (Kim et al., 2013)). Stabilization of receptors in clathrin plaques may mediate modulation of receptor signaling, in contrast to internalized receptors that would desensitize signaling. Clathrin plaques have been described as actin-controlled hubs for the signaling and endocytosis of the LPA receptor 1 (Leyton-Puig et al., 2017). On the other hand, it has been shown that receptors associated with flat clathrin lattices are not internalized (Grove et al., 2014; Kim et al., 2013). The mechanism of how receptors are internalized or stabilized at clathrin plaques and how this process is controlled is still unknown.

Integrins, extracellular matrix (ECM) receptors, have been found to be localized in clathrin plaques, therefore their function as adhesions is now increasingly recognized (Lampe et al., 2016). A physiological function of clathrin plaques is the organization of costamers, specific attachment sites of sarcomeres to the cell membrane in skeletal muscle (Vassilopoulos et al., 2014). Tubular clathrin/AP2 lattices have also been described that pinch collagen fibers and appear to be important for cell adhesion and migration in a 3D collagen matrix (Elkhatib et al., 2017). However, the physiological significance of clathrin plaques for cell adhesion and migration in various cells and tissues remains unclear.

1.2 Cell adhesion and migration

1.2.1 Integrins

In multicellular organisms, cell adhesion to the extracellular matrix (ECM) is essential for development, organization, and repair of tissues. The ECM is a meshwork of collagens, glycoproteins, and proteoglycans, whose biochemical and biophysical properties can be sensed and remodeled through cell-to-substrate contacts (Sun et al., 2019). Such contacts mediate the connection between the ECM and the cytoskeleton of the cell and regulate numerous downstream signaling pathways (Colognato et al., 2004).

Integrins are the major transmembrane receptors that mediate this connection (Huttenlocher and Horwitz, 2011). Integrins are heterodimers with a large extracellular domain that recognizes specific extracellular ligands and a short cytoplasmic tail that binds to numerous adaptor, scaffold, and signaling proteins. Currently, 24 unique mammalian integrins are known to exist, consisting of 18 α- and eight β-subunits with distinct and overlapping ECM ligands (Hynes, 2002). Although different integrin receptors can recognize the same ligand, they affect adhesion dynamics and cell motility differently (Huttenlocher and Horwitz, 2011).

Activation of integrin dimers is associated with three distinct conformations that correspond to a transition from low to high ligand affinity (Figure 1.4). Resting receptors change from a bent-closed to an extended-closed to a ligand-bound extended-open configuration (Peterson and Koval, 2021). Once activated, integrins cluster together and recruit adaptor and signaling molecules to form a dynamic macromolecular complex. This complex, known as the integrin adhesome, contains over 200 described proteins in different layers, thereby mediating cellular processes such as mechanotransduction, signal transduction, and migration (Humphries et al., 2019). These integrin complexes can be visualized as nanoclusters with different integrin activities using super-resolution microscopy (Spiess et al., 2018).

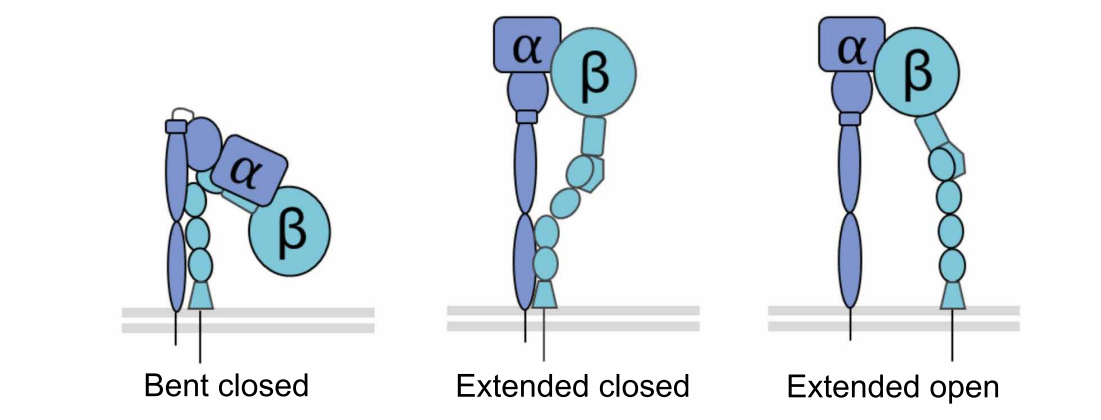

Figure 1.4: Integrin activation. Schematic representations of integrin conformation. Illustrated is the inactive bent-closed conformation with low affinity of external ligand, the intermediate extended-closed conformation and the active extended-open conformation with a high affinity for external ligands. Modified from: Peterson and Koval 2021.

It is well established that the ubiquitously expressed talin and kindlin proteins are essential for integrin activation. These bind directly to NPXY motifs in cytoplasmic ß-integrin tails via their FERM-domain and recruit further adaptors (Bachmann et al., 2019). Ligand-mediated activation is the so-called outside-in signaling, as integrin activation depends on the external environment of the cell. Remarkably, activation of integrins can also occur in the opposite direction to strengthen cell adhesion or remodel the ECM (inside-out signaling) (Shattil et al., 2010). Integrin-mediated adhesions are very complex, occur in different sizes and morphologies, and can also form different subclasses.

1.2.2 Focal adhesions

Focal adhesions are the best characterized integrin adhesions, forming large complexes associated with the actin cytoskeleton (Burridge and Chrzanowska-Wodnicka, 1996; Yamada and Geiger, 1997). Focal adhesions are organized in a three-dimensional structure with interconnected modules. In the z-direction, an integrin activation/signaling layer at the plasma membrane is followed by a force transfer layer and finally an actin regulatory layer (Kanchanawong et al., 2010) (Figure 1.5).

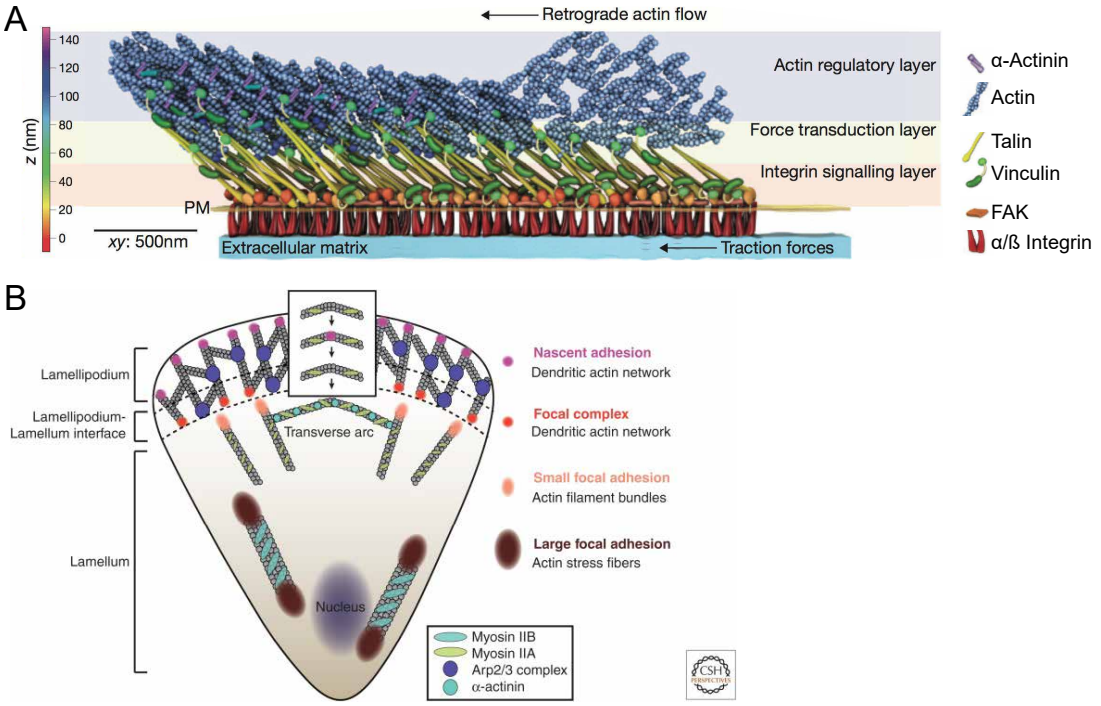

Figure 1.5: Structure of focal adhesions. (A) Schematic representation of a focal adhesion. Illustrated are the three layers in z-direction: The integrin activation/signaling layer at the plasma membrane, the force transfer and the actin regulatory layer. As maturation progresses (from right to left), density within the focal adhesion increases as a result of the recruitment of additional FA components. Characteristic components of FAs are indicated on the right side.
Modified from: Case and Waterman 2015. (B) Schematic representations of FA maturation. Small nascent adhesions residing within the lamellipodium grow into focal complexes at the lamellipodium–lamellum interface and mature further into focal adhesions that are associated with the actin cytoskeleton. Source: Bachir et al. 2017.

Over 2400 proteins have been identified that localize to focal adhesions, of which only about 60 form the core adhesion (Horton et al., 2015). In addition to their structural function FAs also have a signaling function that mediates cellular responses such as migration, proliferation and spreading (Harburger and Calderwood, 2009). Focal adhesions undergo a maturation process that depends critically on the actin cytoskeleton. First, small, short-lived punctate adhesions, called nascent adhesions, form within the protruding front of the lamellipodium (Sun et al., 2014).

The assembly of nascent adhesions requires actin polymerization and an actin flow that reinforces integrin cytoskeleton bonds (Geiger and Yamada, 2011). This actin polymerization is mediated by the Arp2/3 complex, which branches new actin filaments and forms the dendritic actin network (Bachir et al., 2017). When integrins engage and apply force on the substrate, they act like a molecular clutch and mature into focal complexes. Otherwise they are disassembled within seconds through molecular slippage (Hu et al., 2007). This is reflected by the movement of adhesion molecules with the retrograde actin flow (Guo and Wang, 2007).

At the border between the lamellum and the lamellipodium there is a transition zone. Focal complexes that do not disassemble in this region extend centripetally to grow in size (Huttenlocher and Horwitz, 2011). Binding of α-actinin establishes first connections with the actin cytoskeleton (Bachir et al., 2014). Myosin II activity in the contractile actin bundles of the cytoskeleton then generates the necessary force that activates and recruits stretch-sensitive FA proteins, allowing further maturation into large FAs (Vicente-Manzanares et al., 2009). Large persistent FAs (3-10µm) are finally connected with actin stress fibers allowing feed-forward reinforcement (Choi et al., 2008). Adhesion maturation is a continuous process in which the molecular composition of adhesions dynamically changes (Zamir and Geiger, 2001).

1.2.3 Integrin mediated migration

In contrast to amoeboid migration, which is characterized by fast sliding, mesenchymal cell migration relies heavily on integrin adhesions (Huttenlocher and Horwitz, 2011). Migration of mesenchymal cells is a complex cycle consisting of polarized protrusion, adhesion formation and stabilization, and subsequent cell body translocation and adhesion release. The actin-myosin cytoskeleton is the major contractile element regulating the mechanical tension and traction required for translocation of the cell body (Huber et al., 2015). After translocation, a new cycle begins, leading to new adhesion anchorage, FA maturation, and disassembly.

Several mechanisms for the disassembly of FAs are described. Calpain-mediated proteolytic cleavage of talin results in fragments that serve as signal transducers for FA recycling (Calderwood, 2004). Moreover, microtubules have been shown to target focal adhesions and initiate their disassembly (Stehbens and Wittmann, 2012). Here, dynamin is apparently recruited to disassembling FAs to initiate clathrin-mediated endocytosis (Chao et al., 2010). Inhibition of CME impairs focal adhesion turnover and cell migration (Chao and Kunz, 2009). Endocytosis of integrin ß1 was described after disassembly of FAs by the cargo-specific adaptors Dab2 and numb (Ezratty et al., 2009). Furthermore CME seems to play an important role for controlling the availability of integrin receptors at the cell surface thereby regulating cell polarization and directed cell migration (Maritzen et al., 2015). At the rear of the cell, where the focal adhesions are disassembled, integrins may retain some degree of attachment even after the cells have moved forward. These so-called retraction fibers have been observed not only during migration, but also in cells that retract their cell body in preparation for cytokinesis (Mitchison and Cramer, 1996). Cellular footprints, i.e. ruptured retraction fibers that are left behind during migration, were found to represent a spatial memory. Cells that leave permanent footprints on their way can find their way back along these paths (D'alessandro et al., 2021). In mitosis retraction fibers retain the memory of interphase cell shape and tension (Hart et al., 2019).

1.3 Atypical matrix adhesions

Integrin-based adhesions are highly complex structures that vary in size, morphology, and location depending on the cell and its environment. Although FAs are sometimes categorized as a single class, there are several subclasses depending on their maturation state, e.g., nascent adhesions, focal complexes, focal adhesions, and fibrillar adhesions. Most commonly studied integrin adhesions such as FAs, podosomes, and invadopodia are characterized by a common feature. They are closely associated with the cytoskeleton and share a common group of at least 60 canonical proteinss (Bachir et al., 2017; Horton et al., 2015).

Recently, a new type of integrin adhesion has been described and termed reticular adhesion (RA), which was reported to be completely independent of actin and contains only tensin-3 as consensus plaque protein (Lock et al., 2018). This adhesion depends exclusively on the integrin αVß5 and is found in a variety of adherent cell types (Lock et al., 2018). More or less in parallel, mitosis-resistant adhesions were described, which differ from RAs in that they originate from FAs and share the integrin ß1 (Jacquemet and Ivaska, 2018).

Categorization of atypical matrix adhesions is even more difficult than for canonical focal adhesions because of their high variability, lack of a uniform morphology and a unique marker. Footprints for example are atypical integrin matrix adhesion which are known for decades. However, their function was not understood until recently (D'alessandro et al., 2021). In fact, integrin αVß5-positive adhesions now termed RAs were also already seen 30 years ago (Wayner et al., 1991). This also applies to long lived clathrin coated structures (CCS), which were observed more than 40 years ago (Heuser, 1980).

Now long lived CCS are increasingly recognized as adhesion structures, since they modulate cell migration (Bucher et al., 2018b), pinch collagen fibers to support 3D migration (Elkhatib et al., 2017) and are stable features of costameres in the muscle (Vassilopoulos et al., 2014).

Since clathrin plaques and RAs share the αVß5 integrin, it is even assumed that they might be equivalent structures (Lock et al., 2019). However, as my thesis work reveals various subclasses of these adhesions and conversion mechanisms have not been described to date. It is now becoming increasingly evident that these structures likely control adhesion, mechanosensation, endocytosis, and mitosis. Still the exact physiological function of RAs in the organism has not yet been established and motivates further research.

1.3.1 Reticular adhesions

Before cells undergo cytokinesis, they disassemble all focal adhesions to allow the retraction into a spherical shape (Jones et al., 2018). However, to remain attached to the substrate during cytokinesis, the cells employ a special type of adhesion that is connected to the cell body via retraction fibers. These reticular adhesions are formed by the integrin αVß5 and mediate cell attachment during mitosis and during long-term culture (Lock et al., 2018).

RAs differ substantially from classical actin-associated integrin adhesions. However, although they do not depend on actomyosin for their maturation, they clearly contain actin and actin-regulatory proteins such as Arp2/3 and WASP (Lock et al., 2019). Compared to FAs, they are stationary and have a longer lifetime. Using mass spectrometry, many components of the CME machinery, including clathrin itself and a number of adaptors, were found in both RAs and clathrin plaques, stressing the similarity between the two structures (Leyton-Puig et al., 2017; Lock et al., 2018; Zuidema et al., 2018). Comparison of the associated biological pathways shows that proteins of endocytosis, calcium reabsorption, and synaptic the vesicle cycle were enriched (Lock et al., 2019). Interestingly, the organization of integrins into nanoclusters is observed in both FAs and RAs (Lock et al., 2018; Spiess et al., 2018). How integrins are activated in RAs without the necessary talin and kindlin molecules is not known. Since RAs are connected to the actin-positive rectraction fibers in mitosis, actin connection modules must also exist. Further research is needed to clarify this issue.

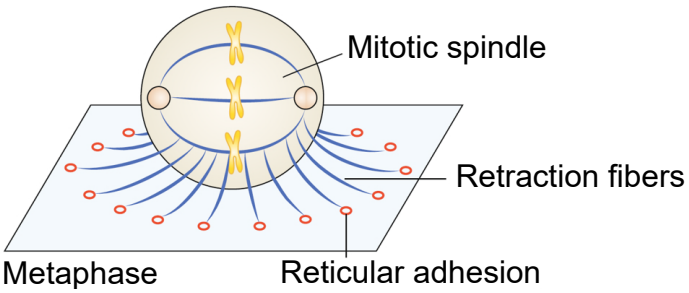

Figure 1.6: Reticular adhesions during mitosis. Schematic representation of a cell that rounds and remains connected to the substrate by reticular adhesions and retraction fibers. Source from: Zaidel-Bar 2018.

1.4 Aims of this study

While focal adhesions have been the focus of attention for decades, it has only become clear in recent years that cells generate a variety of different integrin based adhesions. In line with this, it has taken a long time for clathrin plaques to be recognized as a new class of adhesions. Reticular adhesions and clathrin plaques represent a class of adhesions that is highly enriched in members of the CME machinery.

However, the role of endocytic proteins including cargo-specific adaptors at these adhesions is still very enigmatic, and the careful study of their potential functions will likely expand our understanding of reticular adhesion and clathrin plaque dynamics and functionality. Stonins belong to the group of endocytic adaptors. Although the stonin protein family was identified more than four decades ago, detailed knowledge about stonin1 is still largely lacking.

In a previous study by our laboratory, stonin1 was described as a member of the endocytic machinery which localizes to disassembling focal adhesions (Feutlinske, 2014). In addition, Feutlinske, 2014 showed that stonin1 knockout fibroblasts exhibited altered FA dynamics.

The first aim of this thesis was to dissect the function of stonin1 at cellular adhesion sites by a combination of loss of function approaches and microscopical techniques to understand its impact on adhesion dynamics.

The second aim was to characterize the different types of stonin1-positive adhesions in detail using an array of imaging techniques including live cell confocal microscopy, STED nanoscopy, TEM, and CLEM.

Finally, since the relationship between RAs and other types of integrin-mediated adhesions is still poorly understood, the third aim was to investigate whether connections between these structures exist.

2. Material and Methods

2.1 Materials

2.1.1 General Material

If not indicated otherwise chemicals were purchased from Carl Roth (Germany), Life Technologies (USA), Merck (Germany), Sigma-Aldrich (USA) and Thermo Fisher (USA). Consumables were obtained from B. Braun (Germany), Biozym (Germany), GE Healthcare (UK), Greiner (Germany), Millipore (USA), Sarstedt (Germany) and Schott (Germany).

2.1.2 Buffers, Media, and Solutions

All Buffers were made using ultrapure water from a Milli-Q system (Millipore/Merck, Darmstadt, Germany). The pH was adjusted using NaOH or HCl unless otherwise specified.

Table 2.1: Buffers, media and solutions

Solution/Buffer	**Composition**
Antibiotics (stock solutions)	100 mg/ml Ampicillin 50 mg/ml Kanamycin sterile filtered (0.2 µm)
Bradford reagent (2x)	200 ml 85% H_3PO_4 100 ml Ethanol 140 g/l Coomassie G250
CaCl2 (2 M)	2 M $CaCl_2$ sterile filtered (0.2 µm)
Cell culture medium ($DMEM_{full}$)	DMEM, 4.5 g/l Glucose 10% (v/v) Fetal/ bovine calf serum 100 U/l Penicillin 0.1 mg/ ml Streptomycin
Coomassie destain solution	10% Acetic acid 25% Methanol

Coomassie staining solution	1 g/l Coomassie G250 10% Acetic acid 25% Methanol
DNA loading dye (6x)	0.03% (w/v) Bromphenol blue 0.03% (w/v) Xylene cyanol 60% (v/v) Glycerol
Fixation buffer (4%)	1×PBS 4% (w/v) Paraformaldehyde (PFA) 4% (w/v) Sucrose
Freezing solution (2×)	20% (v/v) DMSO 80% (v/v) Fetal/ bovine calf serum
Goat serum dilution buffer (GSDB)	1×PBS 10% (v/v) Goat serum 0.1% (v/v) TritonX-100
HBS (2x)	50 mM HEPES 280 mM NaCl 10 mM KCl 1.5 mM Na_2PO_4 12 mM Dextrose pH adjusted to 7.0 - 7.1 sterile filtered (0.2 µm)
HBSS/HEPES	HBSS 10 mM HEPES pH 7.4
Imaging buffer	FluoroBrite DMEM, 4.5 g/l Glucose 10% (v/v) Fetal/ bovine calf serum 1x GlutaMAX™ Supplement 100 U/l Penicillin 0.1 mg/ml Streptomycin
Insect lysis buffer	0.5% (v/v) TritonX-100 1 mM DTT 1X Pierce Protease Inhibitor tablet in 50 ml 1x PBS
LB medium	5 g/l Trypton 5 g/l NaCl 10 g/l Yeast extract pH adjusted to pH 7.4

LB plates	15 g/l Agar in LB medium
Lysis buffer	20 mM HEPES pH 7.4 100 mM KCl 2 mM $MgCl_2$ 1% (v/v) TritonX-100 1 mM PMSF 0.3% (v/v) Mammalian Protease inhibitor cocktail (Sigma)
PBS (10×) pH 7.4	1.37 M NaCl 43 mM Na_2HPO_4 14 mM NaH_2PO_4 27 mM KCl
Ponceau destain solution	1% (v/v) Acetic acid
Ponceau staining solution	0.3% (w/v) Ponceau-S 1% (v/v) Acetic acid
Reconstitution buffer (10x)	26 mM $NaHCO_3$ 20 mM HEPES
SDS running buffer (10x)	246 mM Tris 1.92 M Glycine 10% (w/v) SDS
SDS sample buffer (5x)	250 mM Tris pH 6.8 10% (w/v) SDS 0.5% (w/v) Bromphenol blue 50% (v/v) Glycerol 5% (v/v) β-Mercaptoethanol
SDS separating gel buffer (4x)	1.5 M Tris pH 8.8 0.4% (w/v) SDS
SDS stacking gel buffer (4x)	0.5 M Tris pH 6.8 0.4% (w/v) SDS
Stabilization buffer	30 mM HEPES, pH 7.4 70 mM KCl 5 mM $MgCl_2$
TAE (50x)	100 mM glacial acetic acid 50 mM EDTA pH adjusted to 8.2-8.4

TBS (10x)	200 mM Tris pH 7.6 1.4 M NaCl
TE buffer (0.1×)	1 mM Tris 0.1 mM EDTA pH adjusted to 8.0 sterile filtered (0.2 µm)
TE buffer (1x)	10 mM Tris pH 8.0 2 mM EDTA
Western Blot antibody dilution buffer	1×TBS 2% (w/v) Bovine serum albumin 0.03% (w/v) NaN_3
Western Blot blocking buffer	Odyssey® Blocking Buffer-PBS (LI-COR, LI 927)
Western Blot transfer buffer	25 mM Tris 192 mM Glycine 20% (v/v) Methanol

2.1.3 Antibodies

Primary and secondary antibodies were adjusted to 50% (v/v) glycerol for long-term storage at -20°C. The working dilutions listed in table 2.2 refer to the stock concentrations diluted with glycerol. The preparation of full-length antibodies against stonin1 is described in the dissertation of K. Diril (Diril, 2004). Near-infrared fluorescent dye-coupled secondary antibodies used for immunoblotting were diluted in sterile water to 1.0 mg/ml and used for fluorescence detection with an Odyssey® XF Imaging System (LI-COR).

Table 2.2: Primary antibodies

Antigen	Host	Company/ catalog nr.	Dil. IF	Dil. WB
αActinin	ms	Sigma Aldrich/ A5044	1:250	
AP2	ms	Abcam/ ab2730	1:100	
Clathrin HC	rb	Abcam/ ab21679	1:100	1:1000
Clathrin LC	ms	Santa Cruz/ sc-12735	1:100	
Cortactin	ms	Sigma Aldrich/ 05-180	1:500	
CyclinB	ms	Santa Cruz/ sc-245		1:250
Dynamin2	rb	Abcam/ ab3457	1:200	
Eps15R	ms	Gift from Sara Sigismund	1:100	
GFP	ch	Abcam/ ab13970	1:2000	1:5000
Hsc70	ms	Thermo Scientific/ MA3006		1:5000
Integrin αV	rat	BD Bioscience/ 550024	1:50	
Intersectin	ms	Santa Cruz/ sc-136242	1:100	
p34-Arc/ARPC2	rb	Millipore/ 07-227	1:100	
Paxillin	rb	Abcam/ ab32084	1:250	
Stonin1 human	rb	Sigma Aldrich/ HPA005715	1:100	
Stonin1 mouse	rb	Selfmade	1:100	1:500
Stonin2	rb	Sigma Aldrich/ HPA003086	1:200	
Vinculin	ms	Sigma Aldrich/ V9264	1:100	

Table 2.3: Secondary antibodies

Species	Origin	Conjugate	Company/ catalog nr	Dil.
ms	Goat	Alexa Fluor 488	Invitrogen/ A11029	1:200
	Goat	Alexa Fluor 647	Invitrogen/ A21236	1:200
rb	Goat	Alexa Fluor 568	Invitrogen/ A11036	1:200
	Goat	Alexa Fluor 647	Invitrogen/ A31573	1:200
ch	Goat	Alexa Fluor 488	Abcam/ ab150169	1:200
rat	Donkey	Alexa Fluor 488	Invitrogen/ A21208	1:200
	Donkey	Alexa Fluor 647	Dianova/ 712-605-153	1:200
ms	Goat	IRDye® 680RD	Licor/ 926-68070	1:10,000
rb	Goat	IRDye® 800CW	Licor/ 926-32211	1:10,000
ch	Donkey	IRDye® 800CW	Licor/ 926-32218	1:10,000

ch: chicken, rb: rabbit, ms: mouse: WB: Western Blot, IF: Immunofluorescence

2.1.4 Fluorescent reagents

Phalloidin probes were used equivalent to secondary antibodies in immunocytochemistry. Phalloidin was diluted in methanol according to the manufacturer's instructions - no glycerol was added. For super-resolution microscopy and correlative light and electron microscopy, phalloidin was diluted in DMSO according to the manufacturer's instructions to prevent methanol from inducing deterioration of the plasma membrane. DAPI was diluted to a stock concentration of 5 mg/ml and stored at 4 °C. For the preparation of labeled gelatin, a 0.2% gelatin solution (porcine skin; Sigma G-2500) was prepared in PBS. The solution was heated to 37 °C for 30 min to dissolve and sterilized using a syringe filter (0.22 µm, Millipore, SLGS033SB). 500 µl of the gelatin solution were labeled by incubating 5 µl of Atto 647N NHS ester (10 mg/ml, Sigma, 07376-1MG-F) for 1 hour at room temperature. The free dye was removed by dialysis using a Slide-A-Lyzer MINI dialyzer (20 k MWCO, 0.5 ml; Thermo Scientific 88402) against PBS for 2 hours at room temperature. After replacement of PBS, the mixture was dialyzed overnight at 4°C.

Table 2.4: Fluorescent reagents

Probe	**Conjugate**	**Company/ catalog nr.**	**Dilution**
Phalloidin	Alexa Fluor 488	Invitrogen/ A12379	1:50
	Alexa Fluor 568	Invitrogen/ A12380	1:50
	AF 594	Biomol/ ABD-23158	1:1000
Dapi		Sigma/ D9542	1:5000
Gelatin Atto 647N	Atto 647N	Selfmade	1:10

2.1.5 Plasmids

Expression constructs were obtained from addgene, the lab of AG Haucke / Maritzen or obtained by cloning. Since mouse cell lines divide more rapidly than human cell lines and transiently expressed constructs are diluted due to extensive cell division, most expression constructs were stably transduced. We used Moloney murine leukemia virus (MMLV)-based constructs (pLIB), which lead to strong and constitutive expression of the inserted genes under the control of the cytomegalovirus (CMV) promoter. Plasmid DNA was stored in nuclease- and endotoxin-free water at -20°C for long-term storage.

Table 2.5: Plasmids

Construct	Species	Backbone	Tag	Origin
eBFP2-Paxilin	human	pRRL	eBFP2	Fabian Lukas
pceBFP2-ML		pcDNA3	eBFP2	Martin Lehmann
pceGFP-MK		pc-MK	eGFP	Michael Krauß
pCIG3N		pCIG3		Jeremy Luban
pcmCherry-α-Actinin 1		pcmCherry	mCherry	Fabian Lukas
pcmRFP-MK		pcmRFP-MK	RFP	Michael Krauß
pCX-eGFP-ß5-Integrin	human	pCX-eGFP	eGFP	Raymond Birge
pFL 10xHis-Stonin1	mouse	pFL	10xHis	Fabian Lukas
pFL-10xHis		pFL	10xHis	Wen-Ting Lo
piRFP670-N1	mouse	pN1	iRFP	Vladislav Verkhusha
pLIB-CMV-IRES-Puro		pLIB		Reinhard Kofler
pLIB-GFP-MK		pLIB	eGFP	Fabian Lukas
pLIB-ß5-Integrin-iRFP	human	pLIB	iRFP	Fabian Lukas
pLV-F-tractin-mCherry		CSII-EF	mCherry	Tobias Meyer
pMDG.2		pMD2.G		Didier Trono
pRFP-CLC	human	pmRFP	RFP	Fabian Lukas
pRRLSIN.cPPT.PGK		pRRL		Didier Trono
psPAX2		psPAX2		Didier Trono
SpCas9-2A-eGFP		PX458	eGFP	Feng Zhang
Stonin1 full length	mouse	pRRL		Tanja Maritzen
Stonin1HDR-template	mouse	pcEGFP-MK	GFP	Fabian Lukas

2.1.6 DNA oligonucleotides

DNA oligonucleotides used as primers for polymerase chain reactions (PCR) were purchased from BioTeZ as lyophilized powder, dissolved to 100 µM in nuclease-free water, and stored at -20°C.

Table 2.6: DNA oligonucleotides

oligonucleotides	Sequence 5´-3´
CMW-fwd	CGCAAATGGGCGGTAGGCGTG
CRISPR_EGFP-fwd	TCTGGTGGTGGTTCTGGTATGGTGAGCAAGGGCGAG
CRISPR_EGFP-rev	AGGTGACCCAAGATCCCGGGTTTGTAGAATACATGGAT CCCTTGTACAGCTCGTCCATGC
CRISPR_HDR_left-fwd	TAGAGCTGCTGGTTTCAGCC
CRISPR_HDR_right-rev	AGTGAAGGAAGTGTGCCTGC
CRISPR_left_HDR_linker-rev	ACCACCACCAGAACCACCTTGAGTTACACAGCCACCAG
CRISPR_left_HDR-fwd-MluI	GGTGGTACGCGTTCCCTTGGCCTTTGAAGCAT
CRISPR_right_HDR-fwd	ATTCTACAAACCCGGGATCTTGGGTCACCTTTGATGATGAC
CRISPR_rightHDR-rev-NotI	GGTGGTGCGGCCGCGCTCGTGAACCACCTCTGTC
CRISPR-Guide-fwd	CACCGATTCTACAAACCCGGGCAGC
CRISPR-Guide-rev	AAACGCTGCCCGGGTTTGTAGAAT
pc-MK_beforeCMV-fwd	CTGCTTCGCGATGTACGG
pEGFPC1-fwd	GATCACTCTCGG CAT GGA C
pEGFPN1rev	GTCCAGCTCGACCAGGAT G
pRRL-fwd	GACCTCTCTCCCCAGG

RS: Restriction sites, frw: forward; rev: reverse

2.1.7 Software

Table 2.7: Software products, databases and internet tools

Software	Source	Application
Adobe Illustrator 2020	Adobe Systems Incorporated	Preparation of figures
CellProfiler 4.2.1	https://cellprofiler.org/	Automated quuantification of microscopy images
Clustal Omega	https://www.ebi.ac.uk/	Multiple Sequence Alignment

CRISPR gRNA Design tool	https://www.atum.bio	GUIDE DNA design
Fiji	https://fiji.s	Package containing plugins for ImageJ-based analysis
GraphPad Prism 9.0	GraphPad	Statistical analysis and graph preparations
Image J	https://imagej.nih.gov/ij/	Image acquisition of TIRF microscopy
Image Lab	Bio-Rad	DNA gel documentation
LI-COR	LI-COR	Quantitative immunoblot documentation and evaluation
MARS Data Analysis Software	BMG LABTECH	Analysis of microplate reader data
Microsoft Office	Microsoft	Documentations
NCBI/Blast	http://blast.ncbi.nlm.nih.gov/	Homology determination
NetPrimer	Premier Biosoft	Primer design
Primer BLAST	http://blast.ncbi.nlm.nih.gov/	CRISPR primer design
SnapGene viewer 5.0.4	https://snapgene.com/	DNA analysis
Thermo Scientific Web Tools	www.thermofisher.com	Analyzing primers, setting up reactions
Uniprot	https://www.uniprot.org/	Gene and protein research

2.1.8 Mammalian cell lines

Immortalized mouse myoblast cells (C2C12) were used for biochemistry and immunocytochemistry due to their high stonin1 expression. Mouse embryonic fibroblasts from stonin1 wild type and knockout mice were generated by Prof. Tanja Maritzen and Claudia Schmidt. Immortalization was achieved with SV40 large T-antigen on day 10 of in vitro culture. Three independent MEF cell lines were generated to exclude cell-line specific phenotypes. Moreover, three knockout cell lines were stably lentivirally transduced with mouse stonin1 full length for rescue experiments. HEK293T cells were used for retrovirus and lentivirus production. Primary myoblasts were a gift from Dr. Ines Lahmann. Primary astrocytes derived from tamoxifen-inducible conditional AP-2µ knockout (KO) mice were prepared by Dr. Tania López-Hernández.

2.2 Molecular biology

2.2.1 Cultivation of bacteria and glycerol stock preparation

Transformed *E.coli* Top10 were taken from cryopreserved cultures or LB agar plates and inoculated with 5 ml of LB medium for 8 hours. Bacteria were always incubated at 37°C and 180 rpm in a bacterial incubator shaker with appropriate antibiotics (100 µg/ml ampicillin or 50 µg/ml kanamycin). For a higher yield of plasmid DNA, Erlenmeyer flasks containing 100-200 ml of LB medium were inoculated with a 0.1 % (v/v) preculture and incubated overnight (∼15 h). To prepare bacterial glycerol stocks, a 1:1 mixture of sterile 50% glycerol and cell suspension was stored in 2 ml cryotubes at -80°C.

2.2.2 Bacterial transformation

For transformation, 50 µl glycerol stocks of chemically competent *E.coli* Top10 were thawed on ice and mixed with 10 ng of plasmid DNA or 5 µl of ligation products. Samples were mixed gently and incubated at 4°C for 15 min. Uptake of the plasmid DNA was induced by a heat shock of 60 s at 42°C in a heat block. After cooling on ice for 2 min bacteria were suspended with 900 µl LB medium without antibiotics and initially cultured at 37°C and 180 rpm for 1 h to allow expression of the resistance protein prior to exposure to the antibiotics. Bacteria were then pelleted at 700 × g for 2 min and plated on pre-warmed LB agar plates containing 50 µg/ml kanamycin or 100 µg/ml ampicillin. The plates were incubated overnight at 37°C. Newly transformed clones isolated from LB agar plates with sterile plastic tips were transferred to 200 µl LB medium (with appropriate antibiotics) per well of a 96-well plate and cultured for 2 h at 37°C on a Heidolph Titramax 1000 plate shaker at 350 rpm. 1 µl of the suspension was used directly to perform colony PCR for verification of positive clones.

2.2.3 DNA plasmid isolation

Plasmid DNA from small plasmid preparations (5 ml bacterial suspension) was isolated using the Nucleospin Plasmid Kit (Machery-Nagel) according to the manufacturer's instructions and eluted in 30 µl TE buffer. For large-scale plasmid preparations (100-200 ml bacterial suspension), the NucleoBond Xtra Midi Kit (Machery-Nagel) was used according to the manufacturer's instructions. The DNA pellet was dissolved in nuclease- and endotoxin-free water to a concentration of 1 µg/µl. The amount of DNA was determined by spectrometric measurement using a NanoDrop. Protein purity was defined by the ratio 260/280 (∼1.8 for DNA).

2.2.4 Restriction digest and ligation

Restriction digests were performed with FastDigest enzymes from Invitrogen. Plasmids were digested with 1 µl of each restriction enzyme in FastDigest buffer in a total volume of 20 µl for 30 min at 37°C. Plasmid DNA was additionally treated with 10 µl of calf intestinal phosphatase (CIP; New England Biolabs, Frankfurt am Main, Germany) for 10 min at 37°C to prevent re-circularization of the vector without insert. T4 DNA ligase (Thermo Fisher, ELL0016) was used to insert the fragment into the vector. A 5:1 molar ratio of insert to vector backbone was used, with 50-100 ng of backbone in a reaction volume of 20 µl. The reaction tube was incubated either overnight at 16°C or for 1 hour at room temperature.

2.2.5 Polymerase chain reaction (PCR)

The polymerase chain reaction (PCR) is used to amplify specific DNA sequences from a template based on cycles of denaturation of template DNA, annealing of sequence-specific primers, and subsequent elongation by a thermostable polymerase (Saiki et al., 1988). The Phusion™ High-Fidelity DNA Polymerase (Invitrogen) was used in a total reaction volume of 50 µl according to the manufacturer's protocol.

2.2.6 Agarose Gel electrophoresis

DNA was analyzed and purified by agarose gel electrophoresis using 0.5% to 2% agarose (w/v). Agarose was dissolved by heating in TBE buffer, and ethidium bromide was added at a final concentration of 100 ng/ml to allow visualization of DNA with UV light. Gels were poured and polymerized at RT until gelation. DNA samples were set to 1×DNA loading dye (Invitrogen), loaded into the cast agarose gel in 1x TAE buffer and run at 120 V for 30 min. A 1 kb DNA ladder (Invitrogen) was used as a molecular weight marker. To purify DNA fragments from the agarose gels, the desired bands were excised and transferred to a 1.5 ml tube and further processed using the Nucleospin Gel and PCR Clean-up Kit (Machery-Nagel, Düren, Germany) according to the manufacturer's instructions. The DNA was eluted with 30 µl TE buffer.

2.2.7 Colony PCR and sequencing

Colony PCRs were performed in a volume of 20 µl using a master mix containing 1× Taq polymerase reaction buffer, 200 µM of each dNTP, 10 µM of each primer, and approximately 1 unit of Taq polymerase (Fermentas, St. Leon-Rot, Germany) per reaction. 10-15 colonies were transferred with a pipette tip into 96-well plates containing 100 µl of antibiotic-enriched LB medium and incubated at 37°C for at least 4 h. 0.5 µl of the bacterial suspension was then directly transferred into the reaction mixture. Colony PCRs were performed according to the manufacturer's protocol, with an initial denaturation step of 3 minutes at 95°C. DNA samples were sequenced by LGC genomics (Germany) according to the Sanger method (Sanger and Coulson, 1975) using the appropriate sequencing primer.

2.3 Cell biology

2.3.1 Cultivaton of mammalian cell lines

Mammalian cells were cultured in $DMEM_{full}$ at 37°C in a humidified incubator containing 5% CO_2. Cultivation of cell cultures was performed continuously under sterile conditions. Media and wash buffer were always incubated in a water bath at 37°C before use. For passaging, cells were briefly washed with 1× PBS and detached from dishes by incubation with a synthetic trypsin replacement solution (TrypLE; Thermo Fisher, 12605036), which was used in appropriate volumes according to the manufacturer's instructions. The enzymatic reaction was stopped with an equal volume of $DMEM_{full}$, and the cells were seeded into new cell culture dishes. Mouse cell lines were passaged every 2 to 4 days at dilutions ranging from 1:5 to 1:20. Mammalian cells were not used after the 30th passage. Human cells were passaged every 2 to 3 days at dilutions of 1:2 to 1:5. Cell cryopreservation was performed by detaching cells from a confluent dish as described above and pelleting by centrifugation (300 × g, 3 minutes). Cells were resuspended in $DMEM_{full}$ containing 45% FBS (v/v) and 10% DMSO (v/v) and aliquoted into cryotubes. The suspensions were slowly frozen at -80°C overnight before long-term storage in liquid nitrogen. Cell biology experiments were performed on 18-mm glass coverslips and coating was performed overnight at 4°C. The coverslips were coated with 10 µg/ml fibronectin (Roche, MFCD00131062) or 5 µg/ml vitronectin (Gibco, A14700). To create a thin layer of Matrigel, the surface of the coverslip was covered with 5% (v/v) Matrigel (Corning®, 356231) in Opti-MEM ™(Thermo Fisher, 51985-042) and incubated for 10 minutes. This step was repeated.

2.3.2 Generation of HDFC matrices

Collagens are components of the extracellular matrix of connective tissue. The layers of the subcutis, for example, are made of collagen. In the human body, cells such as fibroblasts migrate into connective tissue containing collagen. The collagen proteins polymerize together to form fiber bundles.

We used a protocol to prepare high-density fibrillar collagen matrices (HDFC), which closely resemble the desmoplastic collagenous matrix of malignant tumors (Artym, 2016). To polymerize collagen on the coverslip, it was first neutralized. Rat tail collagen (Corning; formerly BD Biosciences) was first mixed with ice-cold 10X DMEM and then with 10X reconstitution buffer. The collagen solution was centrifuged for 3 min at 9000 g and 4°C. Neutralization was validated with indicator paper. The pre-cooled coverslips were removed with forceps and held in one hand while pipetting 2.5 µl of collagen solution with the other hand and dispensing with the pipette tip. The dishes were incubated on ice for 5 minutes to facilitate flattening of the collagen. The coverslips were then incubated for 30 minutes at 37°C in a humidified CO_2 incubator to polymerize the collagen into fibers. The coverslips were then centrifuged at 3500 g, 4°C to smooth the collagen meshwork into a relatively two-dimensional layer. The dishes were washed 1 x with PBS and filled with medium.

2.3.3 Transfection and RNA interference

Throughout the study, transfection techniques were adjusted to the type of experiment and cell type. Sufficient overexpression in C2C12 could be achieved by JetPrime (VWR). Here, the DNA is complexed with the positively charged reagent that can be taken up by endocytosis. Cells with a confluency of 30% to 40% were transfected according to the manufacturer's instructions. After 4 h incubation, the medium was changed. Knockdown of C2C12 was difficult to achieve due to rapid cell growth and dilution of siRNA with each cell division. It was finally achieved using reverse transfection with INTERFERin (VWR) and low cell seeding according to the manufacturer's instructions. In 12 well plates, 20,000 cells were directly reverse-transfected with 25 nM siRNA on fibronectin coated coverslips. MISSION® siRNA (Sigma, SIC001) was used as a negative control and SMARTpools for silencing of stonin1 (Dharmacon, L-055068) or ß5 integrin (Dharmacon, L-042453). Experiments were performed after 96 hours.

2.3.4 Production of lentiviral particles and transduction

Preparation of lentiviral and retroviral particles and transduction of mammalian cells were performed according to S2 guidelines (LAGESO). In fast dividing mouse cell lines, we usually used stable viral transduction as a method of choice. We used either MMLV (Moloney murine leukemia virus) or lentiviral particles. HEK cells were transfected with three plasmids, each of which includes a component of the virus and therefore begins to produce the virus only when co-expressed. The viral packaging plasmid psPAX2 carries the viral genes pol, gag, rev, tat and the rev response element (RRE). The envelope plasmid pMD2. G encodes the G protein of the vesicular stomatitis virus (VSV-G) envelope for broad host infectivity For retroviral particle production instead of psPAX2 the pCIG3N plasmid was used for the expression of MLV gag-pol. The psPAX2 (Addgene plasmid #12260) and pMD2. G (Addgene plasmid #12259) were a gift from Didier Trono. The pCIG3N plasmid was a gift from Jeremy Luban (Addgene plasmid # 132941) The transfer plasmid contains the protein of interest flanked by long terminal repeats (LTRs) and the respective packaging signal. Lentiviral particles expressing clathrin LC and control shRNA were kindly provided by Dr. Domenico Azarnia Tehran. For viral production, 10 cm dishes of HEK cells with a confluency of 60-80% were transfected using calcium phosphate with 15 µg of transfer plasmids, 4.5 µg of pMD2.G plasmid and 10.5 µg psPAX2 (lentivirus) or pCIG3.NG (retrovirus) plasmid. From this point on, cells were considered to be S2 cultures. After an incubation period of at least 16 hours, new medium was added in a volume reduced by 60% to increase the virus titer. Two subsequent rounds of virus harvest were conducted after 24 and 48 hours. The virus-containing medium was collected and replaced with new medium. Cell debris was then removed from the collected medium by centrifugation at 200 × g for 5 min at RT, and the medium stored at 4°C. The supernatant was pooled and filtered using a 0.45-µm Falcon filter and concentrated 100-fold using an Amicon-15 100-kDa filter column (Merck, Z740210). Aliquots each containing 20% concentrated viral supernatant were stored at -80°C. For high transfection efficiency in mouse cell lines, 100,000 cells were seeded the previous day in 6-well plates and transduced with the contents of an aliquot. Since the retroviral transfer plasmid encodes a puromycin resistance gene, cells were selected after 96 hours with 1 µg/ml puromycin.

2.3.5 Immunocytochemistry

Cells grown on coverslips or cell culture slides (Greiner, 543079) were rinsed with 1x PBS and fixed with ice-cold 4% (w/v) paraformaldehyde (PFA) containing 4% (w/v) sucrose in PBS for 10 min at RT. After washing three times with PBS, cells were simultaneously permeabilized and blocked in goat serum dilution buffer (GSDB) for 30 min. Antibodies were specifically diluted in GSDB (Table 2.2) and incubated for 1 hour. After washing three times with PBS, cells were incubated with secondary antibodies (Table 2.3) in GSDB for 45 minutes. When labeling the actin cytoskeleton, 6 U/ml of phalloidin were added to the solution. After rinsing three times with PBS, cells were incubated with 1 µg/ml 4',6-diamidino-2-phenylindole (DAPI) for 5 minutes and then rinsed two additional times. Glass coverslips were mounted on slides in ImmuMount™ (Thermo Fisher, 9990402). For TIRF microscopy, cell culture slides were not mounted but kept in 1x PBS and imaged on the same day.

2.3.6 Stimulation and inhibitor treatments

All compounds were purchased from Selleckchem and dissolved in DMSO. Stock solutions, working concentrations and incubation times are indicated in table 2.8. Inhibitors were dissolved in 37°C prewarmed DMEM and applied to cells. For starvation, cells were starved overnight in DMEM. Cells were stimulated with either $DMEM_{full}$ or with 50 ng/ml PDGF-BB (Peprotech) in DMEM for 15 min. PDGF-BB was dissolved in sterile commercial water and diluted to 10 µg/ml in water containing 0.1% BSA as a stabilizing carrier protein.

Table 2.8: Inhibitors

Inhibitor	**Stock concentration**	**Working concentration**	**Incubation time**
Blebbistatin	10 mM	50 µM	1 hour
CytochalasinD	5 mM	20 µM	2 hour
Cytostatin	1 mg/ml	10 µg/ml	30 min
Flavopiridol	10 mM	1 µM	12 hours

2.3.7 Fluorescence microscopy

Confocal imaging was performed with a Nikon/Andor spinning disk confocal microscope, equipped with an Andor EMCCD camera, an Okolab environment control chamber for life cell imaging at 37°C and 5% CO_2 and a Nikon PerfectFocus autofocus system. Either a 60x (PLAN APO, NA: 1.40, WD 0.13 mm) oil immersion objective or a 40x (PLAN APO, NA: 0.95, WD 0.25 mm) air objective was used. Excitation was performed at 405 nm, 488 nm, 561 nm and 633 nm for Dapi/eBFP2, Alexa-Fluor488/eGFP, Alexa-Fluor568/mRFP and Alexa-Fluor647/iRFP, respectively. The setup was controlled with the imaging-Software NIS (Nikon). If not indicated otherwise, live-cell imaging was performed with Imaging buffer (Table 2.1). To visualize the dynamics at the plasma membrane over a tiny distance of 100 to 200 nm depth, total internal reflection fluorescence microscopy (TIRF) was utilized (Axelrod, 1981). TIRF microscopy was performed using the Nikon equipment described above, which was equipped with an sCMOS camera and a custom-built solid-state laser. A 60x oil immersion objective (APO TIRF, NA: 1.49, WD 0.13 - 0.21 mm) was used as standard. The setup was controlled with Micromanager (Edelstein et al., 2010), an ImageJ-based open-source microscopy software. Stimulated emission depletion (STED) microscopy was used to image stonin1 containing adhesions on a nanoscale level. STED nanoscopy was performed with a Leica TCS 3X gSTED microscope with 592 and 775 nm depletion lasers. Image acquisition was performed using a 100 x (PLAN APO, NA 1.4, WD 0.13 mm) oil immersion objective. Excitation was at 488 nm, 590 nm, and 640 nm for AF488, AF594, and Atto647N, respectively. Noncommercial secondary antibodies were provided by Dr. Martin Lehmann. AF 594 phallodin (table 2.4) was used to visualize the actin cytoskeleton. For STED microscopy high precision coverslips with a thickness of 1.5 (0,16-0,19 mm) were used and mounted in Prolong Gold (Invitrogen, P36930), 1 day at RT. Microscopy images were imported and analyzed using ImageJ/FIJI (Bioformats importer).

2.3.8 Generation of unroofed membrane sheets for correlative light and electron microscopy

Cells were seeded on gridded glass coverslips (Ibidi, 10816) that were coated with HDFC. Unroofing was performed 16 hours after seeding. The cells were washed two times with stabilisation buffer (Table 2.1). Unroofing was performed in 2% paraformaldehyde (PFA) in stabilization buffer using a 10-ml 22-gauge, 1.5 inch syringe (BD Biosciences 309604). The stabilization buffer was removed and the syringe was used to splash the coverslips. The needle was positioned approximately 1 cm from the coverslips. The coverslip was immediately put into fresh 2% PFA solution and fixed for 20 minutes at room temperature. For correlative light and electron microscopy (CLEM), membrane sheets of endogenously expressing eGFP-Stonin1 C2C12 myoblasts were used that were stably transduced with ß5 integrin-iRFP. After fixation, the cells were washed three times with PBS and incubated with AF 594 phallodin for 30 min. After another 3x PBS washes the membrane sheets were immediately used for spinning disk microscopy. To cover a defined grid of the coverlip a montage of 12 x 12 images with an overlap of 20% for stichting was taken. The immersion oil was carefully removed from the coverslip, and a standard cell culture microscope was used to find the square of the imaged area uniquely defined by numbers and letters. The imaged area was marked with a circle using a diamond scribe. Unroofed membranes were fixed overnight with 2% glutaraldehyde in PBS. Electron microscopy and further preparation was performed by Dr. Claudia Matthaeus at the Leibniz Research Institute for Molecular Pharmacology (FMP, Berlin). Briefly, the samples were dehydrated and dried using critical point drying and coated with a thin layer of platinum and carbon to produce a replica of the membrane surface. The replica were removed from the coverslip using 5% hydrofluoric acid and then transferred to a TEM grid for imaging in the TEM at magnifications of 4,000 to 20,000 times. MATLAB was used to transform the fluorescence image to the corresponding EM montage using phalloidin.

2.3.9 Data analysis and statistical analysis

Image analysis was performed with Fiji, an image processing package based on ImageJ2 (Schindelin et al., 2012). To quantify colocalization between two channels, Pearson correlation coefficients were determined using the Fiji plugin 'Coloc2' with 'Costes Threshold regression'. Prior to image processing, the background was manually removed by measuring pixel intensities in a black area, and background noise was removed by applying a Gaussian filter. The same was done for determining the Mander's overlap coefficient. Here the Fiji plugin "JACoP" was used, and the threshold was set manually.

Image analysis containing a large image set was performed automatically with the modular high-throughput image analysis software CellProfiler (McQuin et al., 2018). For segmentations of particles or cells, the lower quartile of intensities was removed automatically as background and automatic thresholding was performed using the Otsu algorithm (Otsu, 1979). Mean fluorescence intensities were measured using either automatically detected particle or cell segmentations or by manually selecting a region of interest and measuring it using the measurement tool in Fiji.

For the analysis of experiments that included three independent experiments, cells were randomly selected according to the fluorescence signal from the nuclear counterstain. All statistical tests were performed using either the two-tailed unpaired t-test or the one-sample t-test using Prism 8.0 software (GraphStats). Data were usually normalized and displayed as mean +/- standard error of the mean (SEM). Significance levels are shown in each graph: *$p < 0.05$, **$p < 0.01$, ***$p < 0.001$. Experiments with $n < 3$ were typically displayed as box plots with center and box edges indicating the median and 25th or 75th percentile, respectively. The box plot notches indicate an approximate 95% confidence interval. N is represented here as the number of cells or adhesions.

2.4 Biochemistry

2.4.1 Preparation of cell lysates

Cells were washed three times with PBS, and 100 µl of lysis buffer was pipetted directly onto the cells. The lysates were scraped from the cell culture dishes and incubated on ice for 10 minutes, mixing from time to time. The debris was spun at 17,000 × g for 10 minutes at 4°C. The protein content of the supernatant was determined by the Bradford assay (Bradford, 1976). Samples were diluted 1:1000 in 1 × Bradford reagent (Table 2.1) and then incubated at RT for 5 min before measurement with a spectrophotometer. Protein concentration was determined using a bovine serum albumin standard curve. Samples were adjusted to 1 × SDS sample buffer (Table 2.1) and boiled at 95°C for 5 min. Samples that were not immediately loaded were stored long-term at -20°C.

2.4.2 SDS PAGE

Discontinuous sodium dodecyl sulfate-polyacrylamide gel electrophoresis (SDS-PAGE) was done to separate the protein content of cell lysates according to their molecular weight (Laemmli, 1970). All reagents and gel components were prepared according to the Laemmli buffer system. The gel electrophoresis chamber Mini Protean Tetra Cell System (Bio-Rad), plates (1.5 mm thickness), combs and pouring stations were used for gel preparation. SDS-PAGE gels were cast as indicated in table 2.9. To ensure a straight transition between the stacking gel and the separating gel, a layer of 2-propanol was added to the separating gel and washed off with water before the stacking gel was poured. Samples containing 50 µg of protein lysate were loaded into the equilibrated gel pockets in volumes of 20 to 40 µl. SDS-PAGE gels were run at 15-20 mA in 1× SDS running buffer. Pre-stained protein markers (New England Biolabs) were used as molecular weight standards. When the bromophenol blue front line of the sample buffer reached the bottom of the gel, electrophoresis was stopped and gels were either stained with coomassie or used for Western blotting.

Table 2.9: SDS-PAGE gel preparation

Component	Separating gel		Stacking gel
	6%	8%	
1 x buffer	SDS separating gel buffer		SDS stacking gel buffer
Acrylamide/Methylen bisacrylamide - 37.5:1 (v/v)	6%	8%	3%
TEMED (v/v)	0.1%		
APS (w/v)	0.1%		

For coomassie staining, gels were incubated in coomassie solution for 2 hours at RT. Background staining of the gel was removed by two consecutive rounds of incubation in coomassie destaining solution, first for 2 hours at RT and then overnight.

2.4.3 Immunoblotting

Immunoblotting was performed for selective detection of proteins (Western blots). The separated proteins from SDS-polyacrylamide gels were transferred to nitrocellulose membranes (Amersham Protran 0.2 NC; GE Healthcare) using the Tank Electroblotting Mini Trans-Blot System (Bio-Rad). Proteins were transferred using a wet blotting device (Biorad) for 90 minutes at 110 V and 4°C. To assess protein loading and transfer efficiency, nitrocellulose membranes were reversibly stained with a Ponceau staining solution at RT for 5 min. If necessary, the membrane was cut at different molecular weights to allow parallel detection of proteins of different sizes. Ponceau S staining was removed by washing several times with PBS. All the following incubations were carried out on a laboratory shaker. Blots were blocked for 1 hour at RT with Western blot blocking buffer (Table 2.1) against nonspecific antibody binding.

The Western blot was incubated with the primary antibodies in Western blot antibody dilution buffer overnight at 4°C. After incubation of primary and secondary antibodies, blots were washed four times with 1x PBS containing 0.05% Tween. IRDye-conjugated secondary antibodies (Table 2.3) in Western blot antibody dilution buffer were incubated for 40 minutes. Fluorescence signals were acquired using a LI-COR Odyssey® Fc imaging System and recorded and analyzed using Image Studio Lite (LI-COR) software.

2.4.4 Recombinant protein expression in Sf21 insect cells

The recombinant stonin1 was expressed in insect cells using the Bac-to-Bac baculovirus Expression System (Life Technologies). To create the expression vector, the full-length coding sequence of mouse stonin1 was inserted into the pFL10xHis vector using standard restriction enzyme cloning. The final pFL 10xHis-Stonin1 plasmid was transformed into DH10Bac competent cells, and successful recombination into the bacmid was determined by blue-white screening using XGal. Several blue colonies were picked, inoculated and grown overnight. The next day, 1 L LB medium was inoculated with 10 ml of the overnight culture and grown to an OD600 of 0.6 to isolate the bacmid using the Nucleospin Plasmid Kit (Machery-Nagel) as described in section 2.2.3.

Maintenance of Spodoptera frugiperda-21 cells (Sf21; Life Technologies) was performed in suspension culture in Sf-900™ II medium (Life Technologies) at 27°C in a non-humidified incubator at 120 rpm. Three ml of Sf-9 cells (0.2 x 10^6 cells / ml) were transfected in 6-well culture plates (Corning®) using Fugene (Roche) according to the manufacturer's instructions. Successful transfection was assessed by eYFP expression after 48 hours using a cell culture microscope and baculovirus-containing supernatant was removed (P0 virus stock). For the preparation of a large-scale virus stock, 40 ml of Sf21 cells at a cell density of 1 x 10^6 ml were transferred into 300 ml medium and 1 ml of P0 virus stock was added. Cell density was carefully monitored after 2 days until proliferation arrest was detected. After another day, the supernatant was removed, filtered and stored at 4°C.

For purification of 10xHis-Stonin1, 200 ml of Sf21 cells were grown to a density of 6 x 10^6 cells /ml. The cells were divided into two 2 liter flasks and 300 ml of fresh medium was added containing 8 ml virus supernatant. The cells were harvested and aliquoted into 50 ml Falcon tubes after 24 hours. After centrifugation for 800xg for 5 min, the supernatant was discarded and the cell pellet stored at -80°C.

The purification of 10x-His-Stonin1 was done using immobilized metal affinity chromatography. The Sf21 cell pellet from a Falcon tube was lysed in 10 ml insect lysis buffer for 15 min at 4°C on a tube rotator (VWR) and sonicated with 30% power for 30 sec (Branson digital sonifier 450). Cell debris was removed from the lysates by centrifugation in an SS-34 rotor (Sorvall) at 35,000 × g and 4°C for 15 min. 100 µl of equilibrated Ni-NTA agarose (Life Technologies) were applied to the lysate supernatant and incubated for 2 hours at 4°C in a tube rotator. Four wash steps were performed, each by centrifuging at 3,000xg for 3 minutes at 4°C, discarding the supernatant, and applying the new wash buffer. Washing was performed 1x with insect lysis buffer and 3x with 20 mM imidazole in PBS. Elution was performed in 300 mM imidazole in PBS. The eluate was dialyzed first for 2 h and then overnight against PBS with 1 mM DTT or against coupling buffer (table 2.10) with 1 mM DTT in a dialysis tube with a molecular weight cut-off of 6000-8000 kDa (Roth). Final protein concentration was determined by Bradford assay and purification was assessed by SDS-PAGE and coomassie staining.

2.4.5 Affinity chromatography of a stonin 1 specific antibody

Table 2.10: Buffers used for antibody purification

Buffer	Composition
Coupling buffer	0.2 M $NaHCO_3$, 0.5 M NaCl, pH 8.3
Buffer A	0.5 M ethanolamine, 0.5 M NaCl, pH 8.3
Buffer B	0.1 M sodium acetate, 0.5 M NaCl, pH 4.0

An NHS-activated HiTrap affinity column (GE Healthcare) was used to purify a polyclonal stonin1 specific antibodies with a peristaltic pump (Peri-Star PRO) at 4°C and a flow rate of 0.5 ml/min according to the manufacturer's instructions. The column was equilibrated with 1 mM HCl and coupling buffer. A total of 1 mg of 10xHis-Stonin1 purified from Sf21 insect cells in the coupling buffer was recirculated for 4 hours at 4°C using a peristaltic pump for ligand coupling. Excess NHS groups were deactivated, and the nonspecifically bound ligand was washed off by the following procedure:

1. Injection of 3 × 2 ml buffer A

2. Injection of 3 × 2 ml buffer B

3. Incubation of the sealed column for 1.5 h at 4°C

4. Injection of 3 × 2 ml buffer B

5. Injection of 3 × 2 ml buffer A

6. Injection of 3 × 2 ml buffer B

10 ml of rabbit 86.6 immune serum provided by Prof. Tanja Maritzen was diluted 1:5 in PBS and filtered through a 0.2 µm filter. After the ligand-bound column was equilibrated with PBS, the diluted serum was pumped into the column and then washed with 10 volumes of PBS. Stonin1-specific antibodies were eluted from the antigen with 0.1 M glycine, pH 2.8, and collected in 10 fractions of 0.5 ml eluate in 1.5 ml tubes containing 25 µl 1 M Tris-HCl, pH 9. Fractions were tested for the presence of antibodies by determination of A_{280} and analyzed by Western blotting of stonin1 wild-type and knockout MEFs. The antibody was either aliquoted and stored at -80°C or mixed 1:1 with 90% (v/v) glycerol in PBS containing 0.05%(v/v) sodium azide for regular use and stored at -20°C.

2.4.6 Proteomics and kinase screen

The 10xHis-Stonin1 purified from insect cells showed a characteristic double band in SDS-PAGE gels, which was also observed in mammalian cells suggesting posttranslational modifications. Since the characteristic double band was not visible in stonin1-expressing bacteria, we decided to determine the post translational modifications by mass spectrometry. Mass spectrometric measurements and data processing was performed by the group of Dr. Eberhard Krause at the FMP Berlin. Briefly, 500 ng of 10xHis-Stonin1 were reduced with 5 mM dithiothreitol in 1x SDS sample buffer at 55°C for 30 min. Then 40 mM chloroacetamide (CAA, fresh solution) were added and incubated for 30 min at RT in the dark. After an SDS-PAGE was performed the gel was stained with coomassie and sent to the mass spectrometry facility.

For kinase screening, a peptide comprising the proline-rich domain of mouse stonin1 was synthesized by Dr. Rudolf Volkmer at the FMP Berlin. The peptide was N-terminally biotinylated and had the following sequence: WKDEGSASPFPLDSLASRKPFSPKDKEVPIGH (32 aa, pl = 7.8)
The phosphorylation profile of the peptide was determined at 1 µM in a radiometric assay (PanQinase® activity Assay) on a panel of 245 Ser/Thr kinases using streptavidin-coated FlashPlate® HTS PLUS plates by ProQinase, Freiburg.

2.4.7 CRISPR/Cas9 genome editing

The goal was to generate endogenous N-terminal GFP-labeled stonin1 by Cas9 cleavage and homology-directed DNA repair (HDR). For this purpose, a donor vector was generated with the GFP tag and 5' and 3' homology regions (HR) flanking the startcodon of stonin1 genomic DNA. Genomic DNA was isolated from C2C12 mouse myoblast cultivated to 90% confluence with the Blood & Cell Culture DNA Mini Kit (Qiagen) according to the manufacturer instructions. Because we were unable to amplify the HRs, we first performed a nested PCR that enclosed the mouse stonin1 HRs. Primers were designed using primer-BLAST (Ye et al., 2012). From the nested-PCR mixture, 2 µl were used for amplification of the 5' and 3' homology regions of stonin1. The GFP tag was amplified via PCR from the plasmid pcEGFP-MK. PCRs were performed as described in chapter 2.2.5. HRs were then cloned together with GFP via overlap extension PCR in equimolar amounts for 15 PCR cycles without primers at 60°C, followed by a purification PCR using the end primers for another 15 PCR cycles. The gel extracted fragment was then cloned into pcEGFP-MK plasmid using MluI and NotI restriction enzymes. We also introduced a small peptide-gycin-serine linker after the GFP tag in the PCR overlaps. Oligonucleotides are listed in table 2.6.

The Design of a stonin1 specific sgRNA was performed using the CRISPR gRNA Design tool (Atum, Newark). Cas9-GFP together with the sgRNA was expressed from the PX330 plasmid. Cloning of specific sgRNA was performed as described by (Cong et al., 2013). In brief, two complementary oligonucleotides were synthesized with overhangs for cloning into the BbsI site in the px330 vector. 1 µl oligonucleotides (100 mM) were phosphorylated using 0.5 µl T4 polynucleotide Kinase (NEB) in a total volume of 10 µl for 30 min. For annealing of the oligonucleotide to double-stranded DNA, a heating step was performed at 95°C for 5 min, followed by cooling the reaction to 25°C using a thermal cycler with a ramp rate of -5°C/min. The sgRNA was then cloned into the px330 vector using the restriction site BbsI.

Both the donor vector and the px330 vector expressing Cas9-eGFP and stonin1-specific sgRNA were co-transfected with a 5-molar excess of the donor vector in C2C12 myoblasts with JetPrime (VWR). After 48 hours the GFP expressing cells were sorted and transferred as single cells into five flat bottom 96-well plates (Corning®) using fluorescence-activated cell sorting (FACS). FACS was performed by Hans-Peter Rahn of the flow cytometry facility at the MDC, Berlin. Briefly, cells were trypsinized and washed twice at 300 × g for 5 minutes and resuspended in Opti-MEM™.

Cells were filtered using a cell strainer snap cap (Fisher scientific) and kept in 1.5 ml Opti-MEM™ in 5 ml round-bottom polystyrene tubes (Fisher scientific) on ice. The cells were sorted into 150 µl conditioned media. The conditioned media was prepared beforehand by cultivation of C2C12 myoblast in 15 cm dishes to near confluence. The media was then filtered through a 0.45 µm falcon filter and diluted 1:1 in $DMEM_{full}$.

After reaching confluence, cells were transferred to 24-well plates (Corning®) and from there into 96-well glass bottom plates (Cellview®). Positive endogenous eGFP-Stonin1 expressing cells were then screened with a Nikon/Andor spinning disk confocal microscope. Several clones were picked and further investigated using western blot with both a stonin1 and GFP antibody. We could only identify clones with heterozygous eGFP-Stonin1 expression, which were used for further fluorescence microscopy

3. Results

3.1 Stonin1 is a unique marker for reticular adhesions

Stonin1 is considered to be a regulator of FA dynamics and cell motility. Ston1$^{-/-}$ embryonic mouse fibroblasts (MEFs) show smaller focal adhesions as well as altered cellular motility (Feutlinske et al., 2015). However, the underlying mechanism has remained enigmatic. To unravel the role of stonin1 in adhesion dynamics, we capitalized on the one hand on Ston1$^{-/-}$ fibroblast and on the other hand on genetically altered C2C12 knock-in cells which express eGFP-tagged stonin1 from its endogenous locus.

3.1.1 Stonin1 expression is highly regulated and depends on environmental conditions

To find a suitable cell culture system, the expression of stonin1 in different cell lines was examined. Fig. 3.1 shows a western blot of protein extracts prepared from a selection of mouse and human cell lines. The band below 100 kDa indicates stonin1 expression, which is absent in the Ston1$^{-/-}$ MEFs loaded as control. In most tumor cell lines, stonin1 expression could not be detected, for example in the widely used HeLa cells. The fact that stonin1 was expressed in only a few cell lines, suggests a specialized, selective function of stonin1. Embryonic and adult fibroblasts, as well as myoblasts, displayed high stonin1 expression. The myoblast cell line C2C12 showed high stonin1 expression, a prominent cytoskeleton and large focal adhesions. In addition, it had a flat morphology ideal for microscopy and was therefore chosen to study the function of stonin1.
Stonin1 was expected to have a punctate localization pattern similar to that of stonin2, given its potential role in clathrin-mediated endocytosis (CME).

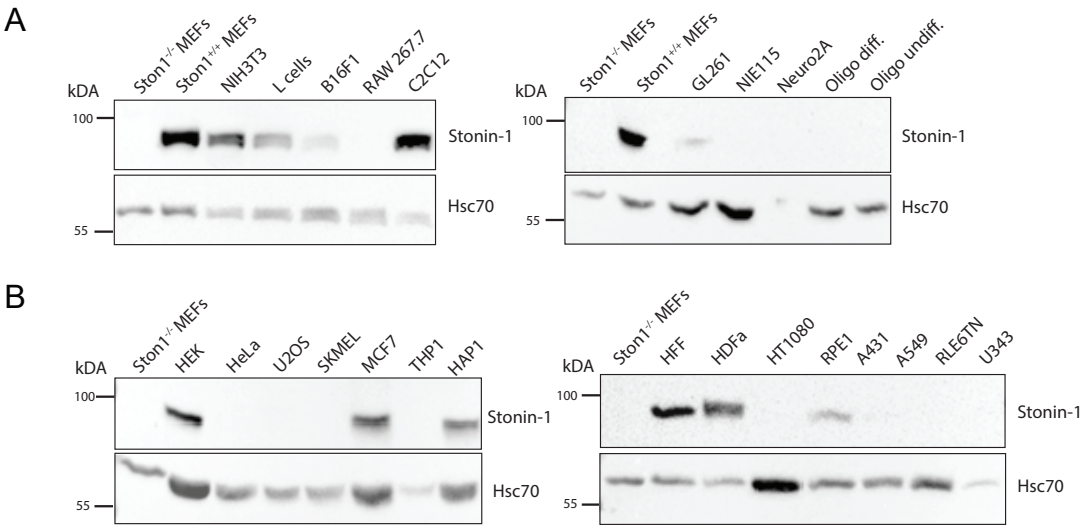

Figure 3.1: Western Blot analysis of the expression profile of stonin1 in various cell lines. Immunoblots for either mouse or human stonin1. 50 µg lysates were loaded on an 8% SDS-PAGE gel. Hsc70 was used as loading control.
(A) Expression of stonin1 in mouse cell lines.
(*MEF: mouse embryonic fibroblasts, NIH-3T3: fibroblasts, L-cells: connective tissue fibroblasts, B16F1: melanoma cells, RAW 267.7: macrophages, C2C12: myoblasts, GL261: glioma cells, NIE115: neuroblastoma cells, Neuro2A: neuroblastoma cells, Oligo diff.: oligodendrocytes differentiated, Oligo undiff.: oligodendrocytes undifferentiated)*
(B) Expression of stonin1 in human cell lines.
(HEK: human embryonic kidney cells, HeLa: cervix cancer cells, U2OS: osteosarcoma cells, SKMEL: melanoma cells, MCF7: breast adenocarcinoma cells, THP1: monocytes, HAP1: fibroblast like leukemia cell line, HFF: foreskin fibroblasts, HDFa: dermal fibroblasts, HT1080: fibrosarcoma cells, RPE1: retinal pigment epithelium cells, A431: epidermoid carcinoma cells, A549: adenocarcinoma alveolar basal epithelial cells, RLE6TN: alveolar type II cells, U343: astrocytoma cells)

However, immunofluorescence images of cells endogenously expressing stonin1 did not show a punctate localization pattern after one day in culture. Instead, the cells showed uniform staining with no specific localization pattern. Occasionally, stonin1-positive fiber-like structures were observed (Fig. 3.2 A). These positive patches increased when cells were grown for a longer time in culture, and also punctate structures appeared.

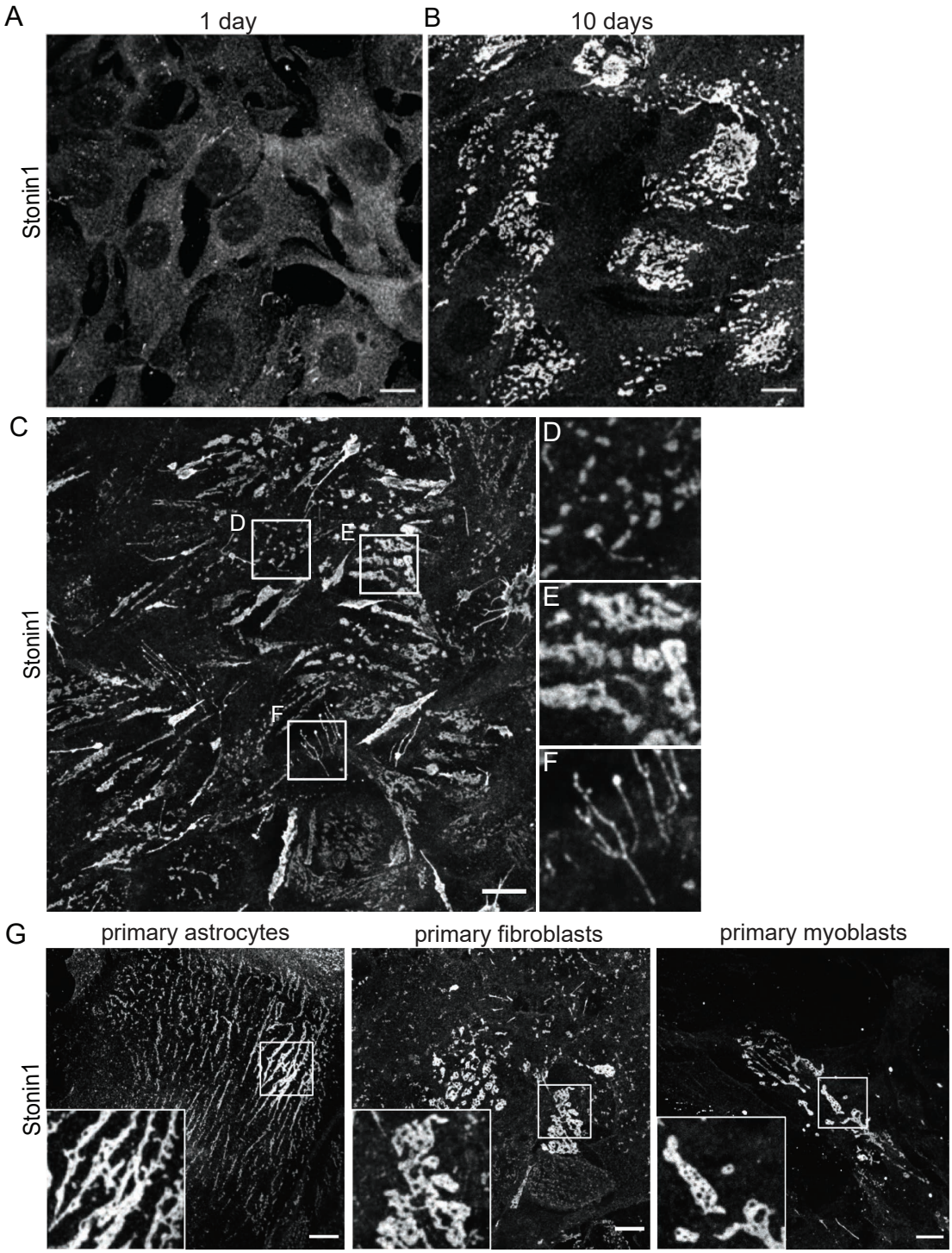

Figure 3.2: Stonin1 expression is dependent on the time in culture. Immunofluorescence images of endogenous stonin1 expression. C2C12 myoblasts were cultured for 1 day (A) or 10 days (B) on vitronectin. (C) C2C12 myoblasts grown for 7 days display morphologically distinct stonin1 structures that were classified as puncta (D), networks (E) and fibers (F). (G) Long-term culture of primary astrocytes, fibroblasts, and myoblasts. Scale bars 10 µm.

Long-term cultures (10 days) of C2C12 myoblasts displayed large stonin1-positive structures which could reach a diameter of over 10 µm (Fig. 3.2 B). Stonin1-positive structures were classified based on their morphology into three categories:

1. puncta (Fig. 3.2 D)

2. fibers (Fig. 3.2 E)

3. networks (Fig. 3.2 F)

The large stonin1-positive structures were heterogeneous in appearance and size. Sporadically they contained holes, and sporadically they were connected with fibers. We have therefore classified these structures as networks. We wondered whether the different stonin1-positive structures might be a common feature of primary cell lines. Indeed, all three types of stonin1-positive structures were also found in primary astrocytes, fibroblasts, and myoblasts (Fig. 3.2 G). Primary cell lines cultured for a short time did not display a specific stonin1 pattern.

Since mouse myoblasts divide rapidly, transient protein expression declines fast due to the high number of cell divisions. In addition, transient expression frequently does not correspond to endogenous expression levels and may lead to artifacts. Therefore, we decided to generate a genetically altered C2C12 knock-in cell line, which expresses an enhanced green fluorescent protein (eGFP)-tagged stonin1 from its endogenous locus (Fig. 3.3 A). Three heterozygous cell lines were verified by western blot and GFP immunoprecipitation using antibodies specific for stonin1 and GFP (Fig. 3.3 B). The clone with the highest eGFP-stonin1 expression was used for further studies. Also in the genome-edited cells stonin1 puncta, fibers, and networks were only observed when culturing the cells for a longer period of time (Fig. 3.3 C).

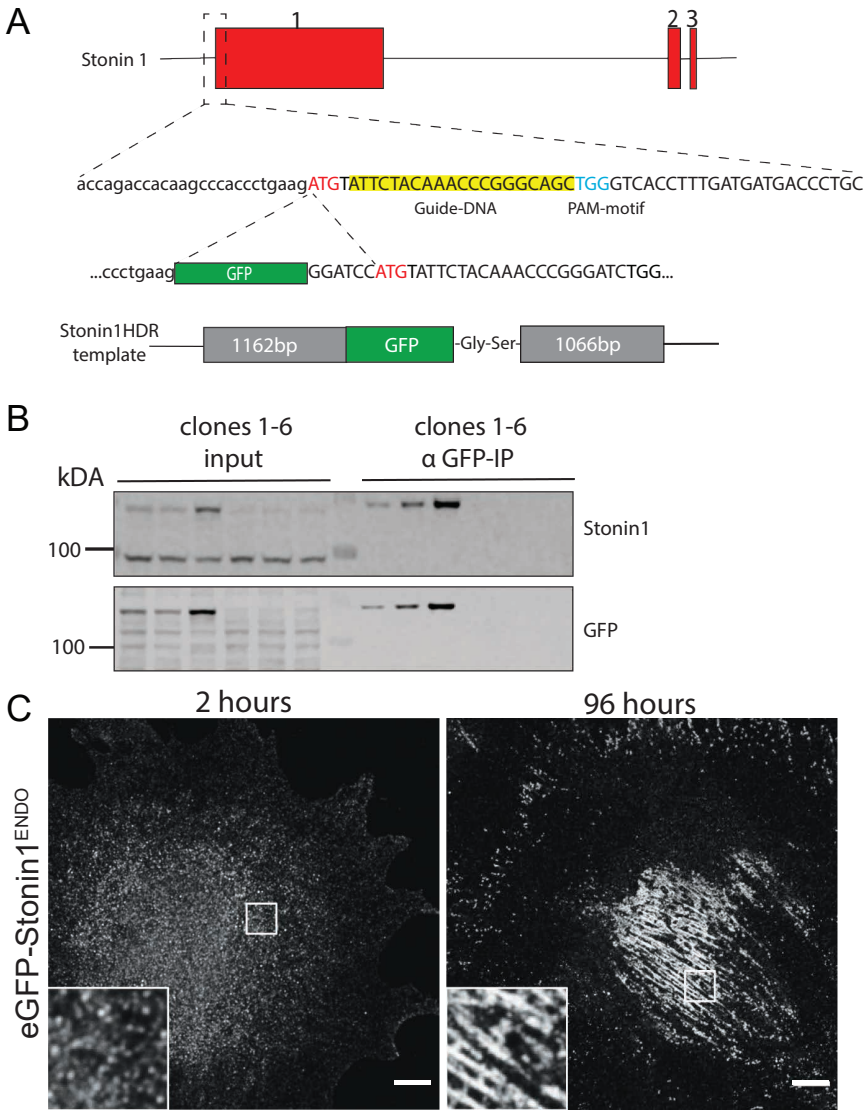

Figure 3.3: Generation of an eGFP-tagged stonin1 knock-in myoblast cell line. (A) CRISPR-Cas9 endogenous tagging strategy. The eGFP tag with a short glycine-serine linker was inserted into the genome before the start codon of stonin1. The Three exons of stonin1 are shown in red. The sequence complementary to the guide RNA is shown in yellow, the PAM-motif needed for activation of Cas9 in light blue. The Stonin1HDR template vector containing the eGFP-sequence flanked by the genomic DNA sequence of the stonin1 gene was used as a template for homology directed DNA repair. (B) Western Blot of the immunoprecipitation with a GFP specific nanobody from C2C12 cell extract of six clones: eGFP-stonin1 was detected in the immunoprecipitation with both antibodies against stonin1 and GFP. 10% Input loaded on an 8% SDS-PAGE gel. (C) Fixed cells were stained with GFP-specific antibodies showing eGFP-stonin1 expression after 2 h and 96 h in culture. Scale bars 10 µm.

3.1.2 Stonin1 only partially colocalizes with the CME machinery

Stonin1 has been speculated to be an endocytic adaptor, as the structurally similar protein stonin2 is an established adaptor for synaptotagmin 1 during clathrin-mediated endocytosis (CME). (Diril et al., 2006). In line with this notion, stonin1 interacts with the general endocytic adaptor AP2 via its WxxF motif (Feutlinske et al., 2015).
Therefore, colocalization of stonin1 with clathrin and other endocytic proteins was investigated in long-term cultured, endogenously eGFP-stonin1 expressing myoblasts. Stonin1 stainings did not completely colocalize with clathrin and other endocytic proteins. In fact, only a subset of stonin1-positive structures exhibited a punctate staining (Fig. 3.4). This subset of puncta was positive for clathrin (Fig. 3.4 A), stonin2 (Fig. 3.4 B) and the two endocytic scaffold proteins Eps15R (Fig. 3.4 C) and intersectin1 (Fig. 3.4 D). However, large stonin1 patches and fibers exhibited only a limited colocalization with the CME machinery. This colocalization appeared in the form of punctate structures that were interspersed in the larger stonin1-positive networks.

This unique localization of stonin1 in comparison to other endocytic proteins was quantified as colocalization of pixels between one channel and the other, as expressed by the Mander's coefficient (Fig. 3.4 E). Paxillin staining was used as a negative control. Indeed, over 50% of stonin1 signals did not colocalize with CME markers.

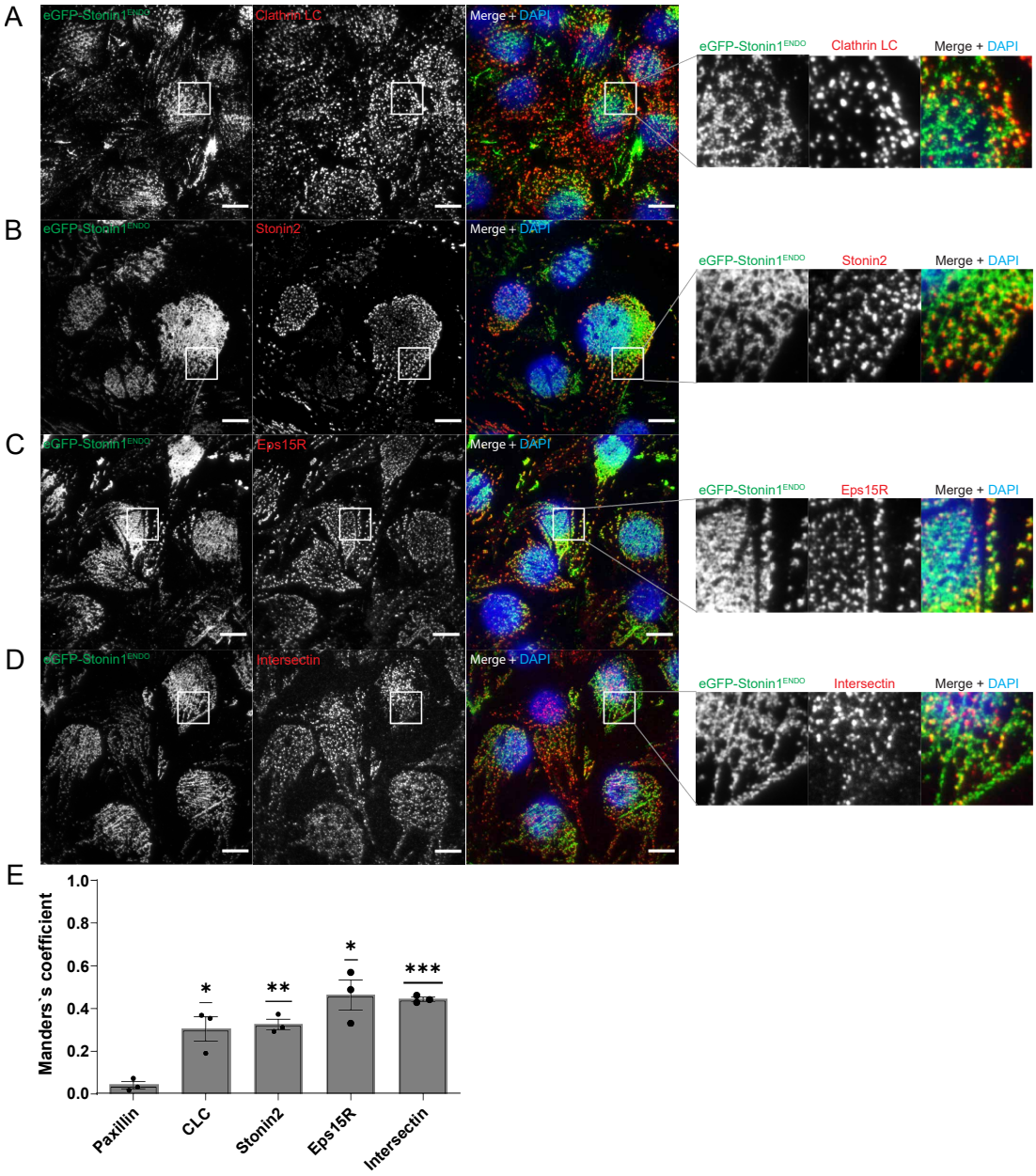

Figure 3.4: Stonin1 only partially colocalizes with the CME machinery. Confocal images of C2C12 myoblasts in long-term culture endogenously expressing eGFP-stonin1 co-stained for GFP and clathrin LC (A), stonin2 (B), Eps15R (C) and intersectin1 (D). Scale bars 10 µm. (E) Quantification of colocalization using the Mander's coefficient: Stonin1 partial correlation with CME markers (* $p<0.05$, ** $p<0.01$, *** $p<0.001$, unpaired t- test with paxillin as negative control, N=3).

3.1.3 Stonin1 resides at long-lived CCS

The formation and endocytosis of clathrin-coated pits (CCPs) during CME is a dynamical process with a short lifetime. Since stonin1 puncta colocalize with clathrin, they could be CCPs. To analyze whether stonin1 exhibits the typical dynamic behaviour of proteins residing at CCPs, we used TIRF life cell imaging of C2C12 myoblasts endogenously expressing eGFP-stonin1 and transiently expressing mRFP-clathrin light chain (mRFP-CLC). A homogeneous distribution of mRFP-CLC showed small and some larger puncta over the entire cell surface (Fig. 3.5 A). In contrast, the subset of clathrin-coated structures positive for stonin1 was larger than the clathrin puncta without stonin1 and preferentially localized at the cell periphery. The lifetime of CCPs ranges from 20 to about 180 s (Lehmann et al., 2021). This observation could be confirmed for clathrin puncta without stonin1, as evident from kymographs (Fig. 3.5 B). However, stonin1-positive clathrin structures never exhibited the typical short lifespan of CCPs but were long-lived with lifetimes of over 10 min.

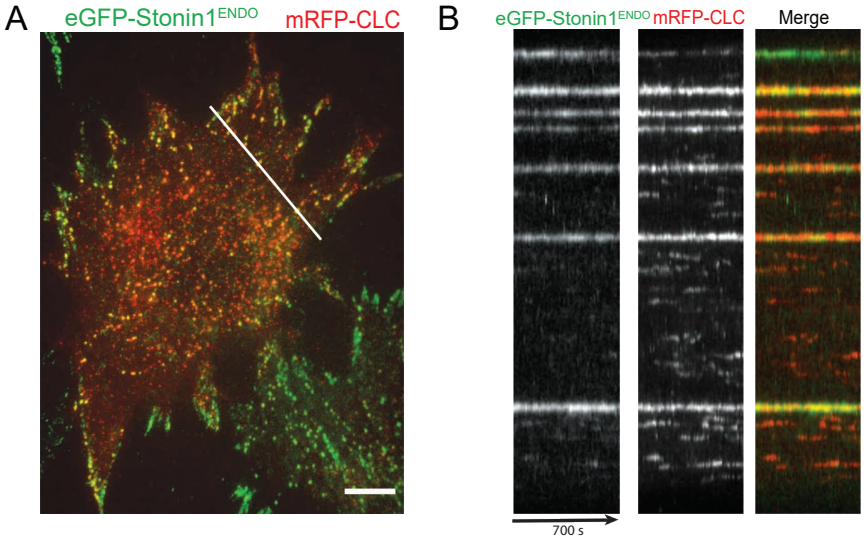

Figure 3.5: Stonin1-positive clathrin puncta exhibit longer life-times than clathrin-coated endocytic pits. (A) Snapshot of life cell TIRF time-lapse imaging of C2C12 myoblasts endogenously expressing eGFP-stonin1 (green) and transfected with mRFP-CLC (red). (B) Kymographs derived from dual-color TIRF microscopy along the line depicted in A (Movie: 700 sec with 10s intervals). Scale bars 10 µm.

This suggests that stonin1 is only found at long-lived CCS, also known as clathrin plaques. Compared to other endocytic adaptors, which are present at short-lived endocytic clathrin-coated pits as well as at long-lived clathrin plaques, stonin1 is unique in that it appears to be recruited exclusively to long-lived clathrin plaques. In addition, stonin1 localizes as already mentioned in the form of large networks that contain interspersed clathrin-positive structures, i.e. clathrin plaques. We went on to examine also these networks for a longer period of time by live cell imaging (Fig. 3.6 A). Stonin1 networks were highly stable and did not change over a six-hour period. However, clathrin localization within these networks was much more dynamic, and clathrin puncta appeared and disappeared frequently (Fig. 3.6 B). Stonin1-positive clathrin plaques were preferentially located at the leading edge of the cell. Retraction of the cell resulted in the disappearance of clathrin, leaving stonin1-positive puncta behind (Fig. 3.6 C). Stonin1 showed a characteristic tendency to form fibers that remained behind as footprints when the cell moved away (Fig. 3.6 D). These fibers are commonly called retraction fibers because they are formed by retraction of the cell body.

Respreading of the cell across stonin1-positive puncta and fibers led to a new accumulation of clathrin at the same site where it was previously located (Fig. 3.6 C). Time-dependent intensity profiles confirmed re-recruitment of clathrin to stonin1-positive patches (Fig. 3.6 E).

While stonin1 and clathrin colocalize in clathrin plaques within stonin1-positive fibers and networks, the majority of stonin1 resides in clathrin negative structures. In line with this, shRNA-mediated silencing of clathrin did not disrupt the localization of stonin1 to large networks, but removed only the stonin1 puncta by eliminating clathrin-coated pits and plaques (Fig. 3.7 A). Overall, the resulting stonin1 staining displayed a more diffuse pattern compared to the sharp stonin1 patches in the control, even though the large stonin1-positive networks were still observed. Our analysis of the stonin1 fluorescence intensity indicated a reduction by about 50% (Fig. 3.7 B).

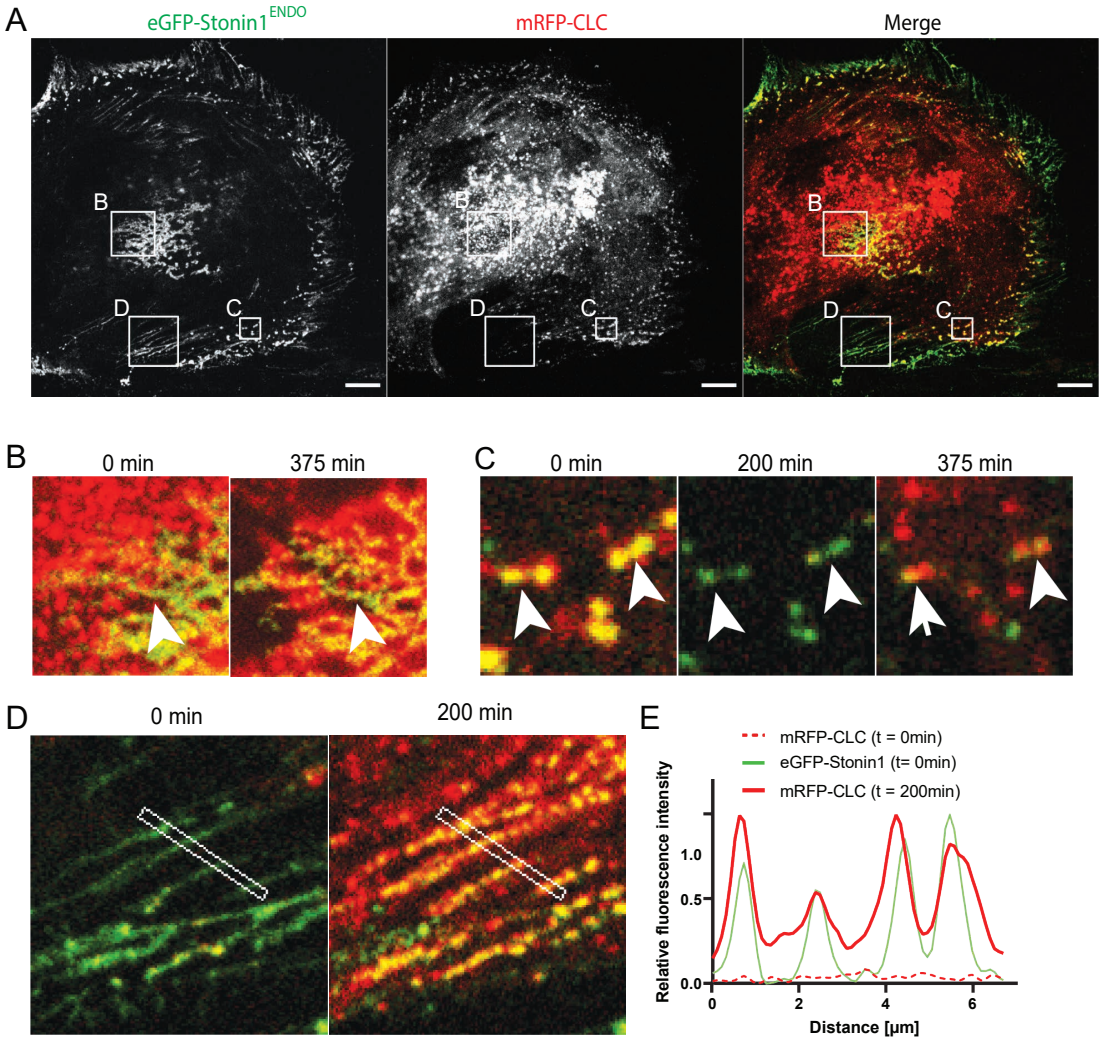

Figure 3.6: Clathrin plaques form after cell respreading on stonin1-positive puncta and fibers.
Life cell confocal time-lapse imaging of C2C12 myoblasts endogenously expressing eGFP-stonin1 (green) and transfected with mRFP-CLC (red). Tracking of stonin1 and clathrin in networks (B), puncta (C) and fibers (D) over a period of 200 to 375 minutes. (D) Time-dependent intensity profiles of stonin1 (green) and clathrin (red) along the line depicted in D. Since this is not TIRF microscopy, in addition to plasma-membrane localized clathrin also the central TGN-associated clathrin pool is visible in A.

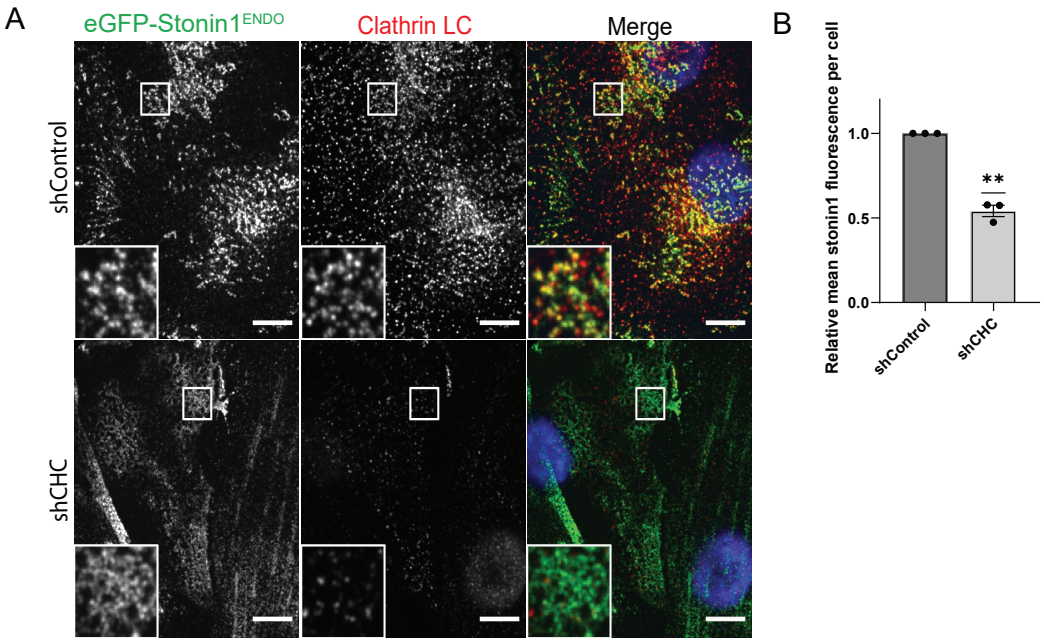

Figure 3.7: Knockdown of CHC does not abrogate stonin1-positive networks. (A) Confocal images of C2C12 myoblasts in long-term culture endogenously expressing eGFP-stonin1, transduced with lentiviral vectors expressing shControl or shCHC and co-stained for GFP and clathrin LC. B) Quantification of relative stonin1 intensity per cell area in cells depicted in (A) (one-sample t-test, N=3).

3.1.4 Stonin1 is a highly regulated phosphoprotein

Stonin1 is visible as a characteristic double band in Western blot analysis when cells are cultured under steady-state conditions (Fig. 3.8 A). It is already known that the upper band represents a highly phosphorylated version of stonin1, which is mainly found in the cytosol, whereas the non-phosphorylated lower band represents the membrane-associated pool (Feutlinske, 2014). Starvation as well as blebbistatin treatment shifts the ratio in favor of the lower band, while the growth factor PDGF-BB leads to an accumulation of the upper band (Fig. 3.8 A). This suggests that stonin1 may be involved in growth factor-triggered signaling events at the plasma membrane. Purification of stonin1 from bacterial cells for affinity purification of a mouse stonin1-specific antibody resulted in a poorly soluble product.

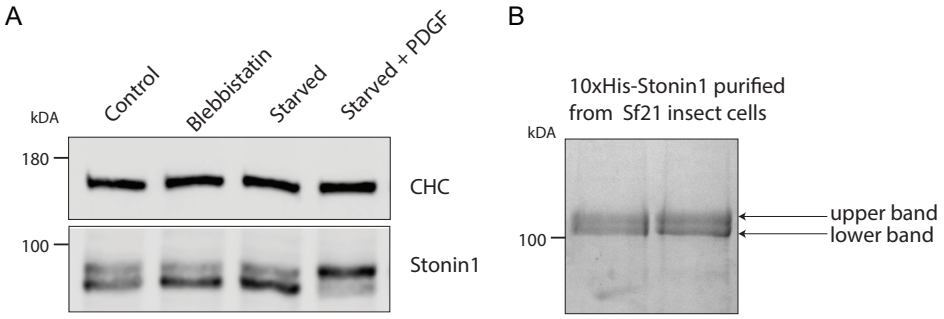

Figure 3.8: Stonin1 is a highly regulated phosphoprotein. (A) The growth factor PDGF induces a shift in the double band of stonin1. C2C12 myoblasts were kept for 1 day in full DMEM (Control) and then treated with either 50 µM blebbistatin for 60 min or serum starved overnight followed by a 15 min washout with DMEM containing 200 ng/ml PDGF-BB. Immunoblots for stonin1 and clathrin HC as loading control. 50 µg cell lysate loaded on an 6% SDS-PAGE gel. (B) 8% SDS-PAGE gel stained with coomassie brilliant blue showing 250ng of 10xHis-stonin1 purified with immobilized metal ion affinity chromatography from Sf21 insect cells overexpressing 10xHis-tagged murine stonin1 after viral transduction.

Therefore, we decided to purify 10xHis-stonin1 from baculovirus-mediated protein expression in insect cells, which resulted in high solubility and a yield of over 1 mg/ml. The insect-cell derived highly purified 10xHis-stonin1 showed the same double band as endogenous stonin1 from mammalian cells on Western blots (Fig. 3.8 B).

Even though stonin1 is not present in insect cells, the posttranslational modifications are apparently conserved in this species which only expresses the stonin2 homolog stonedB. Since we could purify high amounts of insect cell 10xHis-stonin1, we decided to analyze the post translational modification via mass spectrometry. 10xHis-stonin1 containing gel slices were digested with AspN (sequence coverage 45.3%) and trypsin (sequence coverage 90.1%) (Fig. 3.9 A). Thirty-one phosphorylations were detected, four of which were tyrosine phosphorylations. In addition to phosphorylations, several farnesylations were found that could potentially facilitate the attachment of stonin1 to the plasma membrane. A particularly highly phosphorylated region in a proline-rich motif (PRM) was identified in the intrinsically disordered N-terminal region of stonin1 (Fig. 3.9 B).

PRMs often function as docking sites with high discriminatory recognition for multiple proteins in signaling events (Ball et al., 2005). A motif search predicted an SH3 binding domain in the PRM. SH3-mediated interactions are typically found for proteins involved in endocytosis (Tonikian et al., 2009). It is therefore possible that stonin1 might be recruited or stabilized by a putative PRM—SH3 interaction, apart from having been shown to bind to AP2 via its WxxF motif (Bergmann, 2017).

Seven out of the eight discovered phosphorylation sites in the PRM were predicted to be MAPK/CDK motifs with proline in close proximity. These MAPK/CDK motifs and the SH3 binding motif are highly conserved in different species (Fig. 3.9 D). In close c-terminal proximity to the PRM, we identified a conserved PP2A docking motif. A published peptide phage display discovered that the stonin1 docking motif binds the PP2A-B'γ1 holoenzyme and B'α regulatory subunit (Wu et al., 2017). Inhibition of PP2A by Cytostatin indeed resulted in the removal of the non-phosphorylated lower band (Fig. 3.9 C).

To test which kinase phosphorylates the PRM, a screen with 245 serine/threonine kinases was performed using the biotinylated peptide biotin-DFYFSPGPPSNSPLSTPTKDFPGF. Of these 245 kinases, only five were found to phosphorylate the peptide (Fig. 3.9 E). Four of these 5 hits were the cell cycle-dependent kinases (CDKs) CDK1 and CDK2, which were associated with cyclin A and cyclin E, respectively. Cyclins determine the substrate specificity of CDKs during the cell cycle (Lee et al., 2007). It is therefore particularly noteworthy that cyclin B1-associated CDK1 showed no activity toward the peptide. Inhibition of CDKs with the kinase inhibitor Flavopiridol paradoxically led to the disappearance of the unphosphorylated lower band (Fig. 3.9 F), indicating a greater complexity in the phosphorylation of full-length stonin1 as anticipated based on the peptide-based screen.

MAP kinase (p38γ) was the third hit found in the kinase screen. It acts as a CDK-like kinase and cooperates with CDKs to regulate cell cycle entry (Tomas-Loba et al., 2019). In summary, stonin1 is a multi-phospho protein with a highly complex regulatory mechanism.

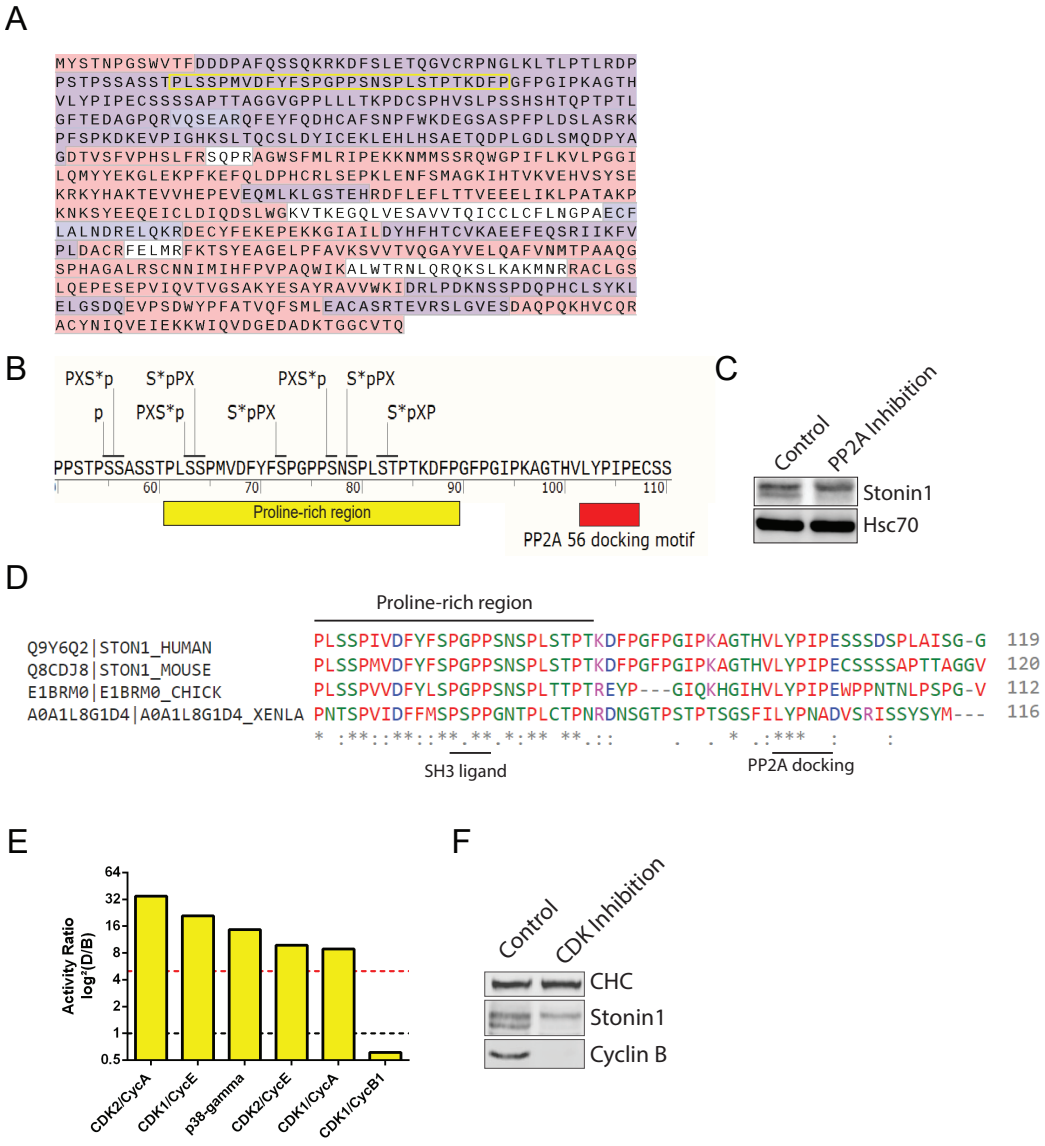

Figure 3.9: Stonin1 is a highly regulated multi-phospho protein.
(A) Peptide coverage of Trypsin (red, 90.1%) and AspN (blue, 45.3%) digests of stonin1. (B) Specific phosphorylation sites in a proline-rich region identified by phospho mass spectrometry; 7 out of 8 phosphorylations were predicted to be MAPK/CDK motifs. A PP2A docking motif is in close proximity. (C) Inhibition of PP2A by Cytostatin (10 µg/ml for 30 min) results in the disappearance of the lower stonin1 band. (D) MAP/CDK motifs in stonin1 are highly conserved in different species. Multiple sequence alignments of stonin1 from human, mouse, chicken, and frog. (E) Top five hits of 245 ser/thr kinases screened for activity with the sample peptide Biotin-DFYFSPGPPSNSPLSTPTKDFPGF. Activity ratios measured as ratios between corrected activity (raw values minus sample peptide background, in cpm) of sample peptide and without sample peptide. (F) Inhibition of CDKs by Flavopiridol (1 µM overnight) results in the disappearance of the lower stonin1 band; complete data in the addendum.

3.1.5 Stonin1 resides at adhesions that mediate attachment during mitosis

Stonin1 shows a characteristic tendency to form fibers that remain behind as footprints on the substrate when cells migrate away. In short-term cultures of one day, stonin1-positive fibers represent the major stonin1-positive structures (Fig. 3.10 A). Only a small amount of stonin1 colocalizes with clathrin in puncta in these short-term cultures. Cells spread for two hours never displayed stonin1 networks as described in Chapter 3.1.1 (Fig. 3.3 C). For a long time, cellular footprints were considered as cellular leftovers, but recently they were found to represent a spatial memory for cell migration (D'alessandro et al., 2021). Footprints are formed at the rear of migrating cells when the retraction fibers are released (Yamada et al., 2013).

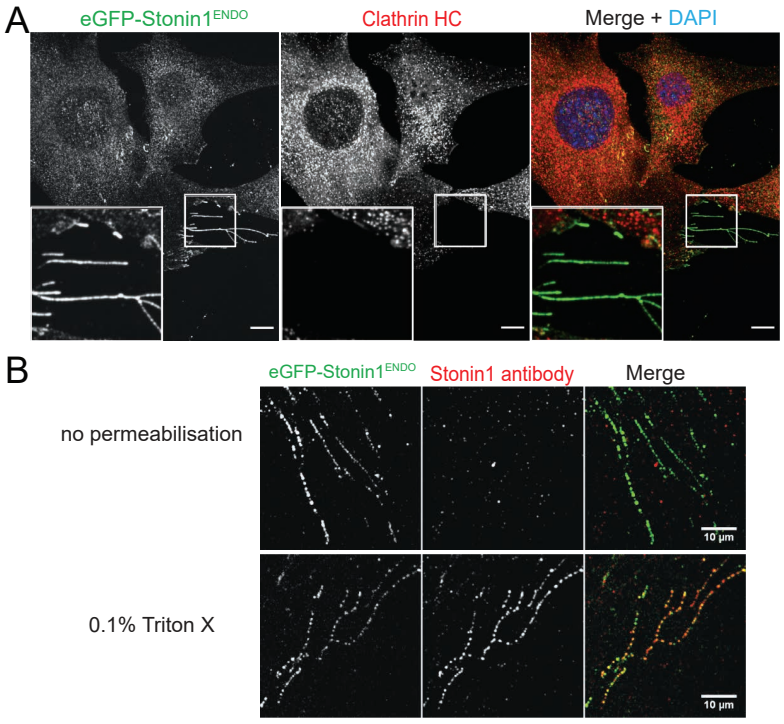

Figure 3.10: Stonin1 is present in cellular footprints. (A) Confocal images of C2C12 myoblasts endogenously expressing eGFP-stonin1 and co-stained for GFP and clathrin HC. Boxed areas are shown as 2.5x Zoom.(B) The cellular footprint was either not permeabilized or treated with 0.1% Triton for permeabilization to allow access with a stonin1 specific antibody. Scale bars 10 µm.

Because we observed re-recruitment of clathrin to stonin1-positive footprints after respreading, we wondered how cells could gain access to them after respreading. We hypothesized that footprints should be surrounded by a membrane, as stonin1 is recruited to the cytosolic inner membrane. To test this hypothesis, samples were either permeabilized with Triton X or left untreated before addition of an antibody against stonin1. Indeed, the stonin1 antibody did not detect any signal at sites where the GFP signal from the endogenously expressed eGFP-stonin1 indicated a footprint (Fig. 3.10 B). Therefore, it can be concluded that footprints containing stonin1 are enclosed by a membrane.

To investigate the formation of stonin1 containing footprints, life cell imaging experiments of endogenously expressed eGFP-stonin1 together with stably expressed mCherry-F-tractin were performed. F-tractin is a probe for filamentous actin suitable for imaging in living cells (Melak et al., 2017). We observed that stonin1 localizes to disassembling actin fibers at the rear-end of migrating cells (Fig. 3.11 A). Stonin1-positive fibers emerged from actin fibers and were left behind as footprints.
Retraction fibers play a prominent function in mitosis, where they retain the memory of interphase cell shape and tension (Hart et al., 2019). Cell adhesion is regulated by CDK1 during the cell cycle, which triggers disassembly of FAs while retraction fibers anchor the cell to the substrate (Jones et al., 2018). In cytokinesis, the cell retracts and rounds up in preparation for dividing its duplicated chromosomes into two daughter cells. Thus, cytosolic proteins are primarily found in the spherical volume of the rounded cell (Fig. 3.11 D). We expressed cytoskeletal markers like α-actinin1 and F-tractin to segment the cell area before and during cytokinesis. Indeed, in cytokinesis the fluorescence signal of both F-tractin and α-actinin1 was concentrated in a small area representing a rounded cell. However, the localization and intensity of stonin1-positive fibers did not change between interphase and mitosis (Fig. 3.11 E). After cytokinesis, the two daughter cells respreaded over the stonin1-positive areas. The retraction fibers of the cell giving rise to stonin1 footprints were indistinguishable in their appearance between migration and mitosis.

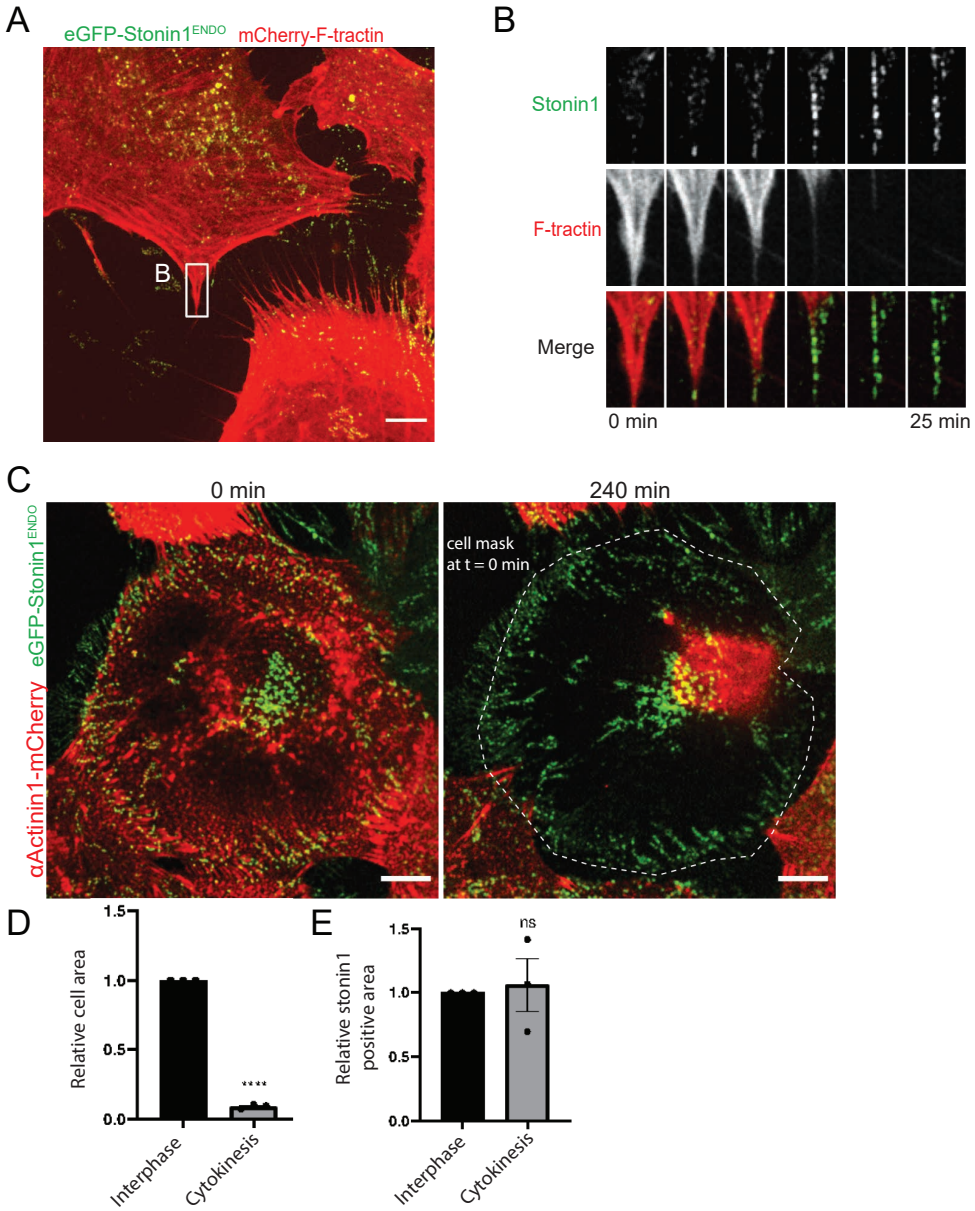

Figure 3.11: Life cell imaging of stonin1 in migrating cells and cells that undergo cytokinesis. (A) Life cell confocal time-lapse imaging of C2C12 myoblasts endogenously expressing eGFP-stonin1 (green) and transduced with mCherry-F-tractin (red). 25 min time-lapse image series with 5 min intervals showing stonin1 localization at the end of a retracting actin fiber. (C) Time-lapse image of a C2C12 myoblast endogenously expressing eGFP-stonin1 (green) and transfected with α-actinin1-mCherry (red) in interphase (0 min, left) and while undergoing cytokinesis based on cytoskeletal markers (240 min, right). (D) Quantification of the relative cell area with cytoskeletal markers before and during cytokinesis. (E) Quantification of the stonin1-positive area before and during cytokinesis. One-sample t-test, N=3 experiments. Scale bars 10 µm.

3.1.6 Stonin1 localizes to distinct αVβ5 adhesion sites

During the course of our experiments a study was published that described very similar mitotic retraction fibers as reticular adhesions (RAs). These RAs are formed by the integrin αVβ5 and mediate cell attachment during mitosis and during long-term culture, and are characterized by the absence of canonical focal adhesions (Lock et al., 2018). In terms of molecular composition, reticular adhesions are defined as adhesions that lack the known markers of focal adhesions but are enriched in markers of CME (Lock et al., 2018). Since we observed stonin1-positive structures that matched the morphology of RAs, we hypothesized that stonin1 might reside at this specific adhesion structure. Indeed, all positive stonin1 structures colocalized with the integrin αV, including the already described large stonin1 networks (Fig. 3.12 C). As shown earlier for the large stonin1-positive structures, the major factor for the appearance of these adhesions was the time in culture.

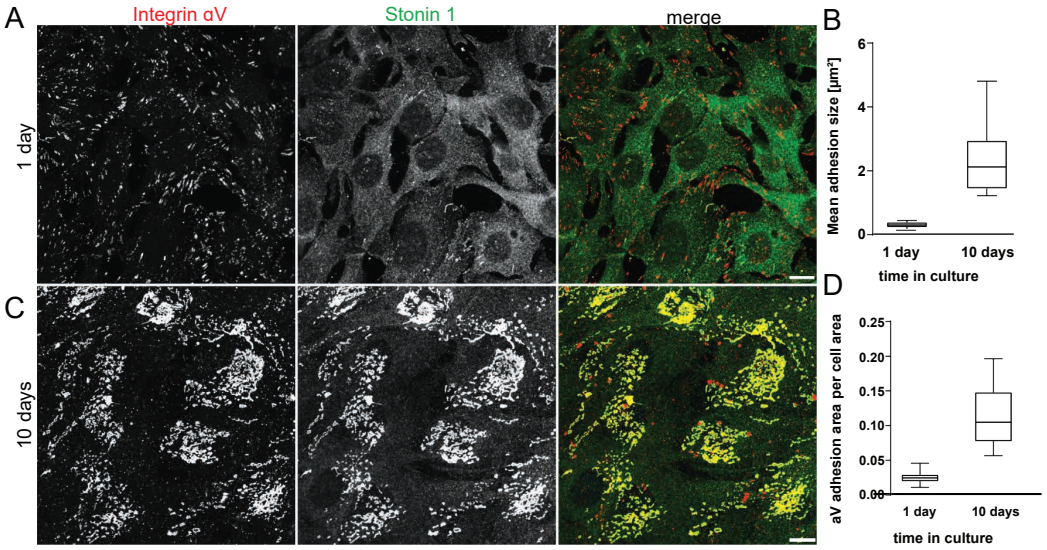

Figure 3.12: Stonin1 localizes to integrin αV positive structures in a time-dependent manner. (A, C) Confocal images of C2C12 myoblasts co-stained for stonin1 and integrin αV cultured for 1 day (A) or 10 (C) days.(B) Quantified mean αV-integrin positive adhesion size per cell. (D) Quantification of αV integrin covered area (percentage) per cell. Data are taken from 20 cells. Boxplot center and box edges indicated median and 25th or 75th percentile, respectively. Boxplot notches approximate 95% confidence interval. Scale bars 10 µm.

The longer the cells were in culture, the larger the adhesions. The corresponding integrin αV positive area per cell increased accordingly (Fig. 3.12 B and D). Stonin1 staining showed a broad cytoplasmic distribution in short-term cultures of one day. Here, cells were seeded on vitronectin, which has been shown to induce RAs and plaques (Lock et al., 2018). However, in our hands, not the coating with vitronectin, but the time in culture was crucial for the formation of stonin1-positive adhesions. In short-term cultures, we observed stonin1-negative αV adhesions, which were also visible in long-term cultures as a distinct pool of adhesions. Since FAs are considered the major adhesion structure, we hypothesized that negative stonin1 adhesions represent FAs.
To characterize the two different types of αV positive adhesions, we analyzed immunofluorescence stainings by TIRF microscopy. Endogenous stainings with the focal adhesion marker vinculin indeed revealed that the stonin1 negative integrin αV positive structures are focal adhesions (Fig. 3.13 A).
In fact, vinculin was anticorrelated with stonin1, demonstrating that stonin1 while being highly enriched at reticular adhesions is excluded from focal adhesions, even when both structures contain the same integrin receptor. (Fig. 3.13 G). The total αV integrin pool can therefore be divided into a pool encompassing focal adhesions and a stonin1-positive reticular adhesion pool. Clathrin plaques can be embedded in the much larger stonin1 patches, but also appear as separate puncta (Fig. 3.13 D). Experimental comparisons of RAs and clathrin plaques have not yet been carried out, and it is suggested that they are in fact equivalent structures (Lock et al., 2019). However, based on our results where we see stonin1 and αVß5 on the one hand together in FA marker negative structures that are positive for other endocytic components like clathrin and on the other hand in FA marker negative structures that are also negative for such endocytic proteins, the relationship between RAs and clathrin plaques is more complex. To avoid misunderstandings, we here define RAs as the umbrella term for all stonin1 and integrin αV positive adhesions that do not contain focal adhesion proteins including clathrin-positive adhesions (i.e. clathrin plaques) and clathrin-negative adhesions.

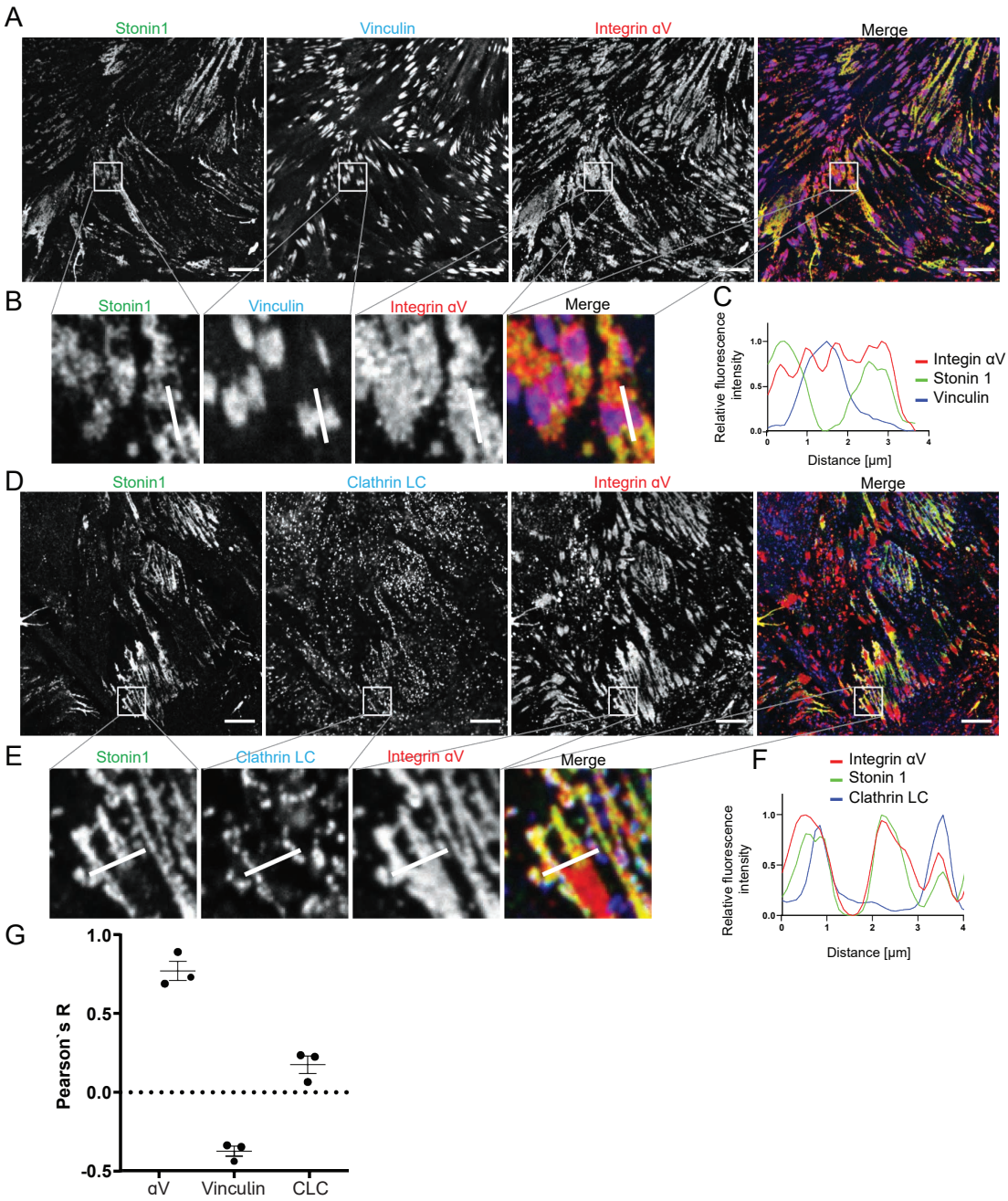

Figure 3.13: Stonin1 localizes to an αV integrin pool that is devoid of FA markers and only partially positive for Clathrin. Immunofluorescence images of endogenous stonin1, integrin αV and vinculin (A) or clathrin LC (D) in C2C12 myoblasts. (B) Zoom of the area marked by the box in A to illustrate FAs and the stonin1-positive integrin pool. (C) Intensity profiles of stonin1 (green), αV integrin (red) and vinculin (blue) along the line depicted in B. (E) Zoom of the area marked by the box in D to illustrate clathrin plaques embedded in reticular adhesions. (F) Intensity profiles of stonin1 (green), αV integrin (red) and clathrin LC (blue) along the line depicted in E. (G) Pearson's correlation analysis of stonin1 with αV integrin, vinculin and clathrin LC, N=3 experiments. Scale bars 10 µm.

3.2 Analysis of stonin1 positive adhesion structures

While RAs have been shown to have a major functional role in mitosis, the mechanisms by which they regulate migration, differentiation, and growth are still enigmatic. In particular, the underestimated link between clathrin plaques and cell adhesion is an open question.
The molecular composition of RAs with stonin1 as a unique marker highlights its peculiarity.

3.2.1 Stonin1 is recruited by the Integrin ß5

Stonin1 likely is recruited downstream of integrins rather than by the endocytic machinery, as stonin1 shows strong colocalization with RAs. To test this hypothesis, we analyzed the effect of knockdown of β5 integrin on the localization of stonin1 in RAs. The depletion of the integrin resulted in the complete loss of stonin1-positive adhesion structures (Fig. 3.14). The already described αV integrin positive puncta, networks, and fibers could not be observed anymore, while the morphological appearance of the networks seemed to be subtly altered which still needs to be investigated in more detail.

The remaining αV integrin positive structures seem to be focal adhesions. Stonin1 depletion on the other hand did not seem to change the size of αV integrin positive puncta and networks (Fig. 3.14 B).
Indeed, β5 integrin depletion has been shown to reduce RAs (Baschieri et al., 2018). Therefore, all observed positive stonin1 structures appear to be β5 integrin dependent RAs.

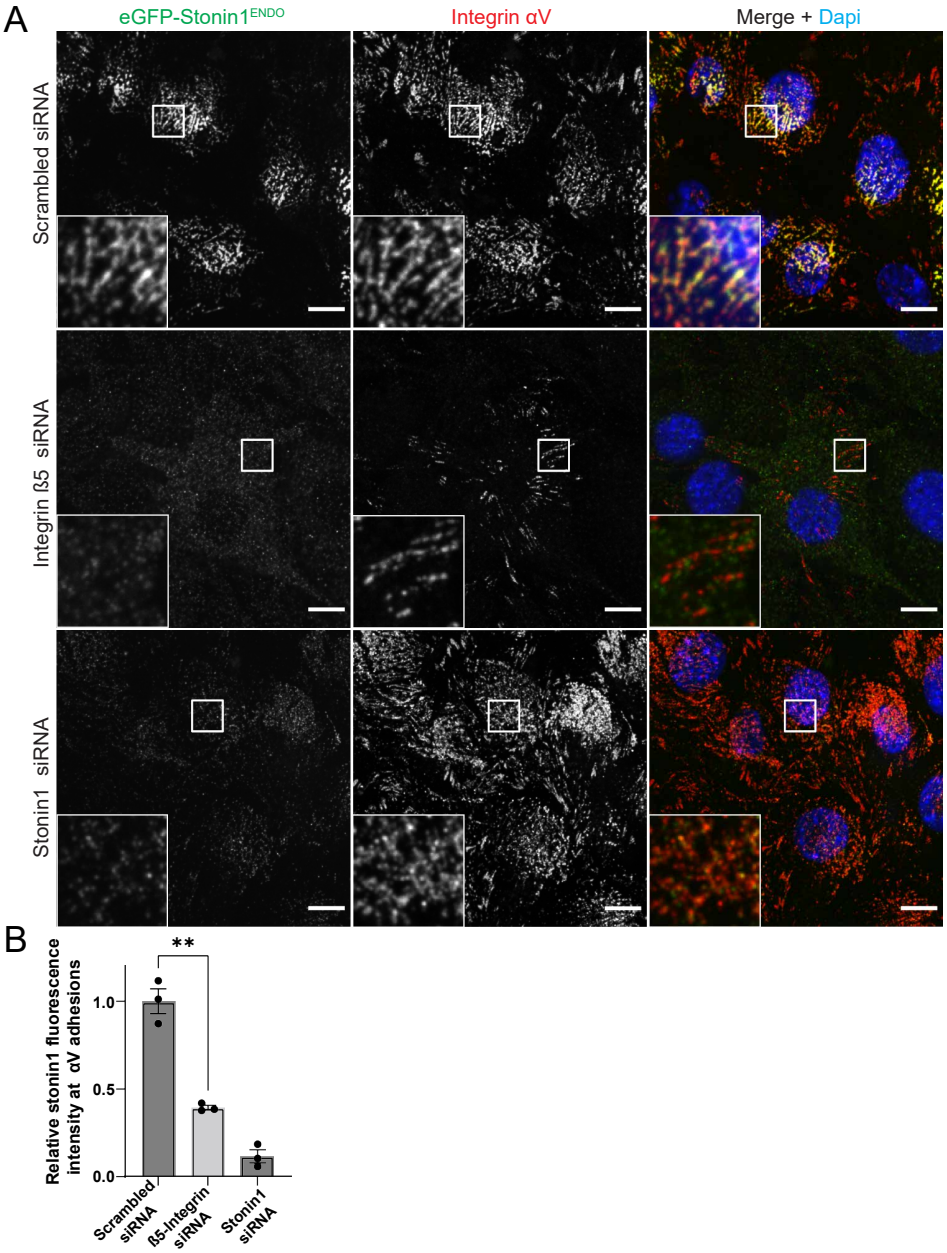

Figure 3.14: Stonin1 localization to αVß5 integrin adhesions is lost upon β5 integrin knockdown. (A) Confocal images of C2C12 myoblasts endogenously expressing eGFP-stonin1, co-stained for GFP and integrin αV and treated with scrambled, β5 integrin or stonin1 specific siRNA. B) Quantification of the relative stonin1 fluorescence intensity at integrin αV adhesions (* $p<0.05$, ** $p<0.01$, unpaired t-test, N=3 experiments). Scale bars 10 µm.

We further studied the consequences of loss of stonin1 on RAs. RAs are inherently heterogeneous and dominate in long-term cultures (Lock et al., 2019). This heterogeneity made quantification of RAs very difficult, as some cells did not have RAs at all. Therefore, we ended up developing a protocol that allowed us to observe homogeneous RAs in each cell. In this protocol, cells were synchronized by starving them for at least 16 hours. However, starvation eventually resulted in more punctate RAs (Fig. 3.15)

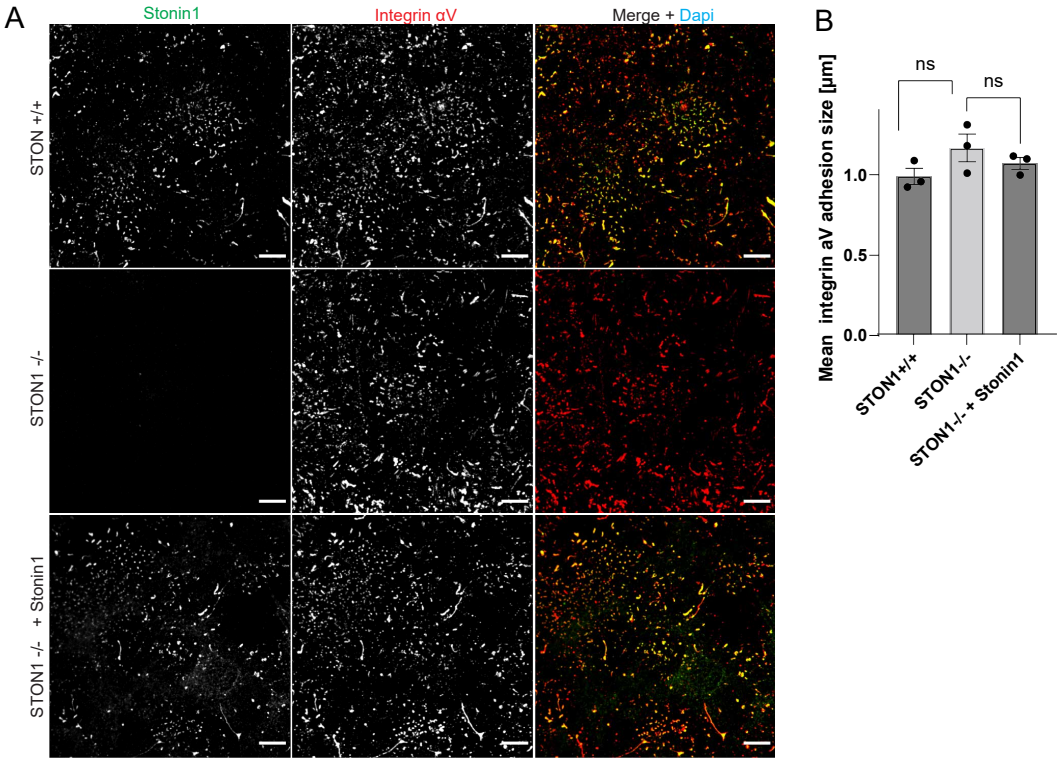

Figure 3.15: Loss and overexpression of stonin1 does not change the size of αV integrin adhesions. (A) Confocal images of stonin1 wild type, knockout, and rescue (knockout + stable stonin1 expression) mouse embryonic fibroblast co-stained for stonin1 and integrin αV. (B) Quantification of αV adhesion size of three wild-type, three knockout and three rescue MEF cell lines. Mean adhesion size was quantified for at least 5000 adhesions per cell line. (ns = not significant, unpaired t-test, N=3 cell lines). Scale bars 10 µm.

Therefore, three stonin1 wild type (wt) and three knockout (ko) embryonic fibroblast cell lines derived from mice were generated. In addition, each knockout cell line was stably transduced with stonin1 via lentiviruses. A 72-hour growth phase followed by 16 hours of starvation resulted in a very homogeneous distribution of integrin αV. We next quantified the area of at least 5000 adhesions per cell line. Neither loss nor overexpression of stonin1 resulted in a change in the size of αV integrin adhesions (Fig. 3.15).

It has been reported that the knockdown of AP2, Numb, Eps15L1 and ARH results in clathrin plaque depletion (Baschieri et al., 2018; Zuidema et al., 2018). To verify this finding and dissect whether AP2 loss would also affect the large networks, we made use of long-term cultured primary astrocytes derived from tamoxifen-inducible conditional AP-2μ knockout (KO) mice (López-Hernández et al., 2020). Indeed, a loss of stonin1 and αV integrin positive puncta was observed in the AP2 knockout. The punctate staining pattern of αV integrin typical of clathrin plaques was lost. However, particularly large adhesion networks positive for stonin1 and αV integrin persisted (Fig. 3.16 A). Thus, AP2 appears to be important for clathrin plaque formation but not for adhesion network formation.

Stonin1 and stonin2 have a very similar structure and share both a central stonin homology domain (SHD) and a C-terminal μ-homology domain (μHD). Both stonins have been reported to interact with AP2 through their WVxF motifs (Bergmann, 2017). In contrast to large stonin1 networks, immunofluorescence of stonin2 in astrocytes showed only puncta that disappeared after depletion of AP2 (Fig. 3.16 C). Large patches as seen for stonin1 (Fig. 3.16 B) were never observed in the AP2 KO astrocytes. This supports the notion that stonin1 is recruited downstream of the integrin and has a unique role compared to other endocytosis adaptors.

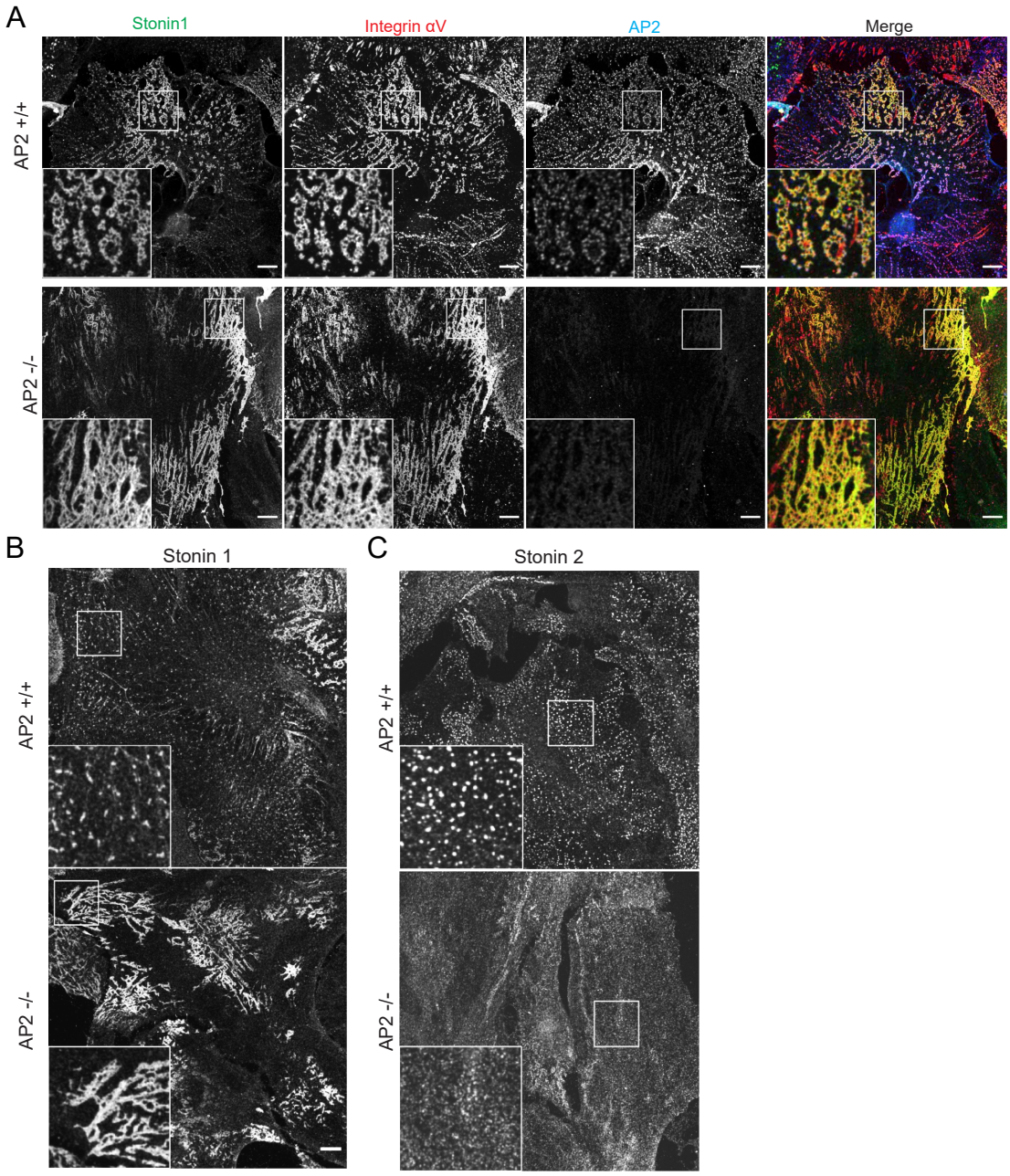

Figure 3.16: Loss of AP2 leaves RA networks intact, while eliminating punctate structures. (A) Confocal images of primary AP2 wild type and knockout astrocytes co-stained for stonin1, integrin αV and AP2. (B) Confocal images of primary AP2 wild type and knockout astrocytes stained for stonin1 to illustrate the loss of stonin1 puncta. (C) Confocal images of primary AP2 wild type and knockout astrocytes stained for stonin2 to illustrate the loss of stonin2 puncta. Scale bars 10 µm.

3.2.2 Stonin1 is an integrin nanospacer

Super-resolution microscopy revealed that integrins segregate into distinct nanoclusters in focal adhesions (Spiess et al., 2018). It was shown that integrin nanoclusters in focal and reticular adhesions are virtually identical (Lock et al., 2018). We wondered how stonin1 might be arranged in integrin adhesions at the nanostructural level compared to focal adhesions. We identified focal adhesions by the presence of αV integrin, the absence of stonin1 and a size of at least one μm^2. Furthermore, we then compared focal adhesions with αV integrin and stonin1-positive puncta, networks, and retraction fibers (Fig. 3.17 A-E). Indeed, we could not detect a difference in the mean αV integrin intensity across all adhesion types (Fig. 3.17 F). Similarly, integrin nanoclusters were found in all adhesion types. Stonin1 did not specifically co-localize with these nanoclusters. On the contrary, stonin1 was located between the nanoclusters and filled the space between them, giving the impression that it might act like a nanospacer setting the distances between the clusters, a hypothesis that awaits further investigation. This observation is particularly evident in the retraction fibers, where the nanoclusters are arranged linearly and stonin1 occupies the space between them (Fig. 3.17 E). Pearson's correlation of STED images of stonin1 with integrin αV supported the idea of an anti-correlation of stonin1 and αV integrin at the nanoscale level in contrast to their colocalization in confocal images (Fig. 3.17 G).

In a second set of STED experiments we addressed the distribution of clathrin and actin within stonin1-positive networks. As seen earlier by confocal microscopy, clathrin puncta are interspersed within stonin1 networks. The STED images confirmed that clathrin puncta within stonin1 networks do not have the typical homogeneously round appearance of clathrin-coated pits, supporting their classification as clathrin plaques. Unfortunately, the staining in the phalloidin channel could not be resolved with super resolution. However, it was evident that actin fibers run through stonin1 networks. Frequently, stonin1 staining was observed between actin fibers and clathrin clusters, suggesting that stonin1 might connect actin fibers to clathrin plaques.

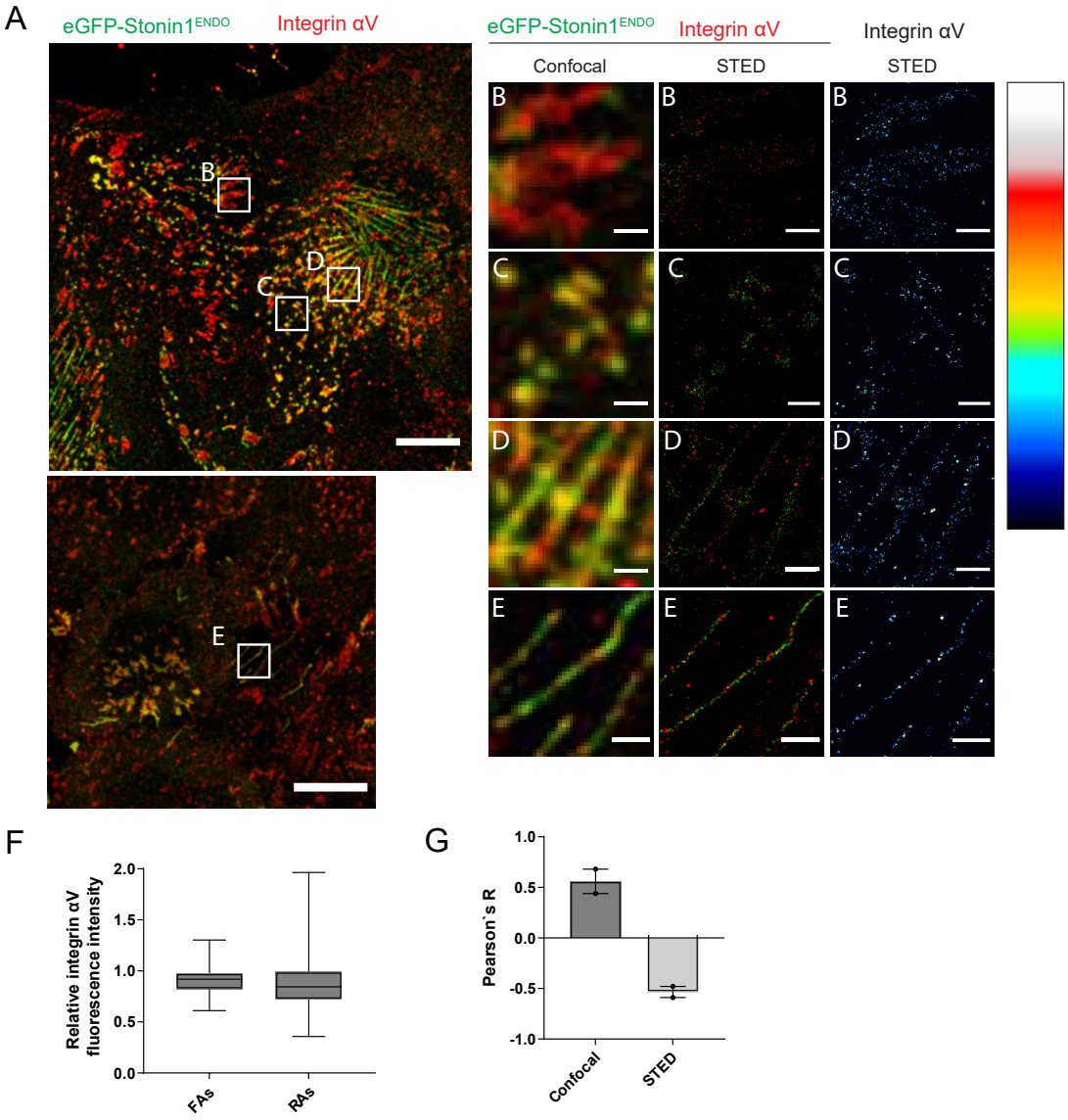

Figure 3.17: Stonin1 is an integrin nanospacer. (A) Confocal images of C2C12 myoblasts endogenously expressing eGFP-stonin1 and co-stained for GFP and αV integrin.(B) Representative images of focal adhesions (B), recognized by the presence of αV integrin and absence of stonin1. Stonin1 puncta (C) stonin1 networks (D) and retraction fibers (E) enlarged from matched confocal and STED images depicted in A. The third panel displays αV integrin signals on a color-coded intensity scale with white denoting the highest intensity. Scale bars, 10 µm (1 µm in cropped images). (F) Relative fluorescence from STED images of αV integrin in focal and reticular adhesions. 50 focal adhesions defined by absence of stonin1 and 162 reticular adhesions were assessed across two experiments. Boxplot center and box edges indicate median and 25th or 75th percentiles, respectively, while whiskers indicate the median ± 1.5 × IQR (interquartile range) or the most extreme observations within these limits. Boxplot notches approximate 95% confidence intervals. (G) Bars show mean Pearson's correlation coefficients of integrin αV with stonin1(± SD) obtained by confocal and STED microscopy (N=2 experiments).

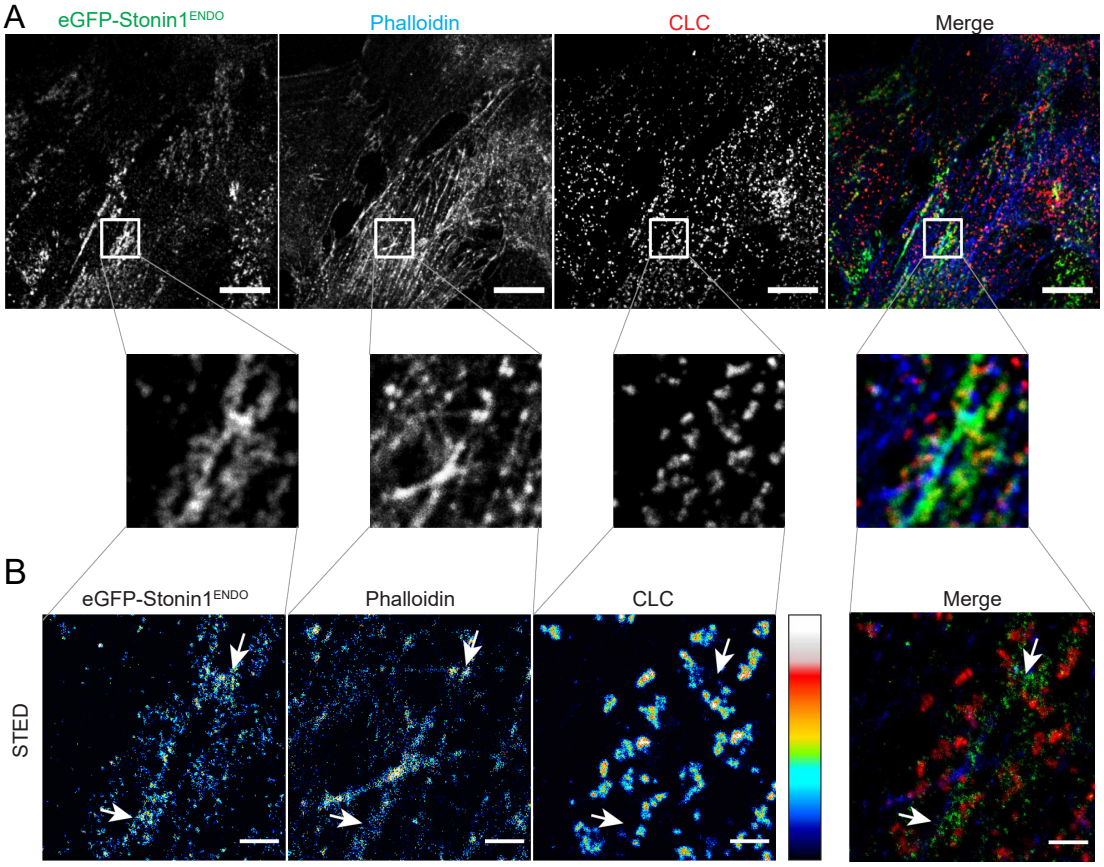

Figure 3.18: Stonin1 is spaced between actin and clathrin.
(A) Confocal images of C2C12 myoblasts endogenously expressing eGFP-stonin1 and co-stained for GFP, actin and clathrin LC. Cropped images from matched confocal image illustrate a large stonin1 patch with interspersed clathrin spots.
(B) STED image of the cropped region depicted in (A). Stonin1, phalloidin and clathrin LC fluorescence intensity signals are depicted on a color-coded intensity scale with white denoting the highest intensity. White arrows point to actin positive structures, which are positive for stonin1 and negative for clathrin LC. Scale bars, 10 µm (1 µm in cropped images).

3.2.3 Stonin1 only partially overlaps with flat clathrin lattices in αV integrin adhesions

STED microscopy revealed the nanospacing of stonin1 between integrin nanoclusters but was unable to fully resolve the ultrastructure of clathrin and actin in stonin1 adhesion networks. Since reticular adhesions so far are believed to be equivalent to clathrin plaques and thus supposed to contain an underlying flat clathrin lattice, we wanted to exactly dissect the ultrastructural relationship between clathrin lattices and stonin1-positive networks. An excellent method for visualizing the polyhedral structure of clathrin lattices is the transmission electron microscopy (TEM) of metal replicas from unroofed cells. This approach has gained additional power lately by its combination with fluorescence microscopy in the method of correlative light and electron microscopy (CLEM). TEM of membrane sheets and correlation of EM images with fluorescence images via the phalloidin staining was performed by Claudia Matthaeus. In our hands, carrying out an immunostaining protocol had a negative impact on the quality of membrane sheets. The omission of immunostaining also greatly reduced background fluorescence from secondary antibodies.

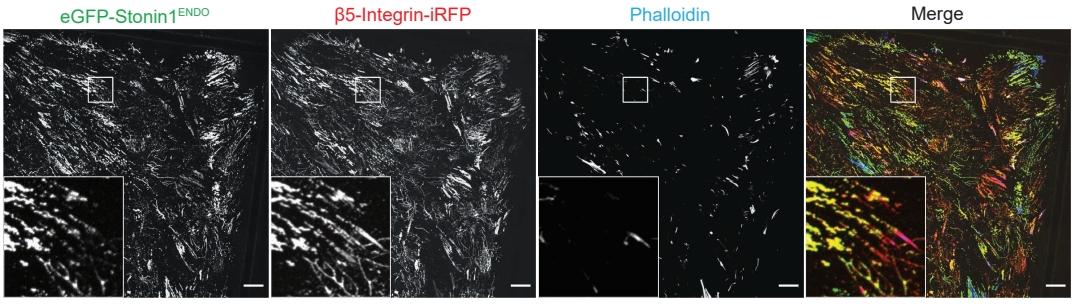

Figure 3.19: Stonin1 is tightly associated with integrin ß5 adhesions.
Confocal images of C2C12 myoblasts endogenously expressing eGFP-stonin1 and stably transduced with ß5-Integrin-iRFP were grown on collagen coated coverslips and unroofed. Actin was stained with phalloidin.
Breakdown of cells and ventral membranes by the unroofing procedure leaves ß5 integrin and stonin1-positive adhesions on the coverslip. The phalloidin staining shows the complete breakdown of cells with actin remnants at ß5 integrin adhesions (Scale bars, 20 µm).

Therefore, we used our endogenously expressing eGFP-stonin1 cell line that was stably transduced with ß5-Integrin-iRFP for correlation. Ventral membranes were identified by a faint phalloidin fluorescence intensity originating from the still attached underlying cortical actin cytoskeleton. The first attempts to produce membrane sheets in confluent cell culture resulted in the complete breakdown of cells, including the ventral membranes. This was not only evident by the absence of the faint phalloidin intensity, but also confirmed with a plasma membrane marker and TEM imaging (data not shown). Strikingly, despite the removal of ventral membranes, ß5 adhesions and eGFP-stonin1 remained on the coverslip (Fig. 3.19). All adhesion types including focal adhesions could be identified on the coverslip despite the loss of ventral membranes. Since stonin1 fluorescence was equally present in RAs and networks despite the loss of the cell membrane, this demonstrates a tight association of stonin1 with these adhesion structures. After reducing the cell density and adjusting the unroofing procedure, we were finally able to generate membrane sheets of stonin1 networks.

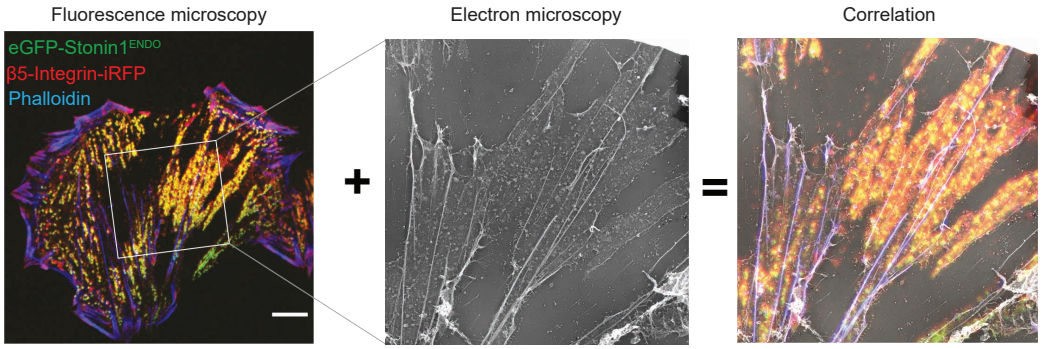

Figure 3.20: CLEM procedure.
Confocal images of C2C12 myoblasts endogenously expressing eGFP-stonin1 and stably transduced with ß5-Integrin-iRFP. Adhesion network with still attached plasma membrane sheet; Scale bars: 10 µm. After fluorescence microscopy (FM) of expressed eGFP-stonin1 and ß5 integrin-iRFP as well as labeled phalloidin the samples were dried, and a metal replica was made, which was lifted from the sample onto a grid for imaging in TEM. The white inset box in the FM image represents the area observed by TEM (4kx EM magnification). The FM and TEM pictures were then correlated to combine their information.

The investigation of CCSs on the plasma membrane sheets of adhesion networks revealed that clathrin was arranged there almost exclusively as a flat lattice. We classified CCS as either flat, dome-shaped or deeply invaginated structures (Bucher et al., 2018a). When quantifying the types of clathrin structures within the ß5 integrin positive area on membrane sheets, we found only 0.67 % of all clathrin structures to be deeply invaginated structures (Fig. 3.21 G). We also observed only a few dome-shaped structures (2.9 %), which were often also embedded in large flat clathrin lattices. Stonin1 fluorescence peaks were occasionally found in close proximity to clathrin and were sometimes partially or completely overlapping clathrin. However, more than 82 % of stonin1-positive fluorescence spots were not found to overlap with clathrin in TEM images at all (Fig. 3.21 A and H). Consequently, our data suggest that stonin1/αVß5 adhesion networks are clearly distinct from clathrin plaques, which however can be found embedded within the networks

Although stonin1 fluorescence was broadly distributed over ß5 integrin adhesions sometimes partially or completely overlapping flat clathrin lattices, fluorescence peaks could also be observed on actin fibers (Fig. 3.21 E). In fact, stonin1-positive spot showed an association to actin fibers connecting them to flat clathrin lattices (Fig. 3.21 F). It has to be noted that unroofing procedure removes the cell body and therefore the actin cytoskeleton as well. However, actin fibers were stably integrated into the membrane sheets of ß5 integrin and stonin1-positive adhesions. This suggests that the stonin1 networks represent an adhesion that stably connects the cytoskeleton to the substrate.

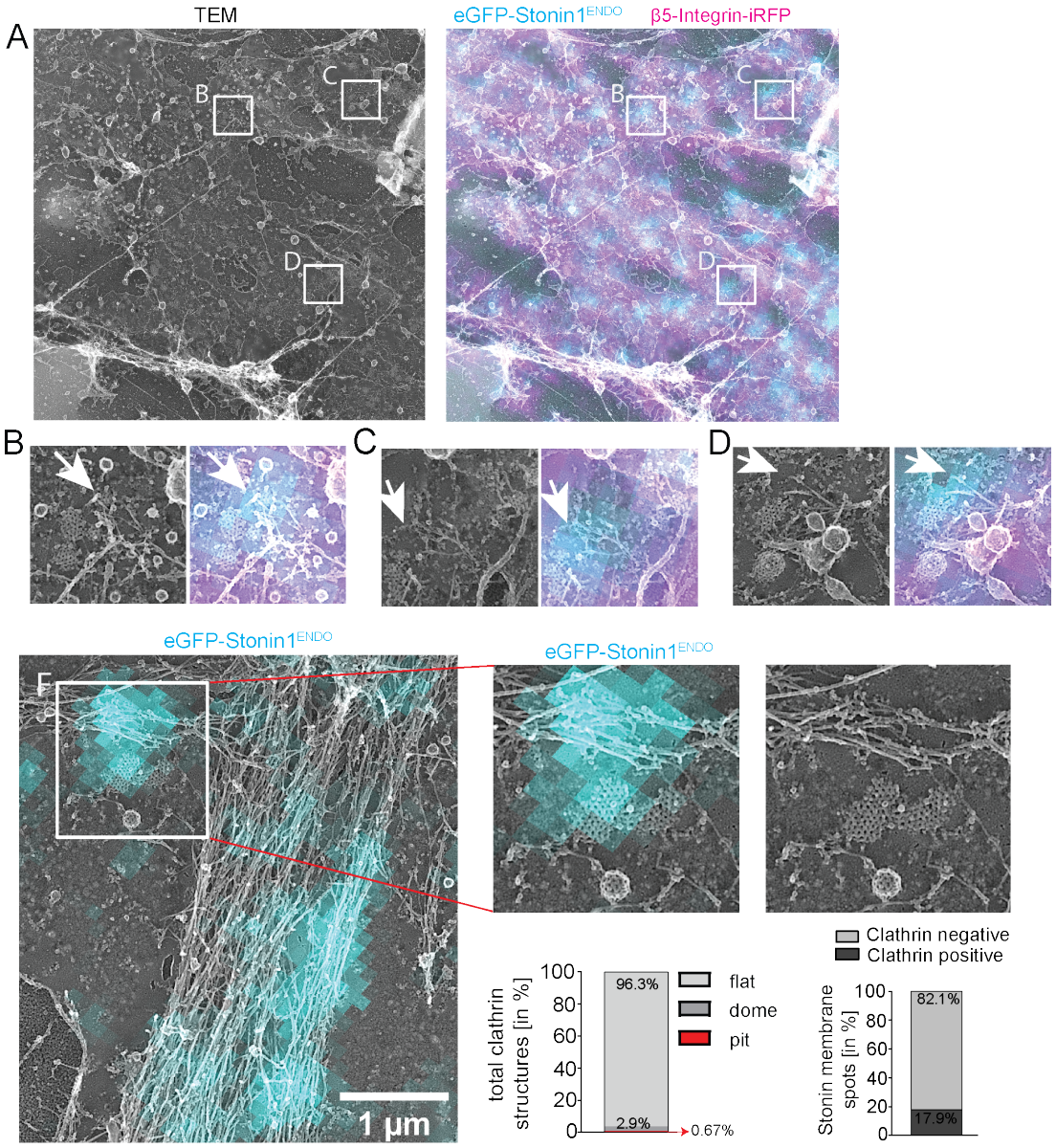

Figure 3.21: Stonin1/αVß5 positive reticular adhesions only partially overlaps with flat clathrin lattices.
CLEM of C2C12 myoblasts endogenously expressing eGFP-stonin1 and stably transduced with ß5-Integrin-iRFP. (A) Overview image (10kx EM magnification). Magnification of the areas marked by the boxes in A show examples of discrete stonin1 puncta in the adhesion network which only partially overlap with flat clathrin lattices (B-D illustrated with white arrowheads)
(E) Example of stonin1 overlapping clathrin and actin fibers. (F) Zoom in on the areas marked by the box in E shows stonin1 connecting flat clathrin lattices with actin fibers. (G) Percentage of flat, dome-shaped and deeply invaginated CCS within ß5 integrin adhesions. (H) Percentage of stonin1-positive spots that are positive for clathrin. Results are calculated from four different membranes.

3.2.4 Stonin1 networks are associated with the actin cytoskeleton

Compositional analyses show that RAs in contrast to FAs lack almost all integrin-F-actin linkage modules and therefore were supposed to have no connection to the actin cytoskeleton (Lock et al., 2019). Therefore, we wondered how stonin1 networks might be linked to the actin cytoskeleton, since stonin1 is largely present at networks but also co-localized with clathrin plaques. Using TIRF microscopy we could show stonin1-positive stress fibers at the plasma membrane (Fig. 3.22 A and B). Clathrin plaques appeared in close proximity to stress fibers, which were distributed across stonin1-positive adhesions but showed no strong overlap with stress fibers. In contrast, punctate actin structures were found to colocalize with clathrin plaques (Fig. 3.22 C).

Using CLEM we could confirm the association of actin fibers with RAs (Fig. 3.22 D). Large actin fibers were embedded in the adhesion and branched into smaller filaments. Stonin1 seems to play a crucial role as a marker for these adhesion networks, since clathrin lattices were not necessarily observed. Therefore, the role of clathrin as a marker of RAs should be reconsidered.

Currently, only FAs are known to link stress fibers with the substrate. Since stonin1 can be localized to both clathrin plaques and actin structures, we wondered how loss or overexpression of stonin1 would affect the actin cytoskeleton at clathrin plaques. Therefore, we used our stonin1 wt, ko and rescue fibroblast cell lines and evaluated the actin distribution. Using TIRF microscopy, we found that knockout of stonin1 resulted in the disappearance of actin puncta at the membrane. Stable lentiviral transduction of stonin1 into the knockout cell line reintroduced these actin puncta and rescued the phenotype (Fig. 3.23).

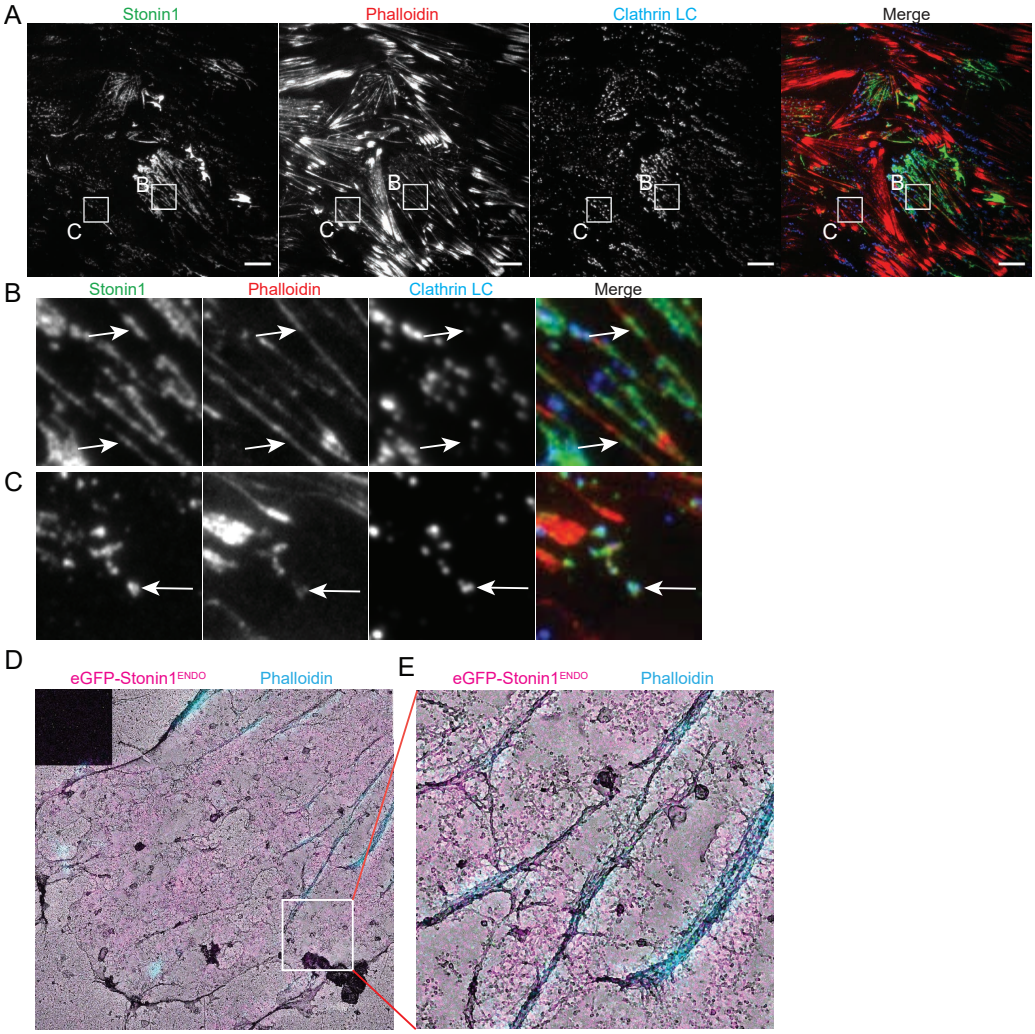

Figure 3.22: Stonin1 is associated with actin fibers and puncta. (A) TIRF images of C2C12 myoblasts co-stained for stonin1, clathrin LC and labeled with phalloidin. (B) Magnifications of stress fibers marked by phalloidin. White arrows point to actin fibers positive for stonin1 and negative for clathrin. (C) Magnification of actin puncta labeled by phalloidin. The white arrow points to an actin spot colocalizing with stonin1 and clathrin. Scale bars: 10 µm. (D) CLEM of C2C12 myoblasts endogenously expressing eGFP-stonin1 (20kx EM magnification). Adhesion network with attached plasma membrane sheet stained for GFP and labeled with phalloidin for STED fluorescence microscopy. (E) Magnification of the area marked by the box in D shows actin fibers embedded in an adhesion network (EM pixel size: 1.5 nm, STED pixel size: 19nm).

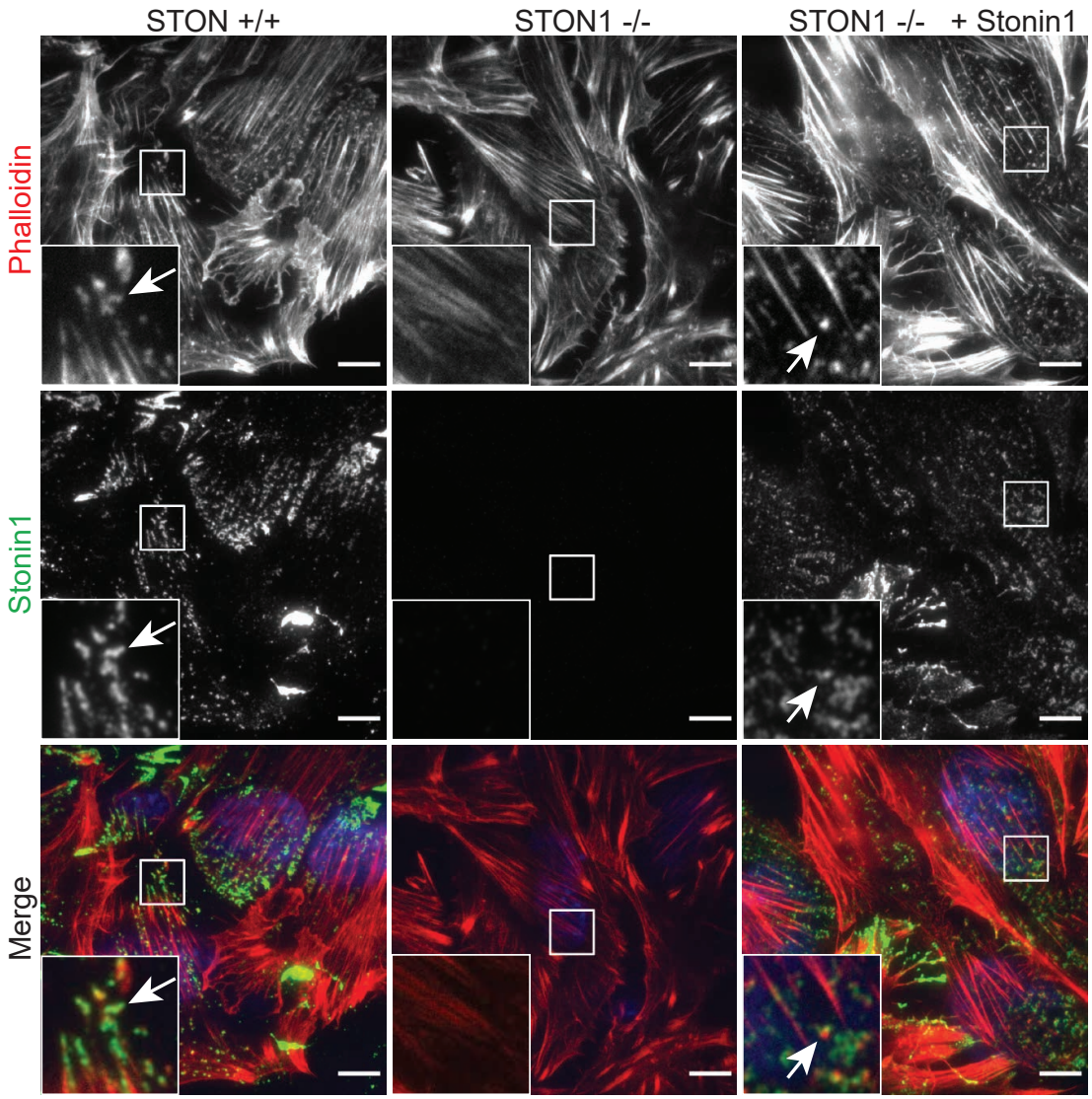

Figure 3.23: Actin puncta at the plasma membrane are stonin1 dependent. Representative TIRF images of stonin1 wild type, knockout and rescue (knockout + stable stonin1 expression) mouse embryonic fibroblasts stained for stonin1 and labeled with phalloidin. White arrows point to stonin1 dependent actin puncta. Scale bars: 10 µm.

3.2.5 Actin recruitment to clathrin plaques is stonin1 dependent

The disappearance of plasma membrane-bound actin puncta was the most striking cytoskeleton-associated phenotype resulting from the loss of stonin1, and actin stress fibers showed no obvious difference. However, stonin1 adhesions are of heterogeneous nature and show no uniform actin localization at steady state. Therefore, we used the same protocol as described in chapter 3.21 to achieve a more uniform and homogeneous distribution of actin and stonin1 puncta. Actin puncta were either partially or completely overlapping clathrin (Fig. 3.24 A). We detected an increased phalloidin intensity selectively at clathrin plaques compared to the average phalloidin intensity in the cell. This actin increase was lost in stonin1 knockout cell lines, and re-expression of stonin1 rescued actin levels at plaques (Fig. 3.24 D).

We wondered how actin is polymerized at clathrin plaques. Two possible candidates for the nucleation of actin polymerization are Arp2/3 and formins. While we could not observe formins with the antibodies we tested, we found that the Arp2/3 complex and also the actin regulatory protein cortactin were highly enriched at these plaques (Fig. 3.25). In addition, the actin bundling protein α-actinin was also highly enriched. The roundish actin structures we observed within the cell and also under the nucleus were morphologically very reminiscent of actin stainings of invadopodia or podosomes. Indeed, we found that dynamin 2, a marker for invadopodia, was colocalized with the plaques. Finally, we observed the degradation of gelatin from coated coverslips at these actin-rich sites. Podosomes and invadopodia are defined as actin-based dynamic protrusions of the plasma membrane, which are sites of adhesion and degradation of the extracellular matrix (Murphy and Courtneidge, 2011). However, an association with clathrin plaques has not yet been observed.

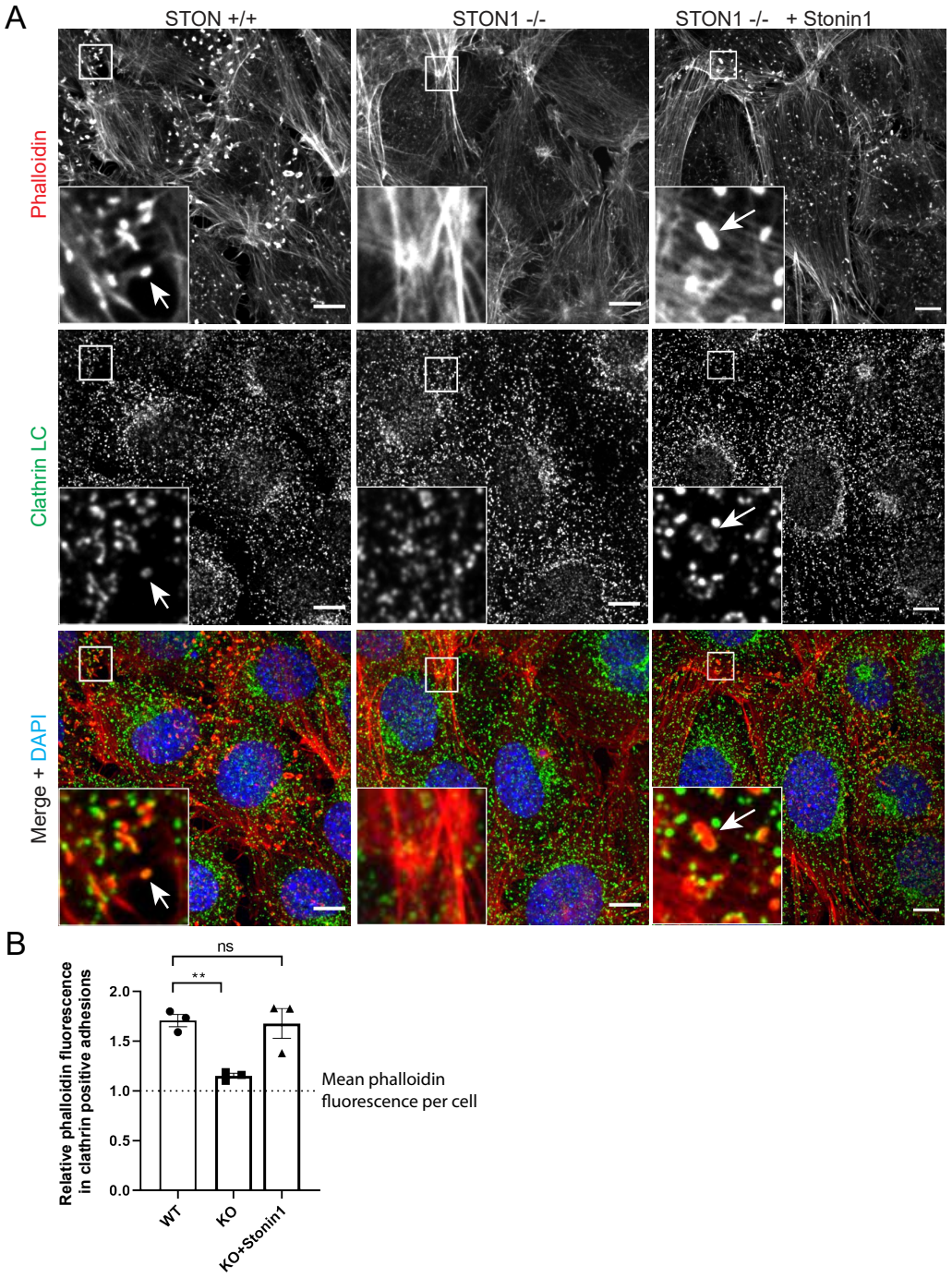

Figure 3.24: Stonin1 recruits actin to clathrin plaques. (A) Confocal images of stonin1 wild type, knockout and rescue (knockout + stable stonin1 expression) mouse embryonic fibroblasts stained for clathrin LC and labeled with phalloidin. White arrows point to clathrin plaques. Scale bars: 10 µm. (B) Quantification of the mean phalloidin fluorescence intensity at clathrin plaques of three wild type, three knockout and three rescue MEF cell lines. Mean phalloidin fluorescence was quantified for at least 5000 clathrin plaques per cell line (ns = not significant, unpaired t-test, N=3 cell lines). Phalloidin fluorescence was normalized to the average mean phalloidin intensity per cell. Scale bars 10 µm.

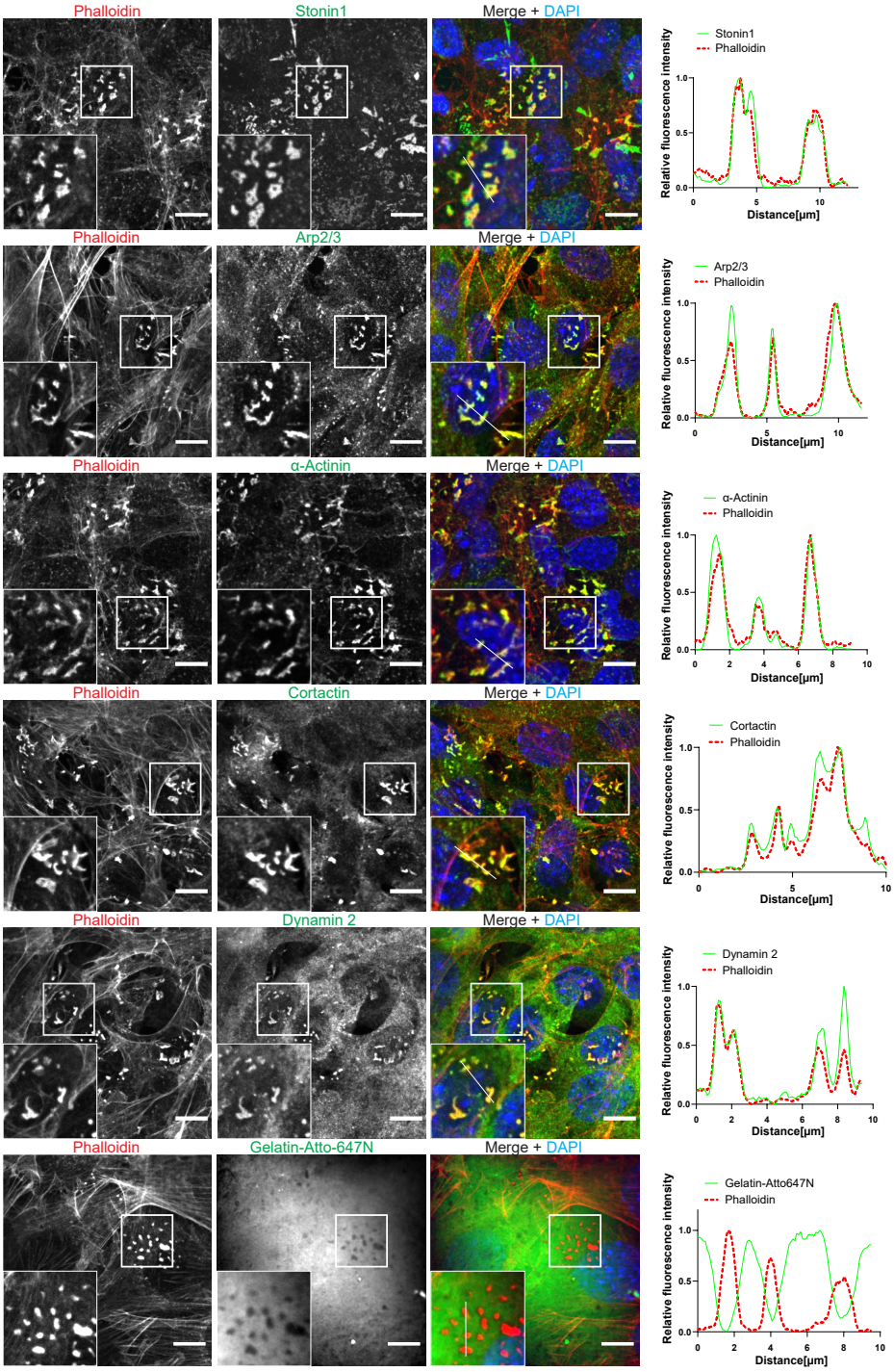

Figure 3.25: Stonin1 dependent actin puncta contain markers of invadopodia. (A) Confocal images of mouse embryonic fibroblasts stained for stonin1 (A), arp2/3 (B), α-actinin1 (C), cortactin (D), dynamin (E) and labeled with phalloidin. (F) Mouse embryonic fibroblasts seeded on gelatin-Atto657N and labeled with phalloidin. Intensity profiles of stonin1 (G), arp2/3 (H), α-actinin1 (I), cortactin (J), dynamin (K), gelatin-Atto657N (L) labeled with phalloidin along the line depicted in the corresponding zooms. Scale bars 10 µm.

3.2.6 Stonin1 positive adhesions depend highly on environmental conditions

Clathrin plaques have been reported to assemble as a consequence of increasing substrate stiffness in a process termed frustrated endocytosis, whereby αvβ5-integrin prevents CCS budding by anchoring the structure to the substrate (Baschieri et al., 2018). It is assumed that frustrated endocytosis occurs on glass (Baschieri et al., 2018) or collagen fibers (Elkhatib et al., 2017).

Long-term cultivation of cells on an initially ECM-covered glass surface might therefore lead to substrate degradation until the cells come into close contact with the glass. Indeed, FAs have been reported to digest the ECM, generating extracellular topographical cues that determine the future location of clathrin plaques (Bucher et al., 2018b).

Assuming that local ECM degradation of gelatin results in clathrin plaques, induced scratches in a gelatin layer would also be expected to trigger such adhesions. Both, the scratch and the local ECM degradation, would lead to the exposure of the glass surface of the coverslip, which might promote formation of clathrin plaques. Indeed, stonin1-positive adhesions were only appearing in an induced scratch, not on gelatin itself when culturing cells overnight (Fig. 3.26 A).

Since stonin1 localization is integrin dependent, we wondered how the scratch would affect αV integrin adhesions. Interestingly, no αV integrin adhesions could be observed on gelatin at all. However, αV integrin adhesions in the form of puncta, fibers, and networks were observed in the scratches (Fig. 3.26 B). As already quantified in (Fig. 3.15 A), the size of integrin αV adhesions in the scratch did not appear to be altered in stonin1 knockout fibroblasts. However, stonin1-dependent actin puncta at the plasma membrane were also not observed in the stonin1 knockout, as described in Fig. 3.25.

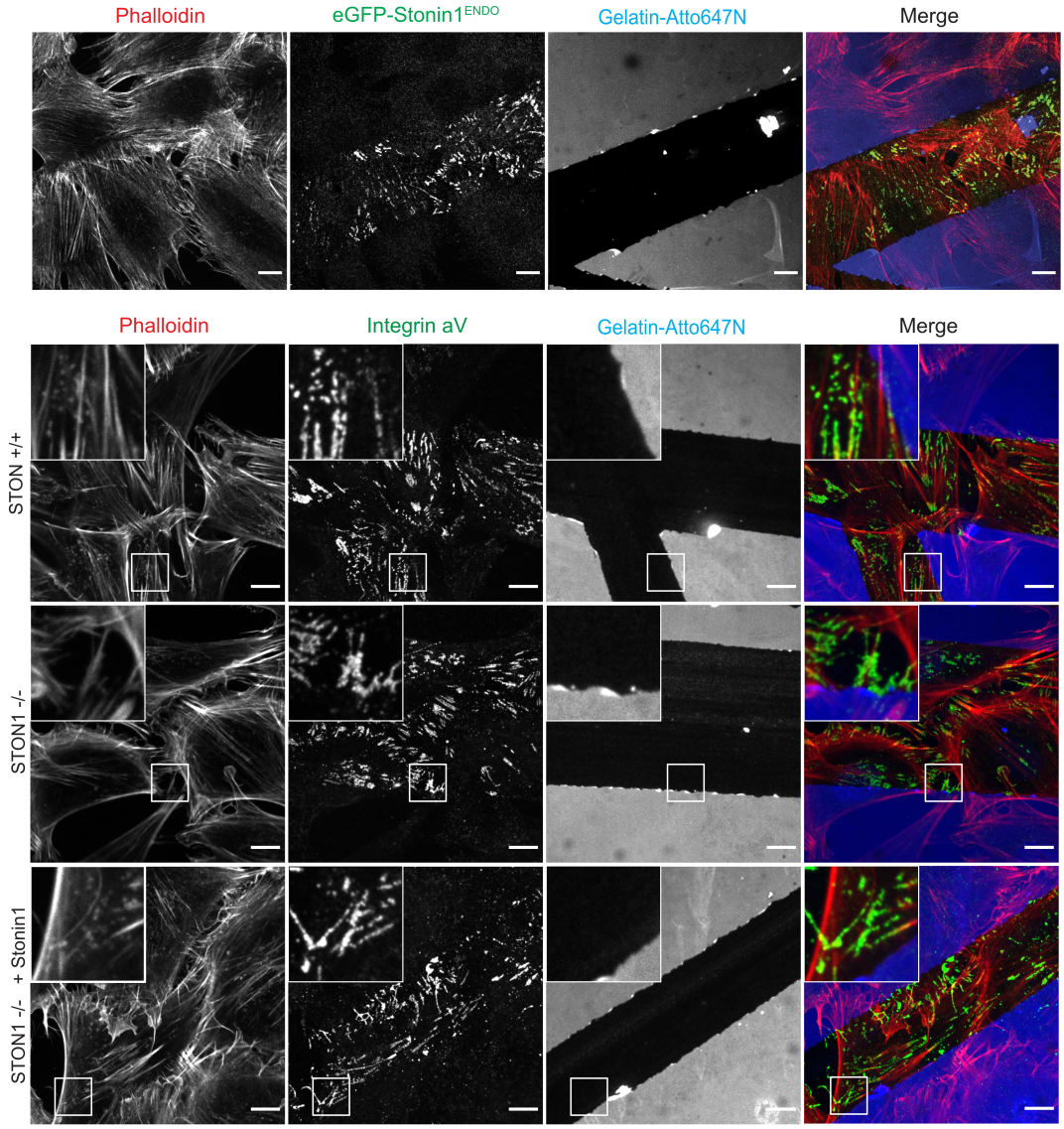

Figure 3.26: Stonin1 adhesions appear on scratches inflicted on the substrate. Coverslips were coated with gelatin-Atto-647N. Then a scratch was inflicted with a small pipette tip, and cells were seeded overnight to reach confluence.
(A) Confocal images of wt C2C12 myoblasts endogenously expressing eGFP-stonin1 and co-stained for GFP and actin (scale bar 10 µm).
(B) Large tiled image of embryonic fibroblasts co-stained for αV integrin and actin (scale bar 20 µm).

Flat clathrin lattices were also observed in a more physiological context than on the stiff glass surface. In fact, flat clathrin lattices also wrap around collagen fibers in a structure termed tubular clathrin/AP2 lattices (Elkhatib et al., 2017). To simulate a more physiological substrate, we therefore chose a high-density fibrillar collagen (HDFC) matrix that mimics desmoplastic tumor stroma.

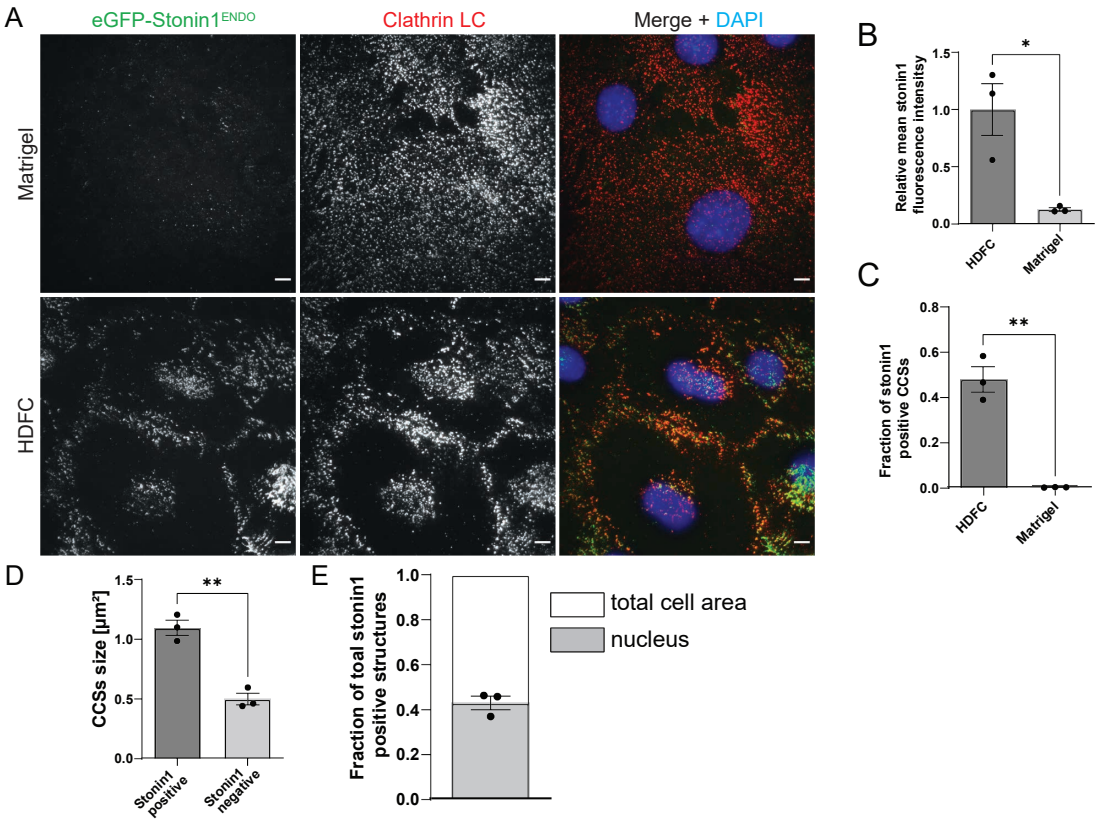

Figure 3.27: Stonin1 adhesions form on collagen.
(A) TIRF images of C2C12 myoblasts endogenously expressing eGFP-stonin1, and co-stained for GFP and clathrin LC and seeded on matrigel or high density fibrillar collagen (HDFC). Quantification of the relative mean stonin1 fluorescence of the total cell area (B) and the fraction of CCSs that was positive for stonin1 (C). (D) Quantification of the size of stonin1-positive or negative CCSs from cells seeded on HDFC. (E) Fraction of the relative mean stonin1 fluorescence under the nucleus compared to the total cell area from cells seeded on HDFC. (*p < 0.05, *p < 0.001 N=3 experiments). Scale bars 10 µm. Dapi staining was imaged via brightfield microscopy.

We compared cells grown overnight on the high-density fibrillar collagen matrix (HDFC) (Artym, 2016) with cells grown on a thin layer of matrigel to analyze if the collagen coating has a selective effect in inducing reticular adhesions that is not exerted by other matrices. As expected, cells grown on matrigel showed no stonin1-positive structures at all, while clathrin was homogeneously distributed over the cells in small puncta likely reflecting CCPs. However, cells grown on HDFC displayed stonin1 adhesion networks that were otherwise only observed after long-term culture (Fig. 3.27 C). Here, clathrin was very differently distributed with puncta localizing either to the cell periphery or the center while the intermittent space remained free. Half of all clathrin positive structures were also positive for stonin1 (Fig. 3.27 D). These clathrin-coated structures were also more than twice the size of clathrin structures that did not contain stonin1, effectively identifying them as plaques. Interestingly, almost 40% of stonin1 fluorescence was detected under the nucleus.

3.2.7 FAs assemble under the nucleus

RAs in contrast to FAs are thought to lack the association with actin. Disruption of the actin cytoskeleton by Cytochalasin D leads to the disassembly of FAs, but not RAs (Lock et al., 2018). In addition, clathrin plaques are formed after treatment with a Rock inhibitor or the myosin II inhibitor blebbistatin, which also trigger the degradation of FAs (Bucher et al., 2018b).

We therefore tested the actin inhibitors cytochalasin D and blebbistatin with respect to large stonin1 networks. We found that stonin1 networks did not disassemble upon treatment with either inhibitor, whereas FAs disassembled completely (Fig. 3.28). Indeed, using TIRF microscopy, we showed that these adhesion networks remained localized under the cell nucleus.

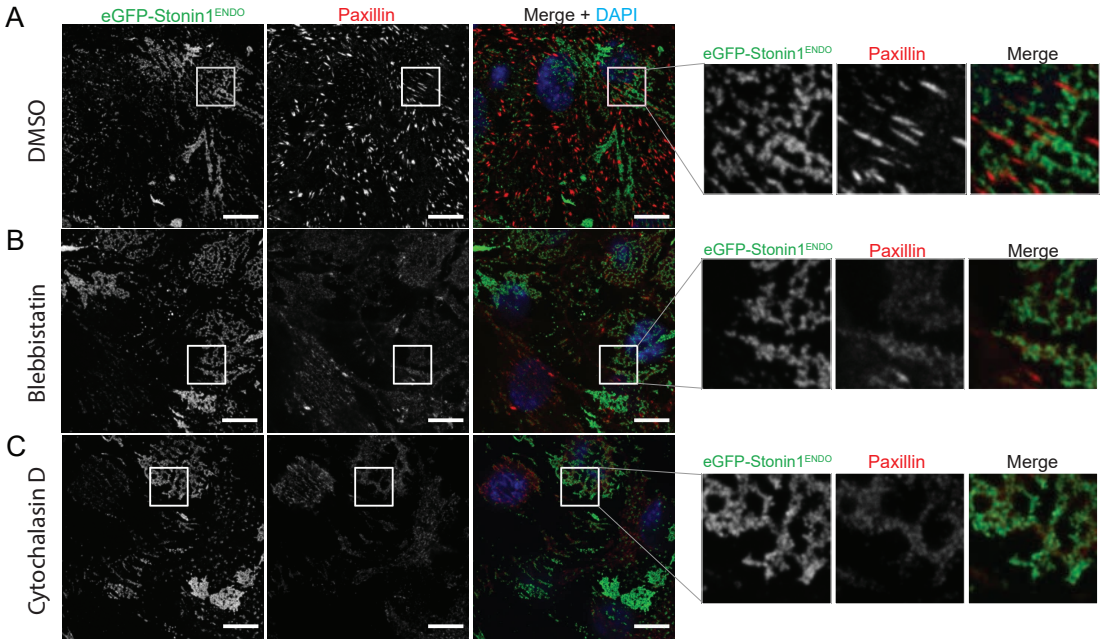

Figure 3.28: Stonin1 networks persist following disruption of the actin cytoskeleton. TIRF images of C2C12 myoblasts endogenously expressing eGFP-stonin1, co-stained for GFP and paxillin, seeded on high density fibrillar collagen (HDFC) and treated with DMSO (A), cytochalasin D (B) or blebbistatin (C) for 1 h. Magnifications of the area marked by the boxes show representive stonin1 adhesion networks. Scale bars 10 µm.

We wondered how protrusion-mediated FA assembly proceeds in confluent cells, where migration of single cells seems to be difficult due to lack of space. Since we observed that FAs in confluent cells are closely associated with the stonin1 adhesion networks below the nucleus, we asked ourselves whether FAs can also be formed there independently. Therefore, we used blebbistatin to disassemble all focal adhesions and then performed a washout with serum-containing medium to synchronize FA assembly. Since stonin1 adhesion networks do not form on Matrigel, we used this condition as a negative control. Indeed, on Matrigel new FAs formed after washout only at the cell edge and not in the cell center. However, cells seeded on HDFC that exhibited adhesion networks displayed small focal adhesions in close proximity to these adhesion networks.

We assume that FAs are formed directly by the adhesion network and not by a lamellipodial protrusion-based mechanism. Therfore, we hypothesize that FAs on collagen are formed simultaneously by the canonical lamellipodial protrusion-based mechanism at the cell edge and by an alternative mechanism under the nucleus that might involve reticular adhesion networks.

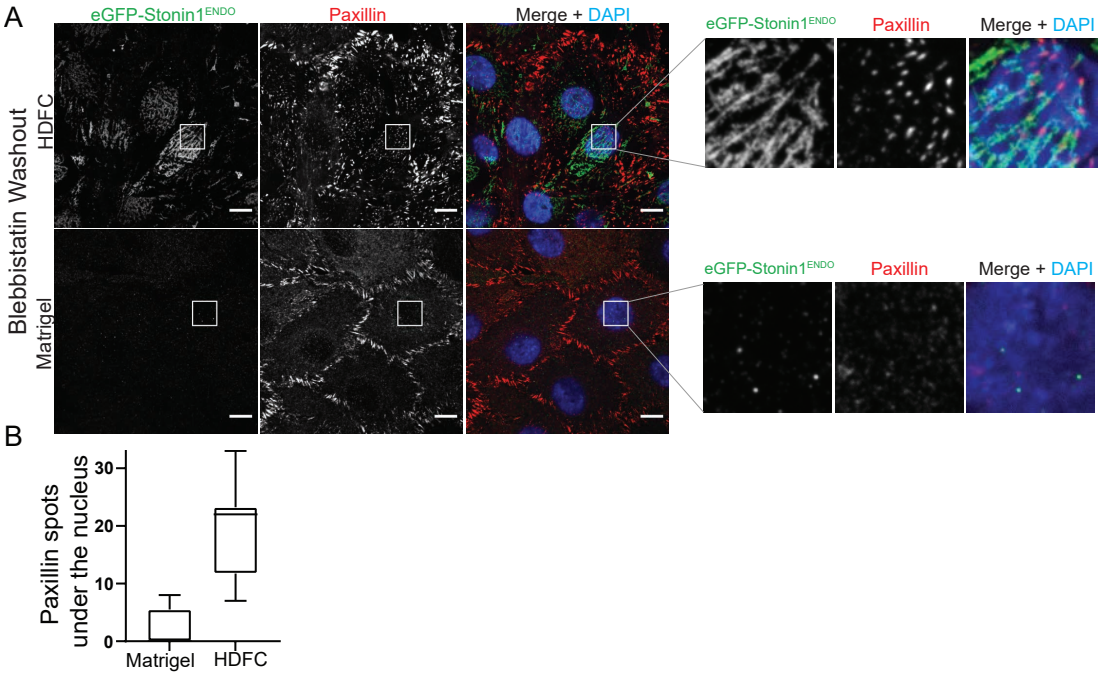

Figure 3.29: FAs assemble under the nucleus in close proximity to reticular adhesion networks. (A) TIRF images of C2C12 myoblasts endogenously expressing eGFP-stonin1 co-stained for GFP and paxillin, seeded on HDFC or Matrigel, treated with blebbistatin for 1 h and washed out with serum-containing medium for 30 min. Magnification of the area marked by the boxes illustrate FA assembly under the nucleus on HDFC. Scale bars 10 µm. Dapi staining was imaged via brightfield microscopy. (B) Quantifcation of segemented paxillin spots with a pixel intensity > 10 under the nucleus using Dapi as mask. Data are taken from 13 nuclei. Boxplot center and box edges indicated median and 25th or 75th percentile, respectively. Boxplot notches approximate 95% confidence interval.

3.3 Dynamic interconversion of FAs and RAs

While the generation of FAs at the cell edge is understood in great mechanistic detail, the biogenesis of RAs is only partially understood. Earlier work has shown that RAs can assemble at sites of FA disassembly (Bucher et al., 2018b), but also de novo (Lock et al., 2018). Therefore, there are close links between both types of adhesions. Based on the results presented in the previous paragraph we wondered whether RAs might also give rise to FAs. To investigate this question, we chose C2C12 myoblasts endogenously expressing eGFP-stonin1 as a model since they form the characteristic stonin1-positive reticular adhesion networks. We used live-cell multi-colour fluorescence microscopy to unravel the dynamics between RAs and FAs and could show that both can dynamically convert into each other.

3.3.1 Stonin1 is recruited to integrin ß5 while FAs are disassembled

It has been shown that clathrin plaques appear where focal adhesions are disassembled (Bucher et al., 2018b). Since we have demonstrated a ß5 integrin dependent recruitment of stonin1 to αV integrin adhesions, we wondered in which chronological order the other components of clathrin plaques appear. To investigate the recruitment of stonin1 and clathrin to the disassembling αVß5 based FAs, we used live-cell microscopy of an endogenously eGFP-stonin1 expressing C2C12 cell line that was stably transduced with paxillin as canonical FA marker, clathrin and ß5 integrin. The live cell imaging revealed that paxillin was first replaced by stonin1 when focal adhesions were disassembled (Fig. 3.30). At this point clathrin was not yet detectable. Stonin1 appeared at focal adhesions, while paxillin was still localized there, and gradually replaced with paxillin (Fig. 3.30 C and D). Interestingly, the size, shape and fluorescence intensity of ß5 integrin was unaffected by this process (Fig. 3.30 E). Stable clathrin puncta appeared after focal adhesion disassembly as described by (Bucher et al., 2018b).

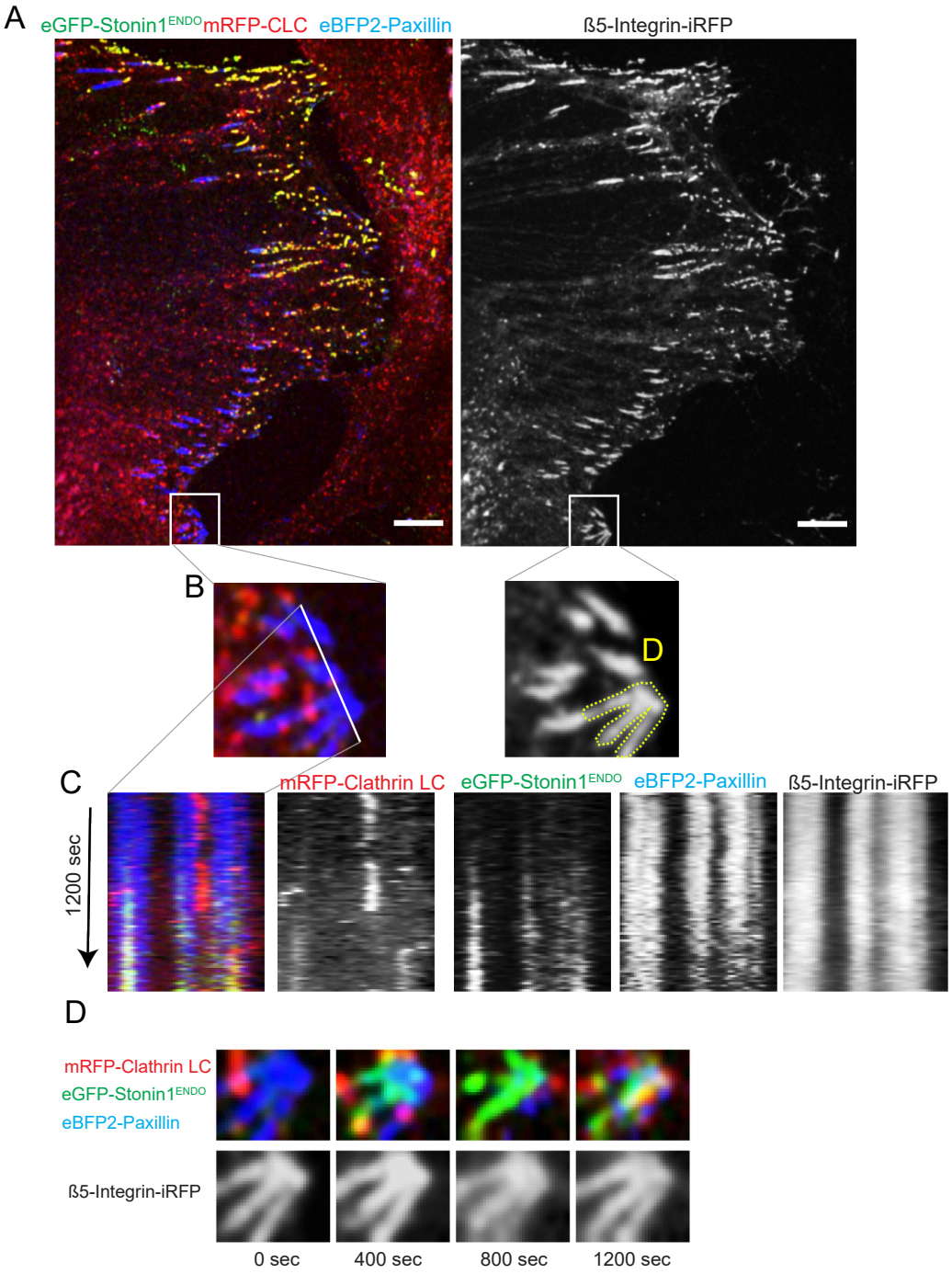

Figure 3.30: Stonin1 is recruited to integrin ß5 while FAs are disassembled. (A) Live-cell confocal spinning disc microscopy of C2C12 myoblasts endogenously expressing eGFP-stonin1 and stably expressing eBFP2-paxillin, mRFP-CLC and ß5 integrin-iRFP. (B) Magnification of FAs before disassembly. (C) Kymograph of FA disassembly along the line shown in (B) for 24 min. (D) Overview of representative disassembling FAs that convert into stonin1-positive RAs. Scale bars 10 µm.

To date, no intermediate structure between FAs and clathrin plaques has been described. Our data now points to αVß5/stonin1-positive structures as intermediary stage on route from αVß5/stonin1/paxillin positive FAs to αVß5/stonin1/clathrin positive reticular adhesions. Stonin1 could therefore represent a link between clathrin and non-clathrin containing adhesions. Stonin1 still localizes to the integrin even after full FA disassembly, and remains as a stable feature of integrin ß5 adhesions, suggesting a special role beyond a possible function as an FA disassembly factor.

3.3.2 Stonin1 is recruited simultaneously with integrin ß5 during the formation of RAs

Although we have shown that stonin1 is recruited to the integrin after retraction-mediated FA disassembly, we also observed an FA independent accumulation of positive ß5 integrin and stonin1 puncta at the leading edge of the cell. (Fig. 3.31 A).

Stonin1 and ß5 integrin localized simultaneously and formed puncta after the protrusion of the leading edge of a migrating cell (Fig. 3.31 C). Actin was recruited right after the formation of these puncta suggesting an actin coupling or bundling mechanism.

We therefore could confirm the FA independent formation of reticular adhesion as described by (Lock et al., 2018) as well the FA dependent clathrin plaques formation as described by (Bucher et al., 2018b). Both are considered to be the same clathrin containing adhesions (Lock et al., 2019). Indeed, we were able to reproduce both observations, and the localization of stonin1 at both described adhesions / mechanisms supports this assumption. F-tractin dynamically colocalized with stonin1-positive RAs when cells formed de novo RAs. However, F-tractin was not always associated throughout the lifetime of RAs, indicating a highly regulated actin coupling mechanism to RAs.

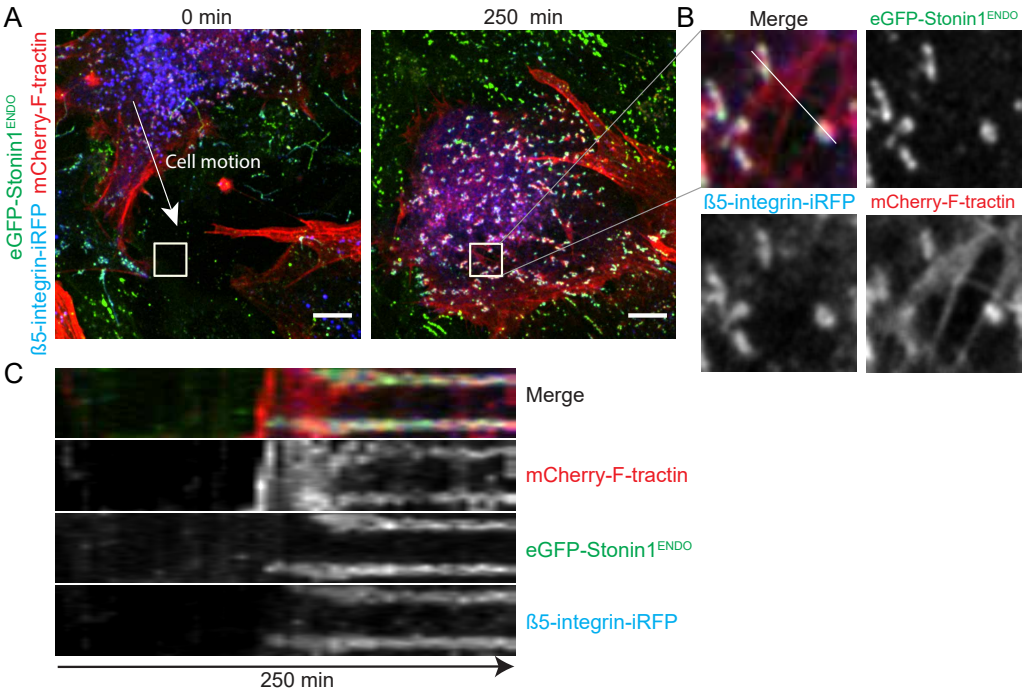

Figure 3.31: Stonin1 is recruited simultaneously with integrin ß5 during the assembly of RAs. (A) Live-cell confocal spinning disc microscopy of C2C12 myoblasts endogenously expressing eGFP-stonin1 (green) and stably mCherry-F-tractin (red) and ß5 integrin-iRFP (blue). Overview of a representative migrating cell at time 0 (left) and after 250 min (right). A white arrow indicates the direction of cell movement. Scale bars 10 µm. (B) Zoom on RAs after 250 min showing association with F-actin. (C) Kymograph of RA assembly along the line depicted in B during the 250 min time period.

3.3.3 The conversion of sliding FAs into retraction fibers is accompanied by stonin1 recruitment

In addition to the disassembly of stationary adhesions, FAs exhibit another specific behaviour: When cells retract their cell membrane, FAs are often observed to "slide" back by a Rho/myosin II-dependent mechanism (Parsons et al., 2010). At the position where the sliding occurs, a retraction fiber frequently originates. Thus the sliding mechanism can be considered as a form of FA disassembly where the FA end pointing to the cell periphery is shrinking by being converted into a retraction fiber while the opposite end is being elongated.

We wondered whether stonin1 also in this case would be recruited early on in the conversion process analogous to the sequence of events in the conversion of stationary FAs to clathrin plaques. To investigate this question, we used the endougenously stonin1 expressing C2C12 cells in combination with stable eBFP2-Paxillin and mCherry-F-tractin expression. We included the actin marker to investigate simultaneously the role of FA-associated stress fibers in this process. Our live cell imaging did indeed reveal that stonin1 recruitment coincides with the partial disassembly/sliding of FAs when the cell retracts (Fig. 3.32) starting at the peripheral tip of the FA. During retraction of the cell and sliding of FAs, the stonin1-positive adhesion progressively elongated into a retraction fiber which stayed connected to the cellular actin cytoskeleton even if the thickness of the associated stress fiber bundles decreased over time (Fig. 3.32 D).

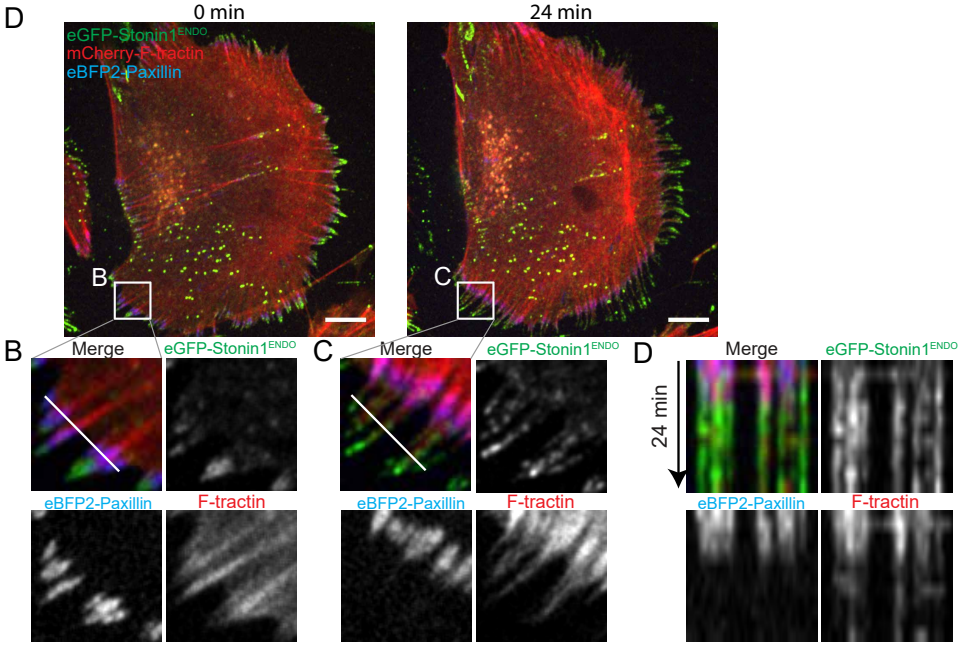

Figure 3.32: Conversion of FAs into retraction fibers involves stonin1 recruitment. (A) Live-cell confocal spinning disc microscopy of C2C12 myoblasts endogenously expressing eGFP-stonin1 and stably expressing eBFP2-paxillin and mCherry-F-tractin. Magnification of FAs before (B) and after disassembly (C). (D) Kymograph of FA disassembly shown in (B) and (C) for 24 min. Scale bars 10 µm.

3.3.4 Focal adhesions assemble at stonin1 positive adhesions

Even though retraction fibers (which turn into footprints once the connection to the migrating cell breaks off) and reticular adhesion networks differ substantially in terms of their morphology, we assume that these adhesions are very similar judged by their identical molecular composition (αVß5, integrin, stonin1, no canonical FA proteins, no clathrin). To better understand their life cycle we went for long-term multi-colour live cell imaging. In doing so we made the surprising discovery that not only FAs can turn into reticular adhesions and retraction fibers (as described in the previous section), but that retraction fibers (Fig. 3.33) and reticular adhesions (Fig. 3.34) can act as templates for the generation of new FAs. This appears for example to contribute to fast respreading of cells over an area they previously occupied. Using paxillin as a focal adhesion marker, we observed FA assembly at retraction fibers after cellular respreading along these retraction fibers. The newly formed focal adhesions originated at integrin ß5 positive retraction fibers until completely overlapping these structures. This was both the case for respreading of cells over retraction fibers formed during migration (Fig. 3.33 A) or respreading over retraction fibers generated during mitosis (Fig. 3.33 B). Since focal adhesions are connected to the substrate via integrins, we assume that the newly formed FAs use the pre-existing integrin in the retraction fiber as building material and also "recycle" the retraction fiber connection to stress fibers to link to the actin cytoskeleton. This might explain the rapid transformation of a retraction fiber into a mature FA.

In addition, we could demonstrate that FAs can originate intracellulary at the sites of reticular adhesion networks without the need for a lamellipodium (Fig. 3.34). These FAs appeared to grow out from RAs and "slide" outward. Here, we did not observe a conversion as the one we had seen when cells respread over retraction fibers since the "parental" RA structure was not consumed in the process, but remained unaltered. Instead, new integrin ß5 together with paxillin was deposited right next to the stonin1-positive RA , but all newly formed FAs originated from stonin1-positive adhesions and used the same integrin (Fig. 3.34 B).

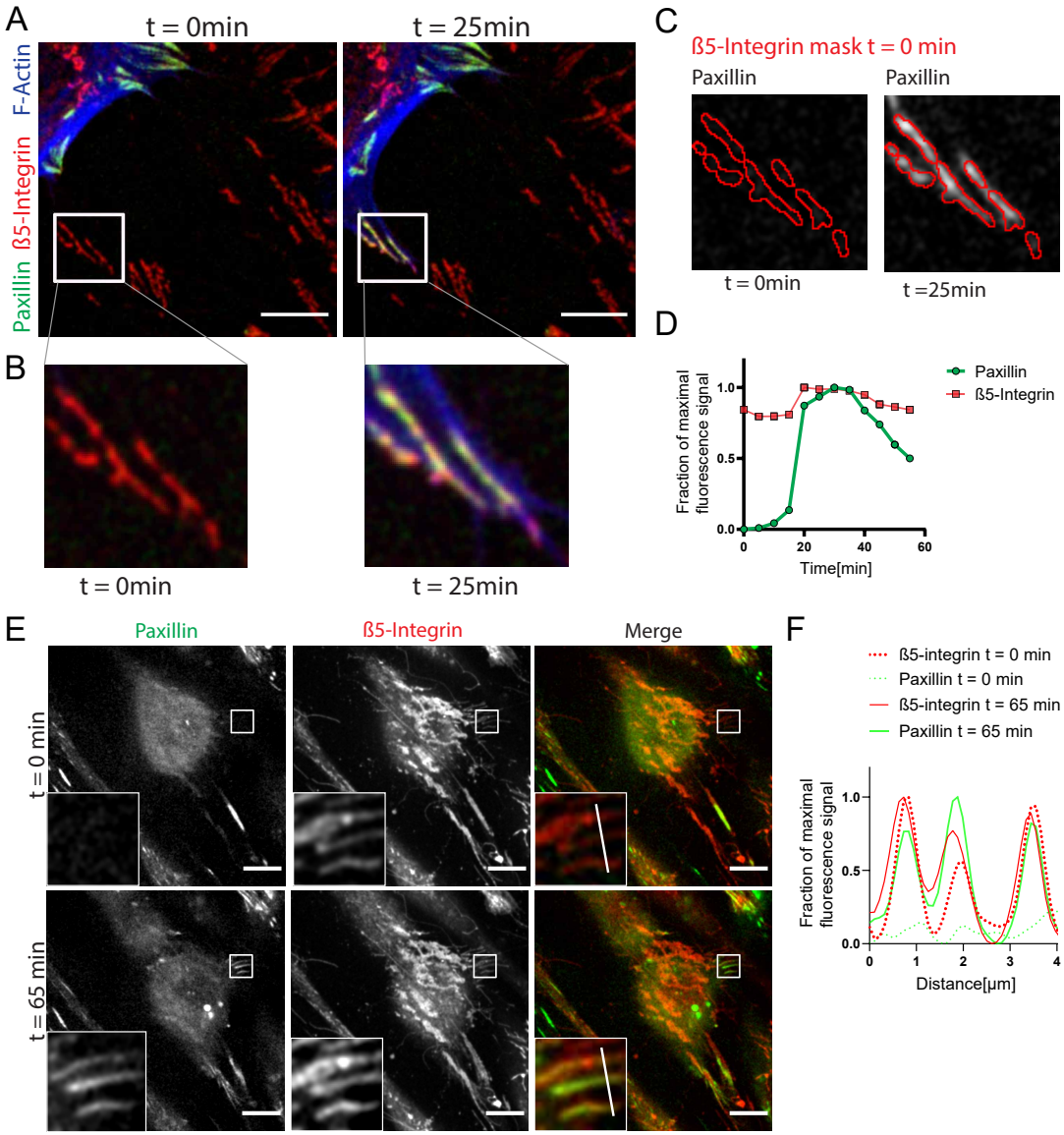

Figure 3.33: Focal adhesions assemble at ß5 integrin-positive retraction fibers. (A) Live-cell confocal spinning disc microscopy of C2C12 myoblasts stably expressing eBFP2-paxillin (green), mCherry-F-tractin (blue) and ß5 integrin-iRFP (red). (B) Magnification of retraction fibers that are converted to FAs, displayed (t = 0 min) and after cell respreading (t = 25 min). (C) Mask marking the integrin ß5-positive retraction fiber (red) and the paxillin signal at time point 0 and after 24 min. (D) Normalized fluorescence intensity of eBFP2-paxillin (green) and integrin ß5-iRFP (red) within the ß5 integrin mask shown in (C) depicted over time. (E) Representative cell at time point 0 min where it is in cytokinesis and has disassembled its FAs and 65 min later where new FAs are assembled on ß5 integrin-positive retraction fibers. (F) Time-dependent intensity profiles of eBFP2-paxillin (green) and ß5 integrin (red) at cytokinesis
(t=0) and after 65 min along the line depicted in E. Scale bars 10 µm.

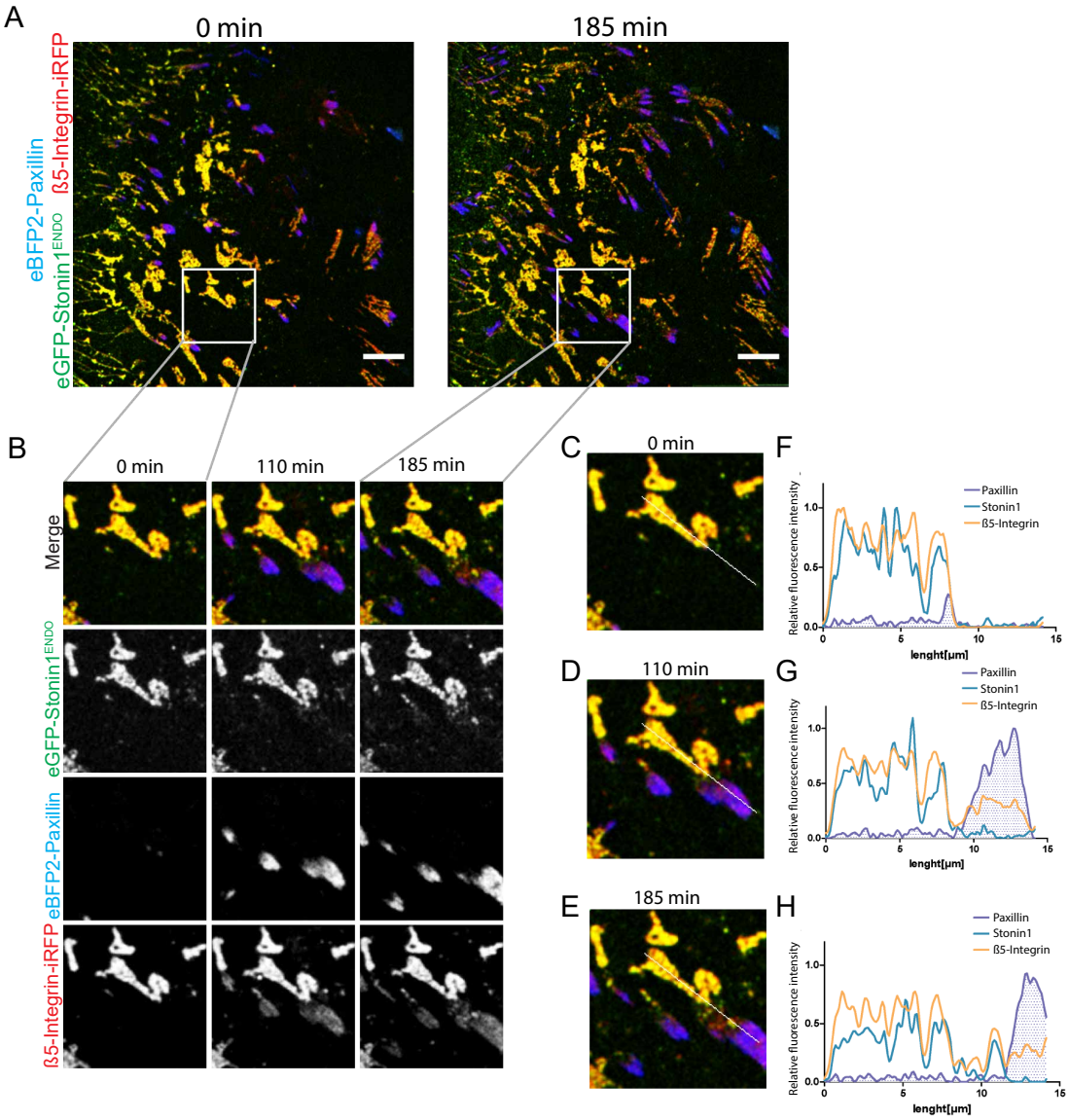

Figure 3.34: Focal adhesions assemble at RAs.
(A) Live-cell confocal spinning disc microscopy of C2C12 myoblasts endogenously expressing eGFP-stonin1 (green) and stably expressing eBFP2-paxillin (blue) and ß5 integrin-iRFP (red). (B) Maginification of ß5 integrin-positive FA assembly originating from RAs after 0, 110 and 180 min. Merged images showing FA assembly and "sliding" at a RA along the indicated line at time 0 min (C) 110 min (D) and 180 min (E). Time-dependent intensity profiles of eBFP2-paxillin (blue), ß5 integrin (yellow) and eGFP-stonin1 (cyan) during FA assembly along the line depicted in C at time point 0 min (F), along the line depicted in D at time point 110 min (G) and along the line depicted in E at time point 180 min (H). Scale bars 10 µm.

When the newly formed FAs started to "slide" away from the "parental" RAs, stonin1 is recruited to the site where the FAs were previously located, leaving a typical "trail" (Fig. 3.34 E). At this point we have no direct experimental evidence that the "parental" RA is truly "parental" in the meaning of causing the "birth" of the new FA. Theoretically, it would still be possible that the generation of the FA adjacent to an RA is purely coincidental. However, the location of newly formed FAs within the cell without a lamellipodium or nascent adhesions suggests a novel mechanism of FA assembly.

3.3.5 F-actin fiber/bundle at the front of newly emerging FAs

F-actin plays an important role in the biogenesis of FAs at lamellipodia. The retrograde actin flow is thought to remodel lamellipodial actin filaments into stress fibers and to contribute to the maturation of FAs (Yamashiro and Watanabe, 2014). Therefore, we wondered about the involvement of F-actin in the assembly of FAs at RAs. To address this question we performed live cell imaging of paxillin and ß5 integrin together with the F-actin marker F-tractin (Fig. 3.35) We observed F-actin fibers to be connected to the protruding end of each of the emerging FAs. Newly assembled stress fibers at FAs could be localized in the middle of the cell and not localized near a lamellipodial protrusion. This suggests an as yet undiscovered mechanism of focal adhesion formation and F-actin bundling at RAs.

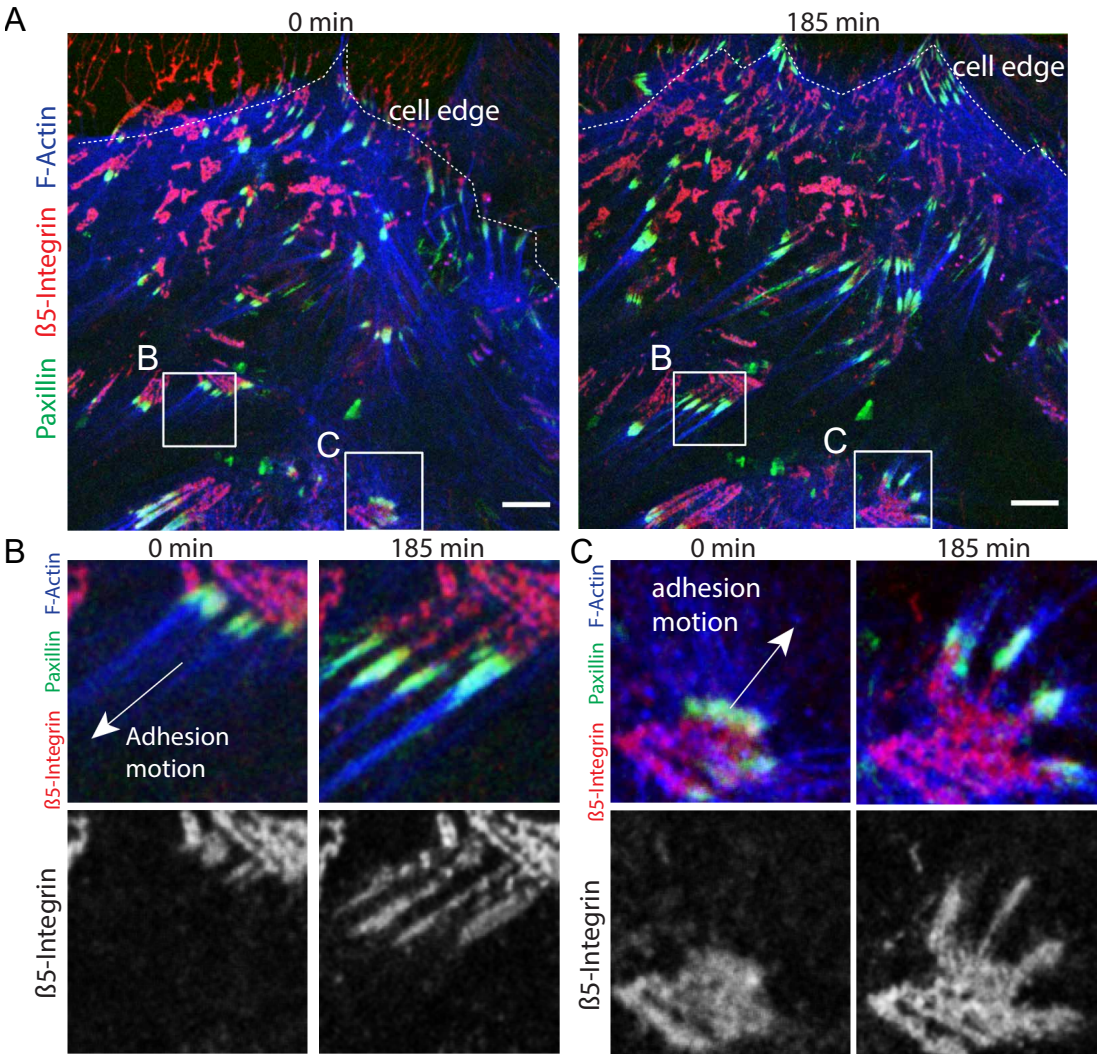

Figure 3.35: Stress fibers assemble at the front of FAs emerging at RA sites. (A) Live-cell confocal spinning disc microscopy of C2C12 myoblasts stably expressing eBFP2-paxillin (green), mCherry-F-tractin (blue) and ß5 integrin-iRFP (red). (B) Magnification of stress fibers originating from FAs at time point 0 min and after 185 min. A white arrow indicates the outward motion of FAs. Scale bars 10 µm.

4. Discussion

Mammalian cells regulate their adhesion activity via integrins and to facilitate cell survival, proliferation, and differentiation (Colognato et al., 2004; Hynes, 2009). In particular, cellular responses to various ECMs have been poorly studied, but are of great importance for aging, tissue repair, and also pathological conditions such as cancer or fibrosis. Integrin-based cell-matrix adhesions are categorized according to the type of integrin receptor used and are found in a wide range of compositions. Different cell types, different extracellular matrix substrates, and even different time points reveal a wide variety of matrix adhesions.

Canonical adhesions comprise focal adhesions that are formed from focal complexes in a well-understood series of events. FAs are dynamic structures that undergo maturation and interconversion, linking the cytoskeleton to the ECM (Geiger and Yamada, 2011).

To date, the role of persistent flat clathrin-coated plaques is controversial, but their function as adhesions is increasingly recognized. These clathrin plaques are characterized by αVß5 integrin that is thought to block the internalization of CCVs by binding tightly to a stiff substrate (Baschieri et al., 2018). Clathrin plaques have moreover been found to be signaling platforms for specific receptors like LPA receptors (Leyton-Puig et al., 2017). Recently, an αVß5 integrin adhesion called RA was discovered to mediate cell attachment in mitosis (Lock et al., 2018). Since these RAs have a similar protein composition as clathrin plaques, they were assumed to be the same (Lock et al., 2019).

Our work contributes to a new picture of RA characteristics and function by shedding light on how FAs and RAs characteristics and function can dynamically interconvert, losing their respective markers during disassembly and assembly, while the underlying integrin remains unaffected. Finally, we propose a novel mechanism of FA assembly that reuses the integrin of RAs/plaques to assemble mature FAs.

4.1 Stonin 1 is a unique marker of adhesion sites that lack canonical FA markers

Since stonin2 is a known adaptor for synaptotagmin1 during CME and since the structure of stonin1 is similar to that of stonin2, it was natural to suspect a similar endocytic role for stonin1. However, we found stonin1 to localize selectively in clathrin plaques but not in individual CCPs. This is the first protein to exhibit this unique localization pattern, suggesting that clathrin coated pits and clathrin plaques are distinct structures with regard to their protein composition. Stonin1 shows a strong colocalization with the integrin αVß5 that is described as the major integrin of RAs and clathrin plaques (Baschieri et al., 2018; Lock et al., 2018; Zuidema et al., 2018).
Indeed, using immunofluorescence and life cell imaging, we could show that stonin1 localizes to all αVß5-positive integrin adhesions except FAs. The recruitment of stonin1 to these adhesions was entirely dependent on the ß5 integrin, since depletion of the latter removed all stonin1-positive structures. On the other hand, depletion of AP2 or clathrin did not abolish the localization of stonin1 to integrin adhesions, which appeared as larger networks rather than as puncta. Stonin1 is therefore not recruited by the CME machinery, but downstream of the αVß5 integrin, indicating a specific role beyond endocytosis.

A strong association of stonin1 with adhesions also becomes evident when a complete breakdown of cell membranes is achieved by high shear-flow water pressure, leaving only FAs and stonin1 containing adhesions behind. This strong association is special since many molecular interactions within integrin adhesion complexes have low affinity and are lost after high shear-flow jetting (Schiller et al., 2011).
Indeed, using super resolution microscopy, we demonstrated that stonin1 appears to act as a nanospacer between αVß5 integrin clusters. Stonin1 can therefore be used as a novel marker to visualize the pool of αVß5 integrin adhesions that is characterized by the absence of FA proteins. Examining the stonin1-positive integrin pool, we observed on the other hand integrin αVß5-positive retraction fibers and footprints lacking endocytic proteins such as clathrin as well as FA proteins.

On the other hand, large αVß5-positive adhesion networks showed limited colocalization with the CME machinery and FA proteins, although clathrin plaques were found interspersed within the larger networks. Stonin1 remains as a stable component of αVß5 adhesions even after disassembly of clathrin plaques.

Based on our observations, we suggest that the RAs observed in mitosis are molecularly identical to retraction fibers observed in migration. Both are characterized by the shared integrin αVß5, the presence of stonin1, and the absence and endocytic or FA proteins. In addition, in both cases the assembly is induced by a cell retraction mechanism that disassembles FAs. Therefore, the mere classification into FAs and clathrin containing adhesions does not seem to accurately reflect the adhesion variety and should be reconsidered. We propose classifying αVß5 adhesions into a focal adhesion pool (marker: αVß5, FA proteins) and a reticular adhesion pool which comprises on the one hand clathrin plaques (marker: αVß5, stonin1, endocytic proteins, no FA proteins), and on the other hand reticular adhesion networks (marker; textalpha Vß5, stonin1, no endocytic proteins except for interspersed clathrin plaques, no FA proteins) and retraction fibers and footprints (marker: textalpha Vß5, stonin1, no endocytic proteins, no FA proteins)(Fig. 4.1).

We observed αVß5 adhesions on collagen, but not on matrigel. Interestingly, FA-independent adhesions have previously been observed to wrap around collagen fibers in 3D collagen gels forming structures termed tubular clathrin/AP2 lattices. These adhesions also form independently of clathrin and are thought to promote adhesions in 3D environments (Elkhatib et al., 2017). However, they differ from stonin1-containing adhesions: First, we could not observe tubular lattices on thin 3D collagen matrices by electron microscopy. Second, these adhesions consist of the integrin ß1, which is not co-localized with stonin1 (data not shown). ß1 integrin-positive plaques have also been observed in myotubes, where they stabilize the costameres that connect the sarcomeres to the plasma membrane (Vassilopoulos et al., 2014). Stonin1 containing reticular adhesion networks and retraction fibers appear to be of particular importance because they mediate the not previously described dynamic interconversion into FAs which might be important for respreading after mitosis or in migration.

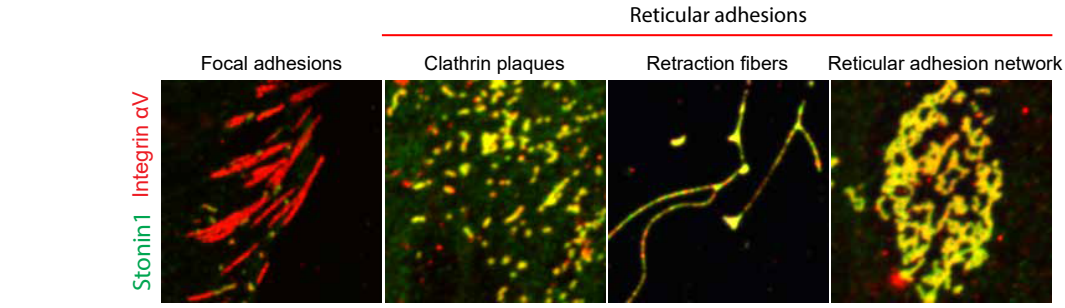

Integrins:	αVß5 & other	αVß5	αVß5	αVß5
Stonin1:	--	stonin1	stonin1	stonin1
FA markers:	yes	--	--	--
CME markes:	--	yes	--	interspersed clathrin puncta
F-actin:	stress fibers	punctate	stress fibers	stress fibers and puncta
		= flat clathrin lattices	= footprints if broken of	

Figure 4.1: Classification of integrin αVß5 adhesions. αVß5 adhesions can be divided into two pools: A stonin1 negative FA pool and a stonin1-positive RA pool. RA is the umbrella term for all αVß5-positive structures that are not FAs. RAs can be further divided into subclasses depending on their morphology and molecular composition. The different adhesion subclasses with their special characteristics are shown below. In contrast to clathrin plaques, retraction fibers and adhesion networks can be associated with actin stress fibers.

4.2 Focal adhesion assembly at reticular adhesions

It has been described that clathrin plaques form where FAs have been disassembled (Bucher et al., 2018b). Although integrin endocytosis is described after FA disassembly (Ezratty et al., 2009), the attachment of the putative endocytic adaptor stonin1 to the integrin apparently rather results in a stable, long-lived structure. Here, we show for the first time that there is an intermediate structure forming during the conversion of FAs into clathrin plaques that is characterized by the presence of stonin1 and the absence of clathrin. This type of FA disassembly is characterized by the gradual exchange of FA proteins such as paxillin with stonin1, leaving the underlying integrin unchanged. Stable, long-lived clathrin puncta appeared only after stonin1 was already recruited.

These clathrin puncta were mostly interspersed and did not completely cover the underlying adhesion. Stonin1 and the integrin ß5 remained in place as retraction fibers even when the cell moved further away and clathrin plaques were disassembled. Interestingly, new plaques emerged right after cell respreading over retraction fibers, where clathrin had previously been dissociated. In fact, it has already been proposed that there is a specific, unknown endocytic protein that determines the future location of clathrin plaques after FA disassembly (Bucher et al., 2018b).

We wondered whether the observed mechanism to assemble clathrin plaques at the sites of retraction fibers would also work once the retraction fibers are broken off and left behind as footprints. Since our experiments showed that these footprints are still membrane-enclosed this would require a membrane fusion mechanism in order for the cell to gain access to the enclosed proteins. In our hands, however, we could only observe the reappearance of clathrin plaques at sites which appeared to be still connected retraction fibers rather than footprints. This view is supported by the fact that we did not observe any cell that formed a new clathrin plaque on a bona fide footprint of another cell.

It has also been shown that reticular adhesions/plaques can form independently of FAs (Lock et al., 2018). Indeed, we could observe the FA independent appearance of αVß5 integrin puncta in migrating cells. Here, stonin1 was recruited simultaneously with the integrin.

These puncta showed a dynamic recruitment of actin. However, throughout the lifetime of RAs, actin was mostly not colocalized with RAs, suggesting a tight regulatory mechanism for the recruitment of actin polymerizing factors. Actin polymerization in clathrin plaques is promoted by N-WASP through the Arp2/3 complex that provides mechanical force for the rearrangement of the flat clathrin lattice into a curved lattice (Leyton-Puig et al., 2017). Consistent with this finding, drugs that stop actin dynamics inhibit CCV formation and prolong CCS lifespan (Yarar et al., 2005). In addition, the disruption of actin polymerization by cytochalasinD or latrunculinA leads to disassembly of FAs but retention of RAs (Lock et al., 2018).

It can be speculated that a flat clathrin lattice might prevent the access of F-actin linking modules to the αVß5 integrin adhesions. These F-actin linking modules are needed for linking stress fibers to FAs or to retraction fibers and RAs. We therefore argue that retraction fibers in mitosis and migration should be regarded as a separate subclass of adhesions because they do not contain clathrin and are connected to F-actin modules. RAs provide a potential mechanism for spatial memory storage after mitotic cell respreading (Lock et al., 2018). It has not yet been considered that RAs could be reused for FA assembly, thereby bypassing the need for the buildup of new nascent adhesions. Indeed, we observed the conversion of retraction fibers into FAs. In particular, new mature FAs emerged at retraction fibers after the respreading of cells following cytokinesis or the respreading of migrating cells.

Newly formed ß5 integrin-positive FAs formed at the exact position of ß5 integrin-positive retraction fibers and grew outward. Since the intensity of the integrin did not change during the interconversion, we assume that the underlying integrin is reused. During a conventional FA assembly new integrin is clustered at the site of the nascent adhesion, which was not observed.

Therefore, we propose an alternative mechanism of FA assembly (Fig. 4.2). This FA assembly does not require a lamellipodium, but uses the integrin present in retraction fibers as a nucleation point for the formation of FAs. We assume that the subsequent molecular mechanism of this alternative FA assembly is similar to the other stages of conventional FA assembly. Here, retraction fibers appear to transform into mature FAs instead of focal complexes. We observed not only the conversion of retraction fibers to FAs after respreading, but also the assembly of new FAs from reticular adhesion networks in the center of the cell. Here, we did not observe a conversion; instead, FAs and stress fibers grew out of the reticular adhesion network.

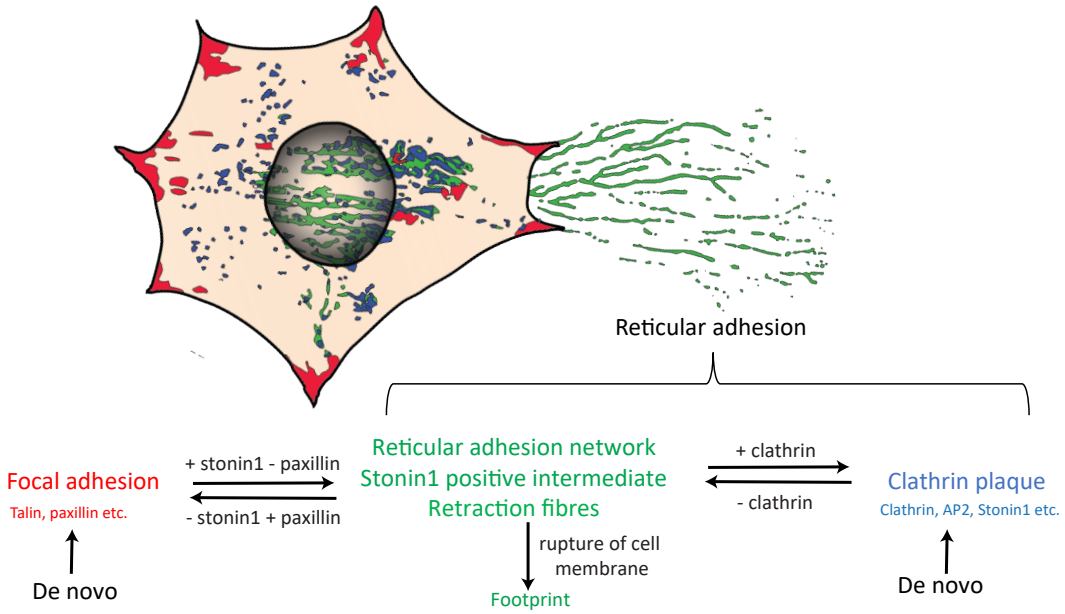

Figure 4.2: Interconversion of αVß5 integrin adhesions. Schematic representation of a cell with different αVß5 integrin adhesions. FAs and RAs can be converted into each other by a stonin1-positive intermediate structure. Stonin1-positive adhesions include retraction fibers and large adhesion networks that may be interspersed with clathrin plaques.

The assembly of FAs generally requires actin polymerization and a retrograde actin flow that reinforces integrin–cytoskeleton bonds (Geiger and Yamada, 2011). This actin flow happens inside the lamellipodium, where it occurs centripetally at a rate of a few micrometers per minute (Ponti et al., 2004).

Quite interestingly, FAs from neighboring adhesion networks can grow outwards in completely opposite directions. Even the opposite growth direction of two FAs from one and the same network was observed. Therefore, actin flow and stress fiber buildup should originate from the adhesion network itself.

Indeed, using transmission electron microscopy, we observed a closely meshed actin network in stonin1-positive adhesion networks. Thus, it appears that the actin cytoskeleton is associated with-positive stonin1 adhesions and that new FAs can be assembled from it without the presence of a lamellipodial protrusion.

4.3 Stonin1 function in adhesion dynamics

Stonin1 becomes associated with the αVß5 integrin during FA disassembly. Therefore, we wondered whether stonin1 might be involved in the disassembly of FAs as suggested in an earlier study from our lab (Feutlinske, 2014). However, we have found several observations that argue against this hypothesis. The specificity of stonin1 for αVß5 integrin suggests that stonin1 cannot be part of a general FA disassembly mechanism, but could only assist in the disassembly of FAs built around αVß5 integrin. Currently, 24 unique mammalian integrins are known to exist (Hynes, 2002). Thus, it seems unlikely that there are 24 unique mechanisms for disassembling FAs. Furthermore, stonin1 remains at the adhesion site after the FAs are already disassembled. Finally, we demonstrated that stonin1 is also recruited to newly formed RAs independently of FA disassembly. Another potential function of stonin1 could be to act as an endocytosis adaptor of the integrin αVß5.

Indeed, integrins are endocytosed after FA disassembly (Ezratty et al., 2009). However, endocytosis of clathrin plaques has not yet been observed (Lock et al., 2019). As endocytic adaptor for αVß5 stonin1 could be expected to affect the amount of integrin at the plasma membrane or influence the size of RAs. However, the loss or overexpression of stonin1 does not change the size of αV integrin adhesions. It is also already described that the loss of stonin1 does not show a significant difference in the surface level of integrin αV using flow cytometry (Bergmann, 2017).
Recently, cilengitide was shown to disassembly clathrin plaques by selectively inhibiting integrins that are not bound to RGD motifs in the ECM (Bucher et al., 2018b). Here, further studies with cilengitide are needed to investigate how αVß5 integrin adhesions are dissembled and whether they are eventually endocytosed.

We showed that the depletion of the ß5 integrin results in the loss of all stonin1-positive structures. In fact, the intracellular domain of ß5 is crucial for the appearance of clathrin plaques. Studies with integrin chimeras containing the extracellular and transmembrane domains of β5 and the cytoplasmic domains of β1 or β3, almost exclusively localize in FAs (Zuidema et al., 2018). The clathrin adaptors ARH and Numb have been shown to bind to an NPxY motif and EPS15R has been demonstrated to bind to ubiquitinated residues in the integrin β5 cytoplasmic domain (Zuidema et al., 2018). Stonin1 has no predicted domain that could bind to the NPxY motif directly.
Immunofluorescence analysis of stonin1 together with stonin2, EPS15R and intersectin showed only colocalization in clathrin plaques but not in non clathrin-containing reticular adhesion networks and retraction fibers. Indeed, stonin2, but not stonin1, interacts with the endocytic proteins Eps15, Eps15R, and intersectin1 (Martina et al., 2001). Stonin1 might still be recruited by one of the ß5-integrin binding endocytic proteins but remains behind at the adhesion after clathrin uncoating.

The published molecular composition of RAs shows limited overlap with FAs but a much greater overlap with the clathrin interactome (Lock et al., 2019). However, our new observation shows that a subset of RAs can lose clathrin and other endocytic adaptors, especially during migration or mitosis. We did not find other endocytic proteins than stonin1 under these conditions.

Interestingly, stonin1 is unique in its localization to both clathrin plaques and actin fibers, and recruitment of F-actin to plaques appears to be dependent on stonin1.

Since stonin1 has a PxxP motif, it could potentially interact with the SH3 domains of endocytic proteins such as amphiphysins, pacsins and endophilins. SH3-domain containing proteins also regulate the Arp2/3-dependent actin polymerization (Mason and Soderling, 2010). The SH3 domain protein cortactin colocalized with stonin1 under conditions where the ECM matrix was degraded and clathrin plaques emerged. We could also show stonin1 colocalization with the Arp2/3 complex and α-actinin. Actin polymerization at clathrin plaques is promoted by N-WASP via the Arp2/3 complex (Leyton-Puig et al., 2017). Despite the finding of proteins involved in actin polymerization or regulation, such as the Arp2/3 complex, N-WASP or cortactin in RAs/plaques, the connection of RAs to the cytoskeleton via actin linkage modules is considered to be less prominent or even absent (Leyton-Puig et al., 2017; Lock et al., 2018; Zuidema et al., 2018).

Interestingly, the actin polymerization at clathrin plaques was completely stonin1 dependent. Actin polymerization should be tightly regulated and activated when the conversion of RAs into FAs is required, e.g., after mitotic respreading or respreading during migration. As a stonin1 knockout showed no actin recruitment in RAs/plaques, a possible role of stonin1 in regulating actin polymerization seems likely.

Once mitotic cells have disassembled their FAs, uptake of the integrin should be prevented at this particular stage of the cell cycle to allow attachment to the substrate by RAs. Indeed, during early mitosis endocytosis is temporarily switched off (Fielding and Royle, 2013).

Therefore, we also speculate whether stonin1 might in fact prevent endocytosis of the αVß5 integrin. However, we never observed clathrin-mediated endocytosis of stonin1 or αVß5 from adhesions. Stonin1 was retained at the ß5 integrin even after clathrin uncoating and conversion into retraction fibers. Whether depletion of stonin1 could trigger CME of the integrin αVß5 requires further investigation.

Depletion of ß5 leads to various mitotic defects such as delayed mitosis, repeated cell rounding, and cytokine failure (Lock et al., 2018). These observations should be further investigated in relation to the loss of stonin1. If stonin1 should really be involved in the cytokinesis stage of the cell cyclce, stonin1 could be expected to be subject to a tight cell cycle-dependent regulation. In line with this, we found that the proline-rich motif in the intrinsically disordered N-terminal region of stonin1 is phosphorylated by CDK1 and CDK2 in a cyclin dependent manner. In fact, phosphorylation by CDK1 and CDK2 was observed only when the kinases formed a complex with cyclinA or cyclinE. When CDK1 forms a complex with cyclinB1, representing the stage of mitosis, no phosphorylation was observed. Indeed, cyclins determine substrate specificity of CDKs during the cell cycle (Lee et al., 2007). The inhibition of CDKs and the cell cycle paradoxically lead to the hyperphosphorylation of stonin1.

Stonin1 might be regulated multidimensional and is a highly regulated phosphoprotein. In total, we found 31 phosphorylation sites of stonin1 with different phospho motifs. The proline rich motif of stonin1 contains a PxxP SH3 binding motif. Interactions of proline-rich peptides with SH3 domains are mainly characterized by hydrophobic interactions (Kurochkina and Guha, 2013). Thus, the hyperphosphorylation of eight serine residues in the proline-rich motif of stonin1 might prevent the interaction with a possible SH3 domain. Unphosphorylated stonin1 is located at the plasma membrane while phosphorylated stonin1 is located in the cytoplasm (Feutlinske, 2014). After stimulation with the growth factor PDGF, stonin1 is mostly present in the phosphorylated form, whereas starvation leads to a shift to the unphosphorylated form.

It has been shown that clathrin plaques can be strongly labeled with an anti-phosphotyrosine antibody upon EGF stimulation and can serve as platforms for receptor-dependent signaling (Baschieri et al., 2018). Clathrin plaques persist as stable adhesions even after growth factor stimulation. In line with this, we do not see the removal of stonin1 from αVß5 adhesions after PDGF stimulation. Interestingly, large stonin1 adhesion networks and footprints were not labeled by an anti-phosphotyrosine antibody. Therefore, we assume that these networks are not participating in signal transduction events. In contrast, stonin1 might even prevent receptor signalling or uptake of the integrin at these adhesions.

We further showed that stonin1 is dephosphorylated by the protein phosphatase 2A (PP2A). The docking site of PP2A is only 15 amino acids downstream of the hyperphosphorylated proline rich motif of stonin1 and was identified to bind the regulatory B´ 56 subunit of PP2A in a phage display (Wu et al., 2017). Indeed, all of the identified sequences that contain a PP2A docking motif have known phosphorylation sites nearby (Wu et al., 2017). PP2A acts as a tumor suppressor with more than 300 substrates involved in cell cycle regulation and MAP kinase signalling. Most of the dephosphorylation events mediated by PP2A play a negative regulatory role (Wlodarchak and Xing, 2016). Substrates of CDK1, CDK2, and p38, kinases identified in our screen, are negatively regulated by dephosphorylation with PP2A (Wlodarchak and Xing, 2016).

We assume that for membrane recruitment stonin1 must be dephosphorylated. However, stonin1 is in the unphosphorylated form when cells are seeded on Matrigel, a condition in which αVß5 adhesions are not formed. It is known that both stonins exist as cytosolic and peripheral membrane proteins (Martina et al., 2001). For stonin1, a mostly cytoplasmic distribution was described (Diril et al., 2006). We assume that until stonin1 is recruited first to the plasma membrane and then might be immobilized by the the integrin αVß5.

Kindlin, for example, is a protein that diffuses freely in the plasma membrane until immobilized by integrins (Orré et al., 2021). In pull-down experiments, the β1, β3, and β5 subunits were shown to differ in their ability to bind kindlin-2 (Sun et al., 2016). Interestingly, ß5 integrin plays a special role, not only because it occurs in RAs/plaques, but also because it does not bind kindlin-2 and kindlin-1 (Zuidema et al., 2018). However, unlike kindlin, stonin1 does not have a predicted membrane domain. Using mass spectrometry, we found a farnesylation site at the c-terminus of stonin1.

The farnesylation motif encompasses a specific amino acid sequence, the CAAX box, at the C-terminus, which is conserved in stonin1. Protein farnesylation acts as a membrane anchor and is a prerequisite for recruitment of proteins with a CAAX motif to the plasma membrane (Gao et al., 2009). This may explain why only the c-terminal µHD domain was shown to be sufficient for recruitment of stonin1 to the membrane (Feutlinske, 2014). µHDs are protein-protein interaction modules found in endocytic proteins involved in CME. They facilitate cargo recognition and internalization. It is thought that the µHD domain of stonin2 binds synaptotagmin and is thereby recruited to the plasma membrane (Diril et al., 2006). The µHD of stonin2 exhibits a high homology to µ2-adaptin, a subunit of the the AP2 adapter complex and competes for binding (Walther et al., 2002).

Adaptin µ2 subunits bind to Yxxφ- motifs in a subset of integrin α-cytoplasmic domains (De Franceschi et al., 2016). A direct binding of stonin1 to integrins might therefore be possible and has to be further evaluated. Interestingly, we did not observe endocytosis of the integrin after clathrin uncoating when stonin1 was present. This leads to the speculation that the µHD of Stonin1 might compete with µ2-adaptin to prevent endocytosis.

4.4 Stonin1 might act as an integrin nanospacer

When integrins recognize extracellular ligands, they switch from a low- to a high-affinity conformation to enable cell adhesion. Integrins within FAs form specific nanoclusters in the membrane that are visible by super-resolution light microscopy (Bachmann et al., 2019). With STED microscopy we could show that all αVß5 adhesions contained these typical nanoclusters. Interestingly, large adhesion networks showed the same level of clustering as FAs. Activation of integrins is known to promote their immobilization (Rossier et al., 2012). In fact, for integrin ß3 clustering to occur, integrin activation is a prerequisite (Cluzel et al., 2005). It has been speculated that integrin within RAs and clathrin plaques are present in an active conformation, as they are only found at the contact sites between the cell and the ECM substrate (Lock et al., 2019).

The activation and clustering of αVß3 integrin requires extracellular ligand binding, talin and kindlin binding to phosphoinositol lipids and talin interaction with the integrin ß3 (Bachmann et al., 2019). An alternative mode for integrin activation and clustering has also been described that requires ony the head domain of talin and induces formation of de novo F-actin-independent integrin clusters (Cluzel et al., 2005). Since all stonin1-positive adhesions contain integrin nanoclusters it might be worthwhile to analyze whether calpain-cleaved talin head domains are present at these sites. Integrin nanoclusters do not colocalize with stonin1 in super-resolution light microscopy. Instead, stonin1 is located between the integrins, which is particularly evident in the retraction fibers that look like strings of beads made of integrins. Keeping integrins in an active high-affinity form in RAs / retraction fibers would ensure the fast interconversion into FAs. After mitosis the cell could "reuse" their adhesions without the need of a lamellipodial protrusion to assemble new mature adhesions. Indeed, we are the first to observe the interconversion of RAs into FAs. This interconversion would be a more efficient way of integrin "recycling" and would ensure the fast respreading over already existing adhesions.

Proteins are described that negatively regulate integrin activation in FAs. Sharpin for example binds α-integrin subunits and thereby inhibits recruitment of talin and kindlin to the integrin (Rantala et al., 2011).

Selective inhibition of the integrin αVß5 was described to occur via PAK4 through the phosphorylation of two serine residues in a β5-specific cytoplasmic SERS motif (Li et al., 2010). However, a potential role of negative integrin regulators in RA and plaques has not yet been investigated.

To test whether stonin1 plays a role in keeping integrins clustered and possiblly active, super-resolution light microscopy of adhesions lacking stonin1 should be performed in the future.

4.5 Substrate specificity of stonin1 containing adhesions

Upon transient overexpression or one day in culture on Matrigel stonin1 shows a largely cytoplasmic localization. This observation was already described and distinguishes stonin1 fundamentally from stonin2 that shows the typical punctate staining of an endocytic adapter (Diril et al., 2006). The cytoplasmic localization comes from the fact that stonin1 localizes specifically to integrin αVß5 based reticular adhesions that are not formed during short-term culture on Matrigel. Specific ECM environments activate different integrin receptors which leads to specific cellular responses depending on the type of integrin. The integrin αVß5 was found to dominate in cell adhesions formed in long-term cultures (Lock et al., 2019). We found in addition that αVß5 adhesions emerged at sites where gelatin was degraded while the presence of gelatin prevented the formation of αVß5-positive reticular adhesions. This is in line with the recent observation that clathrin plaques formed where the substrate was degraded by matrix metalloproteinases after FA disassembly (Bucher et al., 2018b).

Bucher et al. 2018b propose that topographical cues determine the future location of clathrin plaques. At the sites where gelatin was degraded we found the typical markers of invadopodia like cortactin and dynamin. However, the presence of clathrin and αV integrin indicated a different molecular composition between invadopodia and the structures we observed since classical invadopodia contain neither clathrin nor integrin αVß5.

Since stonin1-positive reticular adhesions were found only at degradation sites and not on the gelatin itself, we hypothesized that the cell requires contact with a stiff substrate like the glass, which becomes exposed through the gelatin degradation, to trigger the formation of clathrin plaques. By introducing a scratch into the gelatin layer, we could verify that stonin1 containing adhesions formed only in the scratch. The same was seen with scratches inflicted on Matrigel hydrogels. This suggests that the recruitment of stonin1 is rather induced by stiff substrates potentially leading to frustrated endocytosis than by the degradation process itself. Since frustrated endocytosis is also found on collagen fibers (Elkhatib et al., 2017), we seeded cells on a thin high density 3D collagen matrix. We used a protocol that mimics desmoplastic tumor stroma and ensures that cells have no membrane contact to the glass.

However, in contrast to glass with its stiffness in the ∼GPa range, these collagen matrices were previously reported to have a very low stiffness (4 kPa) (Artym, 2016). Like on glass surfaces, stonin1-positive adhesions emerged within one day on HDFC matrices. Interestingly, on coverlips coated with gelatin which is nothing else than an irreversibly hydrolyzed form of collagen αVß5 integrin adhesions did not form at all. The integrin αVß5 has not been described as a receptor of collagen. Furthermore, our myoblast cell line C2C12 is characterized by the absence of endogenous collagen receptors (Tiger et al., 2001) such as α1β1, α2β1, α10β1 and α11β1 which have been shown to bind collagen (Boraschi-Diaz et al., 2017). Since αVß5 integrin adhesions also form on glass in the presence of serum, we assume that the collagen is not the major inducing factor for the assembly of these structures. In line with our results, Bucher et al. 2018b also reported clathrin plaques to form more efficiently on glass and collagen than other substrates.

The integrin αVß5 is known to bind the ECM component vitronectin (Smith et al., 1990). Vitronectin is the main adhesive protein in bovine serum with an affinity for glass and can even be purified by binding to glass bead columns (Hayman et al., 1985). In addition, it has been shown that vitronectin binds to collagen and not to laminin, fibronectin and albumin (Gebb et al., 1986). However, in our hands, the coating of glass coverslips with vitronectin resulted only in αV integrin-positive FAs without the appearance of a stonin1-positive integrin pool after one day in culture. This observation can be explained because the integrin αVß3 is the main vitronectin receptor that dominates cell adhesion of fibroblasts on vitronectin (Missirlis et al., 2016). In human skin fibroblast seeded on vitronectin the integrin αVß3 is found at focal contacts in early spreading and the integrin αVß5 emerged at focal contacts only after 2 hours (Conforti et al., 1994). The integrin αVß3 is therefore considered as the major vitronectin receptor (Missirlis et al., 2016). Moreover, the integrin αVß3 does not show a distinct, nonfocal contact distribution on the cell surface like the integrin αVß5 (Wayner et al., 1991). For the formation of clathrin plaques, not only vitronectin is required but also a stiff substrate (Baschieri et al., 2018). However, also the concentration of vitronectin in the serum might play an essential role to form plaques and other components in the serum might trigger the assembly of large stonin1-positive networks.

The depletion of the ß5 integrin led to the abolition of the stonin1-positive structures, but not to the abolition of αV integrin-positive FAs. This indicates that the remaining αV-positive FAs contain either the ß3 or ß1 integrin subunit. Nevertheless, the appearance of stonin1-positive adhesions on thin 3D collagen matrices mimicking tumor stroma suggests a specific physiological role for stonin1. In summary, stonin1-positive adhesions occur where adhesion to a substrate is required but specific integrin receptors are not present. Stiffness of the substrate could be an additional trigger that needs further investigation.

4.6 Reticular adhesion networks form in long-term culture

We found that stonin1 containing adhesions were especially formed when cells were in long-term culture. In human U2OS cells, the αVß5 integrin is the predominant integrin in long-term culture (Lock et al., 2018). Furthermore, we demonstrated that primary mouse cell lines such as astrocytes, fibroblasts, and myoblasts exhibit large reticular adhesion networks. The question naturally arose as to which aspect of long-term culture actually triggers the formation of reticular adhesion networks. On the one hand long-term culture could lead to collagen production by the cells, which might trigger frustrated endocytosis, on the other hand the cell might degrade matrix components and thereby come into contact with the glass as potential trigger of reticular adhesion formation. A third possibility is that cells reached confluence and stopped growing and migrating, which could have an effect on the formation of reticular adhesion networks. Cell growth in long-term cultures of primary astrocytes was artificially stopped with the cell-cycle inhibitor cytarabine. When cells contact each other and reach high density, they cease proliferation and cell division (Pavel et al., 2018). An additional characteristic of these confluent cells was the appearance of large stonin1 adhesion networks. Interestingly, the large networks appeared preferentially below the nucleus. This suggests that the positive stonin1 adhesion pool is able to restructure in response to environmental factors. The overall geometry of central reticular adhesions has been shown to remain substantially unchanged between generations, providing a possible mechanism for spatial memory storage (Lock et al., 2018). Large networks under the nucleus appear after cells reach confluence, and are therefore seen when cells reach the endpoint of cell growth. Due to their large size, low turnover and the occurrence in contact-inhibited cells, we assume that integrin signalling is turned off in stonin1 containing adhesions.

Integrin signaling determines cellular responses such as migration, growth, proliferation and spreading (Harburger and Calderwood, 2009). Responses that are expected to be turned off in contact-inhibited cells. Confluent cells would also lose their ability to migrate, but still need to be connected to the substrate, among others to receive the appropriate survival signals to avoid anoikis. Cell adhesion under contact inhibition would also be expected to have low integrin turnover, which is seen in stonin1-containing adhesions. In contrast to senescence, contact inhibition is reversible, so stonin1-containing adhesions could switch to adhesions with fast integrin turnover such as FAs when migration would be stimulated. The prevention of integrin signalling might therefore be a possible option for stonin1 functionality.

4.7 Stonin1 acts as a tumor suppressor

Stonin1 knockout mice grow to adulthood without phenotypic abnormalities. Similarly, the ß5 integrin knockout mice surprisingly develop, grow, and reproduce normally. Keratinocytes derived from ß5-integrin knockout mice have impaired attachment and migration on vitronectin, but healing of cutaneous wounds does not differ between wild-type and β5-knockout mice (Huang et al., 2000). Mice lacking vitronectin, the major ligand for integrin αVß5, also develop normally (Zheng et al., 1995). Therefore, cellular responses to vitronectin, which are mediated by integrin ß5 during development, wound healing, or adenovirus infection in mice appear to be compensated by other αVß5 independent signaling pathways (Huang et al., 2000). The only obvious phenotype of ß5 Integrin knockout mice is the development of age-related retinal dysfunction due to the lack of ß5 integrin-dependent phagocytosis of photoreceptors by retinal pigment epithelial cells (Nandrot et al., 2004).

There is high tissue specificity for stonin1, with the highest expression levels in the lung (Feutlinske et al., 2015). Analysis of cell type specific transcriptome profiles showed that expression of stonin1 in the lung came almost exclusively from fibroblasts and macrophages (Uhlén et al., 2015). With immunofluorescence, we showed the appearance of stonin1-positive adhesions in various primary cells. Astrocytes, fibroblasts, and myoblasts all have the ability to migrate within their respective tissue for tissue repair.

Interestingly, most tumor cell lines did not show stonin1 protein expression. Indeed, stonin1 depletion in the tumour environment increases brain tumor growth in mice (Bergmann, 2017). Supporting data using the REMBRANDT platform show that glioma patients with higher stonin1 expression survived significantly longer than patients with low stonin1 expression.

Both β3- and β5-integrins have been linked to angiogenesis because of their expression in vascular sprouts. Mice lacking both β3- and β5-integrins support tumorigenesis and have increased tumor growth due to enhanced pathological angiogenesis (Reynolds et al., 2002). Thus, by regulating integrin ß5 activity, stonin1 could control the oncogenic potential of ß5 integrin and act as a tumor suppressor. Whether stonin1 affects angiogenesis and thus tumor vascularisation needs to be further investigated.

4.8 Summary and outlook

Classical integrin-mediated cell-matrix adhesions, termed focal adhesions, have long been known and are characterized by their connection to the actin cytoskeleton. These canonical adhesions are disassembled before mitotic rounding. However, dividing cells maintain their connection to the substrate through atypical matrix adhesions. Only recently have these adhesions been termed reticular adhesions, while similar structures were previously known as clathrin plaques, and their function in mitotic respreading has been investigated (Lock et al., 2018). Interestingly, although their function was unidentified, atypical matrix adhesions were already seen 30 years ago (Wayner et al., 1991).

We are the first to describe a bona fide marker of these atypical αVß5 cell matrix adhesions that, to our present knowledge, is not found at any other cellular structure. Using stonin1 in combination with additional marker proteins, we were able to distinguish between different sub populations of these adhesions. Based on our observations, we propose to categorize the different types of αVß5 adhesion complexes in the following way: We would like to extend the recently coined term reticular adhesions to encompass all αVß5 adhesions that are negative for canonical FA markers like paxillin. Within this group, the first subtype is classified by the presence of clathrin and other endocytic adapter proteins, and is usually referred to as clathrin plaques. The second subtype is characterized neither by the absence of CME and FA proteins, and mainly positive for αVß5 and stonin1. This second type of adhesion subtype is of particular importance because it mediates conversion between clathrin plaques and FAs. Morphologically, this adhesion type occurs as retraction fibers, which are generated during cell migration and mitosis, and as large reticular adhesion patches and networks which can contain interspersed clathrin plaques. This second type of adhesion is of particular importance because it allows the rapid generation of mature FAs circumventing the canonical FA assembly process that usually starts at the tip of the lamellipodium.

While the conversion of FAs to clathrin plaques has been described previously (Bucher et al., 2018b; Dix et al., 2018), we are the first to observe the conversion of retraction fibers into FAs. This conversion seems to be important for mitotic respreading. Indeed, we demonstrated that cells can use their retraction fibers after mitosis to assemble new FAs. Therefore, we can expand the function of these adhesions beyond spatial memory and adhesion in mitosis. We were astounded by the observation that reticular adhesions do not seem to form on matrigel or gelatin at all. On the other side, glass and collagen seem to favor the formation of reticular adhesions. At adhesions, cells exert traction on the substrate. Presumably, little traction forces are exerted on soft hydrogels. It will be important to check to what extent traction force is required for cell division and reticular adhesions in general. We are also not sure how stiff our generated collagen matrix actually is.

The centrifugation of high density collagen on coverslips mimics tumor stroma (Artym, 2016). Stiff collagen fibrils from tumors are used by malignant cells to facilitate tumor escape (Butcher et al., 2009). Tensile force measurements and gel contraction experiments may indicate whether stonin1 depleted cells have a defect in stiffness recognition and actomyosin contraction generation.

We were also wondering why some cell lines do not seem to express stonin1 but display clathrin plaques. For example, we did not find stonin1-positive reticular adhesion sites in HeLa cells, even though HeLa cells were studied extensively for clathrin plaques (Baschieri et al., 2018; Leyton-Puig et al., 2017). In contrast, we could identify stonin1-positive adhesions in U2OS cells that displayed stonin1-positive networks. In fact, stonin1 and stonin2 were found in the reticular adhesome of U2OS cells (Lock et al., 2018).

Recently, it was found that two different types of division systems exist in human cells in culture (Dix et al., 2018). The first is characterized by excessive cell rounding without the aid of adhesions for division, as seen in HeLa cells, and the second relies on the interaction with the extracellular environment to divide (Dix et al., 2018). Interestingly HeLa cells can divide in suspension, possibly by oncogenic signalling that overrides the need for adhesions (Dix et al., 2018).

Our CRISPR cell line C2C12 never showed cell rounding and therefore appears to be completely dependent on adhesions for cell division. Further experiments need to be performed to determine if stonin1 plays a role in adhesion-dependent mitosis. It would be interesting to see if overexpression of stonin1 in HeLa cells would reduce cell rounding.

Depletion of stonin1 leads to impaired actin recruitment to clathrin plaques. Furthermore, stonin1 shows overlap with both clathrin and actin stress fibers by immunofluorescence and correlative light-electron microscopy. This suggests a previously undiscovered link between the actin cytoskeleton and RAs. As FA adapters connect the cytoskeleton to the substrate, stonin1 could be an adapter for reticular adhesions, connecting them to the actin cytoskeleton. Therefore, to further investigate stonin1 dependent actin recruitment, potential interaction partners need to be evaluated in the future.

References

Justen Andrew, Michiko Smith, John Merakovsky, Michelle Coulson, Frances Hannan, and Leonard E Kelly. The stoned locus of drosophila melanogaster produces a dicistronic transcript and encodes two distinct polypeptides. *Genetics*, 143(4):1699–1711, 1996.

Vira V Artym. Preparation of high-density fibrillar collagen matrices that mimic desmoplastic tumor stroma. *Current protocols in cell biology*, 70(1):10–19, 2016.

Daniel Axelrod. Cell-substrate contacts illuminated by total internal reflection fluorescence. *Journal of Cell Biology*, 89(1):141–145, 1981.

Alexia I Bachir, Jessica Zareno, Konstadinos Moissoglu, Edward F Plow, Enrico Gratton, and Alan R Horwitz. Integrin-associated complexes form hierarchically with variable stoichiometry in nascent adhesions. *Current Biology*, 24(16):1845–1853, 2014.

Alexia I Bachir, Alan Rick Horwitz, W James Nelson, and Julie M Bianchini. Actin-based adhesion modules mediate cell interactions with the extracellular matrix and neighboring cells. *Cold Spring Harbor perspectives in biology*, 9(7):a023234, 2017.

Michael Bachmann, Sampo Kukkurainen, Vesa P Hytönen, and Bernhard Wehrle-Haller. Cell adhesion by integrins. *Physiological reviews*, 99(4):1655–1699, 2019.

Linda J Ball, Ronald Kühne, Jens Schneider-Mergener, and Hartmut Oschkinat. Recognition of proline-rich motifs by protein–protein-interaction domains. *Angewandte Chemie International Edition*, 44(19):2852–2869, 2005.

Francesco Baschieri, Stéphane Dayot, Nadia Elkhatib, Nathalie Ly, Anahi Capmany, Kristine Schauer, Timo Betz, Danijela Matic Vignjevic, Renaud Poincloux, and Guillaume Montagnac. Frustrated endocytosis controls contractility-independent mechanotransduction at clathrin-coated structures. *Nature communications*, 9(1): 1–13, 2018.

Marietta Bergmann. *The endocytic adaptor stonin 1 regulates cell signalling and focal adhesion dynamics*. PhD thesis, Free University of Berlin, 2017.

Vassilis Bitsikas, Ivan R Corrêa Jnr, and Benjamin J Nichols. Correction: Clathrin-independent pathways do not contribute significantly to endocytic flux. *Elife*, 3, jul 2021.

Iris Boraschi-Diaz, Jennifer Wang, John S Mort, and Svetlana V Komarova. Collagen type i as a ligand for receptor-mediated signaling. *Frontiers in Physics*, 5:12, 2017.

Steeve Boulant, Comert Kural, Jean-Christophe Zeeh, Florent Ubelmann, and Tomas Kirchhausen. Actin dynamics counteract membrane tension during clathrin-mediated endocytosis. *Nature cell biology*, 13(9):1124–1131, 2011.

Marion M Bradford. A rapid and sensitive method for the quantitation of microgram quantities of protein utilizing the principle of protein-dye binding. *Analytical biochemistry*, 72(1-2):248–254, 1976.

Delia Bucher, Felix Frey, Kem A Sochacki, Susann Kummer, Jan-Philip Bergeest, William J Godinez, Hans-Georg Kräusslich, Karl Rohr, Justin W Taraska, Ulrich S Schwarz, et al. Clathrin-adaptor ratio and membrane tension regulate the flat-to-curved transition of the clathrin coat during endocytosis. *Nature communications*, 9 (1):1–13, 2018a.

Delia Bucher, Markus Mukenhirn, Kem A Sochacki, Veronika Saharuka, Christian Huck, Chiara Zambarda, Justin W Taraska, Elisabetta Ada Cavalcanti-Adam, and Steeve Boulant. Focal adhesion-generated cues in extracellular matrix regulate cell migration by local induction of clathrin-coated plaques. *bioRxiv*, page 493114, 2018b.

Keith Burridge and Magdalena Chrzanowska-Wodnicka. Focal adhesions, contractility, and signaling. *Annual review of cell and developmental biology*, 12(1):463–519, 1996.

Darci T Butcher, Tamara Alliston, and Valerie M Weaver. A tense situation: forcing tumour progression. *Nature Reviews Cancer*, 9(2):108–122, 2009.

DA Calderwood. Talin controls integrin activation. *Biochemical Society Transactions*, 32(3):434–437, 2004.

Lindsay B Case and Clare M Waterman. Integration of actin dynamics and cell adhesion by a three-dimensional, mechanosensitive molecular clutch. *Nature cell biology*, 17 (8):955–963, 2015.

Wei-Ting Chao and Jeannette Kunz. Focal adhesion disassembly requires clathrin-dependent endocytosis of integrins. *FEBS letters*, 583(8):1337–1343, 2009.

Wei-Ting Chao, Felicity Ashcroft, Alexes C Daquinag, Tegy Vadakkan, Zhubo Wei, Pumin Zhang, Mary E Dickinson, and Jeannette Kunz. Type i phosphatidylinositol phosphate kinase beta regulates focal adhesion disassembly by promoting β1 integrin endocytosis. *Molecular and cellular biology*, 30(18):4463–4479, 2010.

Colin K Choi, Miguel Vicente-Manzanares, Jessica Zareno, Leanna A Whitmore, Alex Mogilner, and Alan Rick Horwitz. Actin and α-actinin orchestrate the assembly and maturation of nascent adhesions in a myosin ii motor-independent manner. *Nature cell biology*, 10(9):1039–1050, 2008.

Caroline Cluzel, Frédéric Saltel, Jost Lussi, Frédérique Paulhe, Beat A Imhof, and Bernhard Wehrle-Haller. The mechanisms and dynamics of αvβ3 integrin clustering in living cells. *The Journal of cell biology*, 171(2):383–392, 2005.

Brett M Collins, Airlie J McCoy, Helen M Kent, Philip R Evans, and David J Owen. Molecular architecture and functional model of the endocytic ap2 complex. *Cell*, 109 (4):523–535, 2002.

Holly Colognato et al. Integrins: versatile integrators of extracellular signals. *Trends in cell biology*, 14(12):678–686, 2004.

Grazia Conforti, Mariagrazia Calza, and Amada Beltrán-nuñez. αvβ5 integrin is localized at focal contacts by ht-1080 fibrosarcoma cells and human skin fibroblasts attached to vitronectin. *Cell adhesion and communication*, 1(4):279–293, 1994.

Le Cong, F Ann Ran, David Cox, Shuailiang Lin, Robert Barretto, Naomi Habib, Patrick D Hsu, Xuebing Wu, Wenyan Jiang, Luciano A Marraffini, et al. Multiplex genome engineering using crispr/cas systems. *Science*, 339(6121):819–823, 2013.

David K Cureton, Ramiro H Massol, Sean PJ Whelan, and Tomas Kirchhausen. The length of vesicular stomatitis virus particles dictates a need for actin assembly during clathrin-dependent endocytosis. *PLoS pathogens*, 6(9):e1001127, 2010.

Joseph D'alessandro, Alex Barbier, Victor Cellerin, Olivier Benichou, René Marc Mège, Raphaël Voituriez, Benoit Ladoux, et al. Cell migration guided by long-lived spatial memory. *Nature Communications*, 12(1):1–10, 2021.

Oliver Daumke, Aurélien Roux, and Volker Haucke. Bar domain scaffolds in dynamin-mediated membrane fission. *Cell*, 156(5):882–892, 2014.

Nicola De Franceschi, Antti Arjonen, Nadia Elkhatib, Konstantin Denessiouk, Antoni G Wrobel, Thomas A Wilson, Jeroen Pouwels, Guillaume Montagnac, David J Owen, and Johanna Ivaska. Selective integrin endocytosis is driven by interactions between the integrin α-chain and ap2. *Nature structural & molecular biology*, 23(2):172–179, 2016.

Kasim Diril. *Genetic analysis of stoned B/stonin 2 function in vivo*. PhD thesis, Georg-August-University Goettingen, 2004.

M Kasim Diril, Martin Wienisch, Nadja Jung, Jürgen Klingauf, and Volker Haucke. Stonin 2 is an ap-2-dependent endocytic sorting adaptor for synaptotagmin internalization and recycling. *Developmental cell*, 10(2):233–244, 2006.

Jeremy Dittman and Timothy A Ryan. Molecular circuitry of endocytosis at nerve terminals. *Annu. Rev. Cell Dev. Biol.*, 25(1):133–160, jul 2021.

Christina L Dix, Helen K Matthews, Marina Uroz, Susannah McLaren, Lucie Wolf, Nicholas Heatley, Zaw Win, Pedro Almada, Ricardo Henriques, Michael Boutros, et al. The role of mitotic cell-substrate adhesion re-modeling in animal cell division. *Developmental cell*, 45(1):132–145, 2018.

Arthur Edelstein, Nenad Amodaj, Karl Hoover, Ron Vale, and Nico Stuurman. Computer control of microscopes using μmanager. *Current protocols in molecular biology*, 92(1):14–20, 2010.

Nadia Elkhatib, Enzo Bresteau, Francesco Baschieri, Alba López Rioja, Guillaume van Niel, Stéphane Vassilopoulos, and Guillaume Montagnac. Tubular clathrin/ap-2 lattices pinch collagen fibers to support 3d cell migration. *Science*, 356(6343), 2017.

Patricia S Estes, Taryn C Jackson, Daniel T Stimson, Subhabrata Sanyal, Leonard E Kelly, and Mani Ramaswami. Functional dissection of a eukaryotic dicistronic gene: transgenic stonedb, but not stoneda, restores normal synaptic properties to drosophila stoned mutants. *Genetics*, 165(1):185–196, 2003.

Ellen J Ezratty, Claire Bertaux, Eugene E Marcantonio, and Gregg G Gundersen. Clathrin mediates integrin endocytosis for focal adhesion disassembly in migrating cells. *Journal of Cell Biology*, 187(5):733–747, 2009.

Tim Fergestad, Warren S Davis, and Kendal Broadie. The stoned proteins regulate synaptic vesicle recycling in the presynaptic terminal. *Journal of Neuroscience*, 19 (14):5847–5860, 1999.

Fabian Feutlinske. *Stonin 1 facilitates endocytosis of NG2 and regulates signaling and cellular motility.* PhD thesis, Free University of Berlin, 2014.

Fabian Feutlinske, Marietta Browarski, Min-Chi Ku, Philipp Trnka, Sonia Waiczies, Thoralf Niendorf, William B Stallcup, Rainer Glass, Eberhard Krause, and Tanja Maritzen. Stonin1 mediates endocytosis of the proteoglycan ng2 and regulates focal adhesion dynamics and cell motility. *Nature communications*, 6(1):1–13, 2015.

Andrew B Fielding and Stephen J Royle. Mitotic inhibition of clathrin-mediated endocytosis. *Cellular and molecular life sciences*, 70(18):3423–3433, 2013.

Juehua Gao, Jie Liao, and Guang-Yu Yang. Caax-box protein, prenylation process and carcinogenesis. *American journal of translational research*, 1(3):312, 2009.

Camilo Garay, Gurjeet Judge, Stefanie Lucarelli, Stephen Bautista, Rohan Pandey, Tanveer Singh, and Costin N Antonescu. Epidermal growth factor–stimulated akt phosphorylation requires clathrin or erbb2 but not receptor endocytosis. *Molecular biology of the cell*, 26(19):3504–3519, 2015.

C Gebb, Edward G Hayman, E Engvall, and E Ruoslahti. Interaction of vitronectin with collagen. *Journal of Biological Chemistry*, 261(35):16698–16703, 1986.

Benjamin Geiger and Kenneth M Yamada. Molecular architecture and function of matrix adhesions. *Cold Spring Harbor perspectives in biology*, 3(5):a005033, 2011.

Thomas A Grigliatti, Linda Hall, Raja Rosenbluth, and David T Suzuki. Temperature-sensitive mutations in drosophila melanogaster. *Molecular and General Genetics MGG*, 120(2):107–114, 1973.

Joe Grove, Daniel J Metcalf, Alex E Knight, Silène T Wavre-Shapton, Tony Sun, Emmanouil D Protonotarios, Lewis D Griffin, Jennifer Lippincott-Schwartz, and Mark Marsh. Flat clathrin lattices: stable features of the plasma membrane. *Molecular biology of the cell*, 25(22):3581–3594, 2014.

Wei-hui Guo and Yu-li Wang. Retrograde fluxes of focal adhesion proteins in response to cell migration and mechanical signals. *Molecular biology of the cell*, 18(11):4519–4527, 2007.

Natalia Gustavsson and Weiping Han. Calcium-sensing beyond neurotransmitters: functions of synaptotagmins in neuroendocrine and endocrine secretion. *Bioscience reports*, 29(4):245–259, 2009.

David S Harburger and David A Calderwood. Integrin signalling at a glance. *Journal of cell science*, 122(2):159–163, 2009.

Madeleine Hart, Ihsan Zulkipli, Roshan Lal Shrestha, David Dang, Duccio Conti, Parveen Gul, Izabela Kujawiak, and Viji M Draviam. Mark2/par1b kinase present at centrosomes and retraction fibres corrects spindle off-centring induced by actin disassembly. *Open biology*, 9(6):180263, 2019.

Edward G Hayman, Michael D Pierschbacher, Shintaro Suzuki, and Erkki Ruoslahti. Vitronectin—a major cell attachment-promoting protein in fetal bovine serum. *Experimental cell research*, 160(2):245–258, 1985.

John Heuser. Three-dimensional visualization of coated vesicle formation in fibroblasts. *The Journal of cell biology*, 84(3):560–583, 1980.

Jennifer Hirst and Margaret S Robinson. Clathrin and adaptors. *Biochimica et Biophysica Acta (BBA)-Molecular Cell Research*, 1404(1-2):173–193, 1998.

Edward R Horton, Adam Byron, Janet A Askari, Daniel HJ Ng, Angélique Millon-Frémillon, Joseph Robertson, Ewa J Koper, Nikki R Paul, Stacey Warwood, David Knight, et al. Definition of a consensus integrin adhesome and its dynamics during adhesion complex assembly and disassembly. *Nature cell biology*, 17(12):1577–1587, 2015.

Ke Hu, Lin Ji, Kathryn T Applegate, Gaudenz Danuser, and Clare M Waterman-Storer. Differential transmission of actin motion within focal adhesions. *Science*, 315(5808): 111–115, 2007.

Xiaozhu Huang, Mark Griffiths, Jianfeng Wu, Robert V Farese Jr, and Dean Sheppard. Normal development, wound healing, and adenovirus susceptibility in β5-deficient mice. *Molecular and cellular biology*, 20(3):755–759, 2000.

Florian Huber, Adeline Boire, Magdalena Preciado López, and Gijsje H Koenderink. Cytoskeletal crosstalk: when three different personalities team up. *Current opinion in cell biology*, 32:39–47, 2015.

Jonathan D Humphries, Megan R Chastney, Janet A Askari, and Martin J Humphries. Signal transduction via integrin adhesion complexes. *Current opinion in cell biology*, 56:14–21, 2019.

Anna Huttenlocher and Alan Rick Horwitz. Integrins in cell migration. *Cold Spring Harbor perspectives in biology*, 3(9):a005074, 2011.

Richard O Hynes. Integrins: bidirectional, allosteric signaling machines. *cell*, 110(6): 673–687, 2002.

Richard O Hynes. The extracellular matrix: not just pretty fibrils. *Science*, 326(5957): 1216–1219, 2009.

Guillaume Jacquemet and Johanna Ivaska. Mitosis-resistant adhesions provide molecular memory to dividing cells. *Developmental cell*, 45(1):5–7, 2018.

Matthew C Jones, Janet A Askari, Jonathan D Humphries, and Martin J Humphries. Cell adhesion is regulated by cdk1 during the cell cycle. *Journal of Cell Biology*, 217 (9):3203–3218, 2018.

Marko Kaksonen and Aurélien Roux. Mechanisms of clathrin-mediated endocytosis. *Nat. Rev. Mol. Cell Biol.*, 19(5):313–326, jul 2021.

Marko Kaksonen, Christopher P Toret, and David G Drubin. Harnessing actin dynamics for clathrin-mediated endocytosis. *Nature reviews Molecular cell biology*, 7(6):404–414, 2006.

Pakorn Kanchanawong, Gleb Shtengel, Ana M Pasapera, Ericka B Ramko, Michael W Davidson, Harald F Hess, and Clare M Waterman. Nanoscale architecture of integrin-based cell adhesions. *Nature*, 468(7323):580–584, 2010.

Ingyu Kim, Weijun Pan, Sara A Jones, Youxin Zhang, Xiaowei Zhuang, and Dianqing Wu. Clathrin and ap2 are required for ptdins (4, 5) p2-mediated formation of lrp6 signalosomes. *Journal of Cell Biology*, 200(4):419–428, 2013.

Tom Kirchhausen. Imaging endocytic clathrin structures in living cells. *Trends in cell biology*, 19(11):596–605, 2009.

Tomas Kirchhausen and Stephen C Harrison. Protein organization in clathrin trimers. *Cell*, 23(3):755–761, 1981.

Jean-Cheng Kuo, Xuemei Han, Cheng-Te Hsiao, John R Yates III, and Clare M Waterman. Analysis of the myosin-ii-responsive focal adhesion proteome reveals a role for β-pix in negative regulation of focal adhesion maturation. *Nature cell biology*, 13(4):383–393, 2011.

Natalya Kurochkina and Udayan Guha. Sh3 domains: modules of protein–protein interactions. *Biophysical reviews*, 5(1):29–39, 2013.

Ulrich K Laemmli. Cleavage of structural proteins during the assembly of the head of bacteriophage t4. *nature*, 227(5259):680–685, 1970.

Marko Lampe, Stéphane Vassilopoulos, and Christien Merrifield. Clathrin coated pits, plaques and adhesion. *Journal of structural biology*, 196(1):48–56, 2016.

Hui Jun Lee, Gek Huey Chua, Arun Krishnan, David P Lane, and Chandra S Verma. Substrate specificity of cyclins determined by electrostatics. *Cell Cycle*, 6(18):2219–2226, 2007.

Martin Lehmann, Ilya Lukonin, Frank Noé, Jan Schmoranzer, Cecilia Clementi, Dinah Loerke, and Volker Haucke. Nanoscale coupling of endocytic pit growth and stability. *Sci. Adv.*, 5(11):eaax5775, jul 2021.

Daniela Leyton-Puig, Tadamoto Isogai, Elisabetta Argenzio, Bram Van Den Broek, Jeffrey Klarenbeek, Hans Janssen, Kees Jalink, and Metello Innocenti. Flat clathrin lattices are dynamic actin-controlled hubs for clathrin-mediated endocytosis and signalling of specific receptors. *Nature communications*, 8(1):1–14, 2017.

Zhilun Li, John G Lock, Helene Olofsson, Jacob M Kowalewski, Steffen Teller, Yajuan Liu, Hongquan Zhang, and Staffan Strömblad. Integrin-mediated cell attachment induces a pak4-dependent feedback loop regulating cell adhesion through modified integrin αvβ5 clustering and turnover. *Molecular biology of the cell*, 21(19):3317–3329, 2010.

John G Lock, Matthew C Jones, Janet A Askari, Xiaowei Gong, Anna Oddone, Helene Olofsson, Sara Göransson, Melike Lakadamyali, Martin J Humphries, and Staffan Strömblad. Reticular adhesions are a distinct class of cell-matrix adhesions that mediate attachment during mitosis. *Nature cell biology*, 20(11):1290–1302, 2018.

John G Lock, Francesco Baschieri, Matthew C Jones, Jonathan D Humphries, Guillaume Montagnac, Staffan Strömblad, and Martin J Humphries. Clathrin-containing adhesion complexes. *Journal of Cell Biology*, 218(7):2086–2095, 2019.

Tania López-Hernández, Dmytro Puchkov, Eberhard Krause, Tanja Maritzen, and Volker Haucke. Endocytic regulation of cellular ion homeostasis controls lysosome biogenesis. *Nature Cell Biology*, 22(7):815–827, 2020.

Tanja Maritzen, Jasmin Podufall, and Volker Haucke. Stonins—specialized adaptors for synaptic vesicle recycling and beyond? *Traffic*, 11(1):8–15, 2010.

Tanja Maritzen, Hannah Schachtner, and Daniel F Legler. On the move: endocytic trafficking in cell migration. *Cellular and Molecular Life Sciences*, 72(11):2119–2134, 2015.

José A Martina, Cecilia J Bonangelino, Rubén C Aguilar, and Juan S Bonifacino. Stonin 2an adaptor-like protein that interacts with components of the endocytic machinery. *The Journal of cell biology*, 153(5):1111–1120, 2001.

Frank M Mason and Scott H Soderling. Wasp and wave family protein complexes. In *Handbook of Cell Signaling*, pages 1265–1270. Elsevier, 2010.

Harvey T McMahon and Emmanuel Boucrot. Molecular mechanism and physiological functions of clathrin-mediated endocytosis. *Nature reviews Molecular cell biology*, 12 (8):517–533, 2011.

Claire McQuin, Allen Goodman, Vasiliy Chernyshev, Lee Kamentsky, Beth A Cimini, Kyle W Karhohs, Minh Doan, Liya Ding, Susanne M Rafelski, Derek Thirstrup, et al. Cellprofiler 3.0: Next-generation image processing for biology. *PLoS biology*, 16(7): e2005970, 2018.

Michael Melak, Matthias Plessner, and Robert Grosse. Actin visualization at a glance. *Journal of cell science*, 130(3):525–530, 2017.

Dimitris Missirlis, Tamás Haraszti, Catharina v C Scheele, Tina Wiegand, Carolina Diaz, Stefanie Neubauer, Florian Rechenmacher, Horst Kessler, and Joachim P Spatz. Substrate engagement of integrins α 5 β 1 and α v β 3 is necessary, but not sufficient, for high directional persistence in migration on fibronectin. *Scientific reports*, 6(1): 1–18, 2016.

TJ Mitchison and LP Cramer. Actin-based cell motility and cell locomotion. *Cell*, 84 (3):371–379, 1996.

Gilles Moulay, Jeanne Lainé, Mégane Lemaître, Masayuki Nakamori, Ichizo Nishino, Ghislaine Caillol, Kamel Mamchaoui, Laura Julien, Florent Dingli, Damarys Loew, et al. Alternative splicing of clathrin heavy chain contributes to the switch from coated pits to plaques. *Journal of Cell Biology*, 219(9):e201912061, 2020.

Danielle A Murphy and Sara A Courtneidge. The'ins' and'outs' of podosomes and invadopodia: characteristics, formation and function. *Nature reviews Molecular cell biology*, 12(7):413–426, 2011.

Emeline F Nandrot, Yoonhee Kim, Scott E Brodie, Xiaozhu Huang, Dean Sheppard, and Silvia C Finnemann. Loss of synchronized retinal phagocytosis and age-related blindness in mice lacking $\alpha v\beta 5$ integrin. *The Journal of experimental medicine*, 200 (12):1539–1545, 2004.

Thomas Orré, Adrien Joly, Zeynep Karatas, Birgit Kastberger, Clément Cabriel, Ralph T Böttcher, Sandrine Lévêque-Fort, Jean-Baptiste Sibarita, Reinhard Fässler, Bernhard Wehrle-Haller, et al. Molecular motion and tridimensional nanoscale localization of kindlin control integrin activation in focal adhesions. *Nature communications*, 12(1):1–17, 2021.

Nobuyuki Otsu. A threshold selection method from gray-level histograms. *IEEE transactions on systems, man, and cybernetics*, 9(1):62–66, 1979.

J Thomas Parsons, Alan Rick Horwitz, and Martin A Schwartz. Cell adhesion: integrating cytoskeletal dynamics and cellular tension. *Nature reviews Molecular cell biology*, 11(9):633–643, 2010.

Mariana Pavel, Maurizio Renna, So Jung Park, Fiona M Menzies, Thomas Ricketts, Jens Füllgrabe, Avraham Ashkenazi, Rebecca A Frake, Alejandro Carnicer Lombarte, Carla F Bento, et al. Contact inhibition controls cell survival and proliferation via yap/taz-autophagy axis. *Nature communications*, 9(1):1–18, 2018.

Raven J Peterson and Michael Koval. Above the matrix: Functional roles for apically localized integrins. *Frontiers in Cell and Developmental Biology*, 9, 2021.

A Ponti, M Machacek, SL Gupton, CM Waterman-Storer, and G Danuser. Two distinct actin networks drive the protrusion of migrating cells. *Science*, 305(5691):1782–1786, 2004.

York Posor, Marielle Eichhorn-Grünig, and Volker Haucke. Phosphoinositides in endocytosis. *Biochimica Et Biophysica Acta (BBA)-Molecular and Cell Biology of Lipids*, 1851(6):794–804, 2015.

Juha K Rantala, Jeroen Pouwels, Teijo Pellinen, Stefan Veltel, Petra Laasola, Elina Mattila, Christopher S Potter, Ted Duffy, John P Sundberg, Olli Kallioniemi, et al. Sharpin is an endogenous inhibitor of β1-integrin activation. *Nature cell biology*, 13 (11):1315–1324, 2011.

Louise E Reynolds, Lorenza Wyder, Julie C Lively, Daniela Taverna, Stephen D Robinson, Xiaozhu Huang, Dean Sheppard, Richard O Hynes, and Kairbaan M Hodivala-Dilke. Enhanced pathological angiogenesis in mice lacking β 3 integrin or β 3 and β 5 integrins. *Nature medicine*, 8(1):27–34, 2002.

Olivier Rossier, Vivien Octeau, Jean-Baptiste Sibarita, Cecile Leduc, Béatrice Tessier, Deepak Nair, Volker Gatterdam, Olivier Destaing, Corinne Albiges-Rizo, Robert Tampé, et al. Integrins β 1 and β 3 exhibit distinct dynamic nanoscale organizations inside focal adhesions. *Nature cell biology*, 14(10):1057–1067, 2012.

Saveez Saffarian, Emanuele Cocucci, and Tomas Kirchhausen. Distinct dynamics of endocytic clathrin-coated pits and coated plaques. *PLoS biology*, 7(9):e1000191, 2009.

Randall K Saiki, David H Gelfand, Susanne Stoffel, Stephen J Scharf, Russell Higuchi, Glenn T Horn, Kary B Mullis, and Henry A Erlich. Primer-directed enzymatic amplification of dna with a thermostable dna polymerase. *Science*, 239(4839):487–491, 1988.

Fred Sanger and Alan R Coulson. A rapid method for determining sequences in dna by primed synthesis with dna polymerase. *Journal of molecular biology*, 94(3):441–448, 1975.

Herbert B Schiller, Caroline C Friedel, Cyril Boulegue, and Reinhard Fässler. Quantitative proteomics of the integrin adhesome show a myosin ii-dependent recruitment of lim domain proteins. *EMBO reports*, 12(3):259–266, 2011.

Johannes Schindelin, Ignacio Arganda-Carreras, Erwin Frise, Verena Kaynig, Mark Longair, Tobias Pietzsch, Stephan Preibisch, Curtis Rueden, Stephan Saalfeld, Benjamin Schmid, et al. Fiji: an open-source platform for biological-image analysis. *Nature methods*, 9(7):676–682, 2012.

Sanford J Shattil, Chungho Kim, and Mark H Ginsberg. The final steps of integrin activation: the end game. *Nature reviews Molecular cell biology*, 11(4):288–300, 2010.

JW Smith, DJ Vestal, Sally V Irwin, Timothy A Burke, and David A Cheresh. Purification and functional characterization of integrin alpha v beta 5. an adhesion receptor for vitronectin. *Journal of Biological Chemistry*, 265(19):11008–11013, 1990.

Tolga Soykan, Natalie Kaempf, Takeshi Sakaba, Dennis Vollweiter, Felix Goerdeler, Dmytro Puchkov, Natalia L Kononenko, and Volker Haucke. Synaptic vesicle endocytosis occurs on multiple timescales and is mediated by formin-dependent actin assembly. *Neuron*, 93(4):854–866.e4, jul 2021.

Matthias Spiess, Pablo Hernandez-Varas, Anna Oddone, Helene Olofsson, Hans Blom, Dominic Waithe, John G Lock, Melike Lakadamyali, and Staffan Strömblad. Active and inactive $\beta 1$ integrins segregate into distinct nanoclusters in focal adhesions. *Journal of Cell Biology*, 217(6):1929–1940, 2018.

Samantha Stehbens and Torsten Wittmann. Targeting and transport: how microtubules control focal adhesion dynamics. *Journal of Cell Biology*, 198(4):481–489, 2012.

Zhiqi Sun, Armin Lambacher, and Reinhard Fässler. Nascent adhesions: from fluctuations to a hierarchical organization. *Current Biology*, 24(17):R801–R803, 2014.

Zhiqi Sun, Hui-Yuan Tseng, Steven Tan, Fabrice Senger, Laetitia Kurzawa, Dirk Dedden, Naoko Mizuno, Anita A Wasik, Manuel Thery, Alexander R Dunn, et al. Kank2 activates talin, reduces force transduction across integrins and induces central adhesion formation. *Nature cell biology*, 18(9):941–953, 2016.

Zhiqi Sun, Mercedes Costell, and Reinhard Fässler. Integrin activation by talin, kindlin and mechanical forces. *Nature cell biology*, 21(1):25–31, 2019.

Sharon M Sweitzer and Jenny E Hinshaw. Dynamin undergoes a gtp-dependent conformational change causing vesiculation. *Cell*, 93(6):1021–1029, 1998.

Carl-Fredrik Tiger, Francoise Fougerousse, Gunilla Grundström, Teet Velling, and Donald Gullberg. $\alpha 11\beta 1$ integrin is a receptor for interstitial collagens involved in cell migration and collagen reorganization on mesenchymal nonmuscle cells. *Developmental biology*, 237(1):116–129, 2001.

Antonia Tomas-Loba, Elisa Manieri, Barbara Gonzalez-Teran, Alfonso Mora, Luis Leiva-Vega, Ayelen M Santamans, Rafael Romero-Becerra, Elena Rodríguez, Aránzazu Pintor-Chocano, Ferran Feixas, et al. p38gamma is essential for cell cycle progression and liver tumorigenesis. *Nature*, 568(7753):557–560, 2019.

Raffi Tonikian, Xiaofeng Xin, Christopher P Toret, David Gfeller, Christiane Landgraf, Simona Panni, Serena Paoluzi, Luisa Castagnoli, Bridget Currell, Somasekar Seshagiri, et al. Bayesian modeling of the yeast sh3 domain interactome predicts spatiotemporal dynamics of endocytosis proteins. *PLoS biology*, 7(10):e1000218, 2009.

Linton M Traub. Tickets to ride: selecting cargo for clathrin-regulated internalization. *Nature reviews Molecular cell biology*, 10(9):583–596, 2009.

Linton M Traub and Juan S Bonifacino. Cargo recognition in clathrin-mediated endocytosis. *Cold Spring Harbor perspectives in biology*, 5(11):a016790, 2013.

Mathias Uhlén, Linn Fagerberg, Björn M Hallström, Cecilia Lindskog, Per Oksvold, Adil Mardinoglu, Åsa Sivertsson, Caroline Kampf, Evelina Sjöstedt, Anna Asplund, et al. Tissue-based map of the human proteome. *Science*, 347(6220), 2015.

Ernst Ungewickell, Huberta Ungewickell, Susanne EH Holstein, Robert Lindner, Kondury Prasad, Winifred Barouch, Brian Martini, Lois E Greene, and Evan Eisenberg. Role of auxilin in uncoating clathrin-coated vesicles. *Nature*, 378(6557): 632–635, 1995.

Stéphane Vassilopoulos, Christel Gentil, Jeanne Lainé, Pierre-Olivier Buclez, Agathe Franck, Arnaud Ferry, Guillaume Précigout, Robyn Roth, John E Heuser, Frances M Brodsky, et al. Actin scaffolding by clathrin heavy chain is required for skeletal muscle sarcomere organization. *Journal of Cell Biology*, 205(3):377–393, 2014.

Miguel Vicente-Manzanares, Colin Kiwon Choi, and Alan Rick Horwitz. Integrins in cell migration–the actin connection. *Journal of cell science*, 122(2):199–206, 2009.

Kristin Walther, Michael Krauss, M Kasim Diril, Steffen Lemke, Doris Ricotta, Stefan Höning, Stephen Kaiser, and Volker Haucke. Human stoned b interacts with ap-2 and synaptotagmin and facilitates clathrin-coated vesicle uncoating. *EMBO reports*, 3(2):197–197, 2002.

Elizabeth A Wayner, Robert A Orlando, and David A Cheresh. Integrins alpha v beta 3 and alpha v beta 5 contribute to cell attachment to vitronectin but differentially distribute on the cell surface. *Journal of Cell Biology*, 113(4):919–929, 1991.

Nathan Wlodarchak and Yongna Xing. Pp2a as a master regulator of the cell cycle. *Critical reviews in biochemistry and molecular biology*, 51(3):162–184, 2016.

Cheng-Guo Wu, Hui Chen, Feng Guo, Vikash K Yadav, Sean J Mcilwain, Michael Rowse, Alka Choudhary, Ziqing Lin, Yitong Li, Tingjia Gu, et al. Pp2a-b holoenzyme substrate recognition, regulation and role in cytokinesis. *Cell discovery*, 3(1):1–19, 2017.

Kenneth M Yamada and Benjamin Geiger. Molecular interactions in cell adhesion complexes. *Current opinion in cell biology*, 9(1):76–85, 1997.

Masashi Yamada, Gabriele Mugnai, Satoshi Serada, Yoshiko Yagi, Tetsuji Naka, and Kiyotoshi Sekiguchi. Substrate-attached materials are enriched with tetraspanins and are analogous to the structures associated with rear-end retraction in migrating cells. *Cell adhesion & migration*, 7(3):304–314, 2013.

Sawako Yamashiro and Naoki Watanabe. A new link between the retrograde actin flow and focal adhesions. *The Journal of Biochemistry*, 156(5):239–248, 2014.

Defne Yarar, Clare M Waterman-Storer, and Sandra L Schmid. A dynamic actin cytoskeleton functions at multiple stages of clathrin-mediated endocytosis. *Molecular biology of the cell*, 16(2):964–975, 2005.

Jian Ye, George Coulouris, Irena Zaretskaya, Ioana Cutcutache, Steve Rozen, and Thomas L Madden. Primer-blast: a tool to design target-specific primers for polymerase chain reaction. *BMC bioinformatics*, 13(1):1–11, 2012.

Ronen Zaidel-Bar. Atypical matrix adhesions guide cell division. *Nature cell biology*, 20 (11):1233–1235, 2018.

Eli Zamir and Benjamin Geiger. Molecular complexity and dynamics of cell-matrix adhesions. *Journal of cell science*, 114(20):3583–3590, 2001.

Xianxian Zheng, Thomas L Saunders, Sally A Camper, Linda C Samuelson, and David Ginsburg. Vitronectin is not essential for normal mammalian development and fertility. *Proceedings of the National Academy of Sciences*, 92(26):12426–12430, 1995.

Alba Zuidema, Wei Wang, Maaike Kreft, Lisa Te Molder, Liesbeth Hoekman, Onno B Bleijerveld, Leila Nahidiazar, Hans Janssen, and Arnoud Sonnenberg. Mechanisms of integrin αvβ5 clustering in flat clathrin lattices. *Journal of cell science*, 131(21): jcs221317, 2018.

List of Figures

List of Tables

Appendix

A. List of Abbreviations

3D	three-dimensional
AA	amino acids
Amp	ampicillin
AP2	adaptor protein 2
APS	ammonium persulfate
ARH	autosomal recessive hypercholesterolemia
BAR	BIN/Amphiphysin/Rsv
BSA	bovine serum albumin
CCP	clathrin-coated pit
CCS	clathrin-coated structure
CDK	cyclin-dependent kinases
ch	chicken
CHC	clathrin heavy chain
CLC	clathrin light chain
CLEM	correlative light and electron microscopy
CME	clathrin-mediated endocytosis
Dab2	disabled homolog 2
DAPI	4',6-Diamidine-2'-phenylindole
DMEM	dulbecco's modified eagles medium
DMSO	dimethyl sulfoxide
DNA	deoxyribonucleic acid
DTT	dithiothreitol
E. coli	escherichia coli
e.g.	exempli gratia, meaning: for example
e.i.	id est, meaning: that is
eBFP	enhanced blue fluorescent protein
eGFP	enhanced green fluorescent protein
eRFP	enhanced red fluorescent protein
ECM	extracellular matrix
EDTA	ethylenediaminetetraacetic acid enhanced
EGFR	epidermal growth factor receptor

EPS15	epidermal growth factor substrate 15
Eps15R	epidermal growth factor receptor substrate 15-like 1
FA	focal adhesion
FBS	fetal bovine serum
Fcho	Fer/Cip4 homology domain-only fast
FM	fuorescence microscopy
GAK	G-associated kinase
GSDB	goat serum dilution bufffer
HBSS	hank's balanced salt solution
HEPES	4-(2-hydroxyethyl)-1-piperazineethanesulfonic acid
Hsc70	heat shock cognate 71 kDa protein
iRFP	near-infrared fluorescent protein
IF	immunofluorescence
Kann	kanamycin
KO	kockout
LPA	lysophosphatidic acid
MAPK	mitogen-activated protein kinase
MEF	mouse embryonic fibroblasts
ms	mouse
NA	numerical aperture
OD	optical density
Opti-MEM	modified Eagle's minimum essential media for optimal cationic lipid transfections
PAGE	polyacrylamide gel electrophoresis
PBS	phosphate buffered saline
PCR	Polymerase chain reactions
PDGF	Platelet-derived growth factor
PFA	paraformaldehyde
Plan Apo	apochromatic and flat field correction
PMSF	phenylmethane sulfonyl fluorid
PP2	Protein phosphatase
PRM	Proline rich motif
RA	reticular adhesion
rb	rabbit
RNA	ribonucleic acid
ROCK	rho-associated protein kinase
ROI	region of interest

RT	room temperature
SDS	sodium dodecyl sulfate
Ser	Serine
Sf21	Spodoptera frugiperda 21
SH3	SRC Homology 3 Domain
SHD	stonin homology domain
shRNA	short hairpin RNA
siRNA	small interfering RNA
STED	stimulated emission depletion transforming
SV40	simian virus 40
TBS	tris-buffered saline
TEM	transmission electron microscopy
TEMED	N,N,N',N'-Tetramethylethylenediamine
Thr	Threonine
TIRF	total internal reflection fluorescence
Tris	Tris(hydroxymethyl) aminomethane
UV	ultraviolet
v/v	volume per volume
WD	working distance
WT	wild type
µHD	µ-homology domain

B. Phospho 10xHIS-stonin1 immunoprecipitation

Mass spectrometric protein identification of 10xHis-Stonin1 purified from Sf21 insect cells, including modifications (Carbamidomethylation, Phosphorylation, and Farnesylation) after trypsin and AspN digestion using NanoLC-ESI-MSMS (OrbiTrap Elite).

Peptides found with high confidence by trypsin digestion

S1(Phospho)	sLGVESDAQPQK
S1(Phospho) C2(Farnesyl)	scNNIMIHFPVPAQWIK
S10(Phospho) C16(Carbamidomethyl)	IDRLPDKNSsPDQPHcLSYK
S18(Phospho)	IDRLPDKNSSLDHPHCLsYK
S2(Phospho)	NsSPDQPHCLSYK
S25(Phospho)	SVVTVQGAYVELQAFVNMTPAAQGsPHAGALR
S25(Phospho)	SVVTVQGAYVELQAFVNMTPAAQGsPHAGALR
S3(Phospho)	NSsPDQPHCLSYK
S3(Phospho) C9(Carbamidomethyl)	NSsPDQPHcLSYK
S31(Phospho)	DPPSTPSSASSTPLSSPMVDFYFSPGPPSNsPLSTPTK
S31(Phospho)	DPPSTPSSASSTPLSSPMVDFYFSPGPPSNsPLSTPTK
S38(Phospho)	LTLPTLRDPPSTPSSASSTPLSSPMVDFYFSPGPPSNsPLSTPTK
S4(Phospho)	KPFsPKDKEVPIGHK
S4(Phospho)	KPFsPKDK
S4(Phospho)	KPFsPK
S5(Phospho)	TEVRsLGVESDAQPQK
S9(Phospho)	IDRLPDKNsSPDQPHCLSYK
S9(Phospho) C16(Carbamidomethyl)	IDRLPDKNsSPDQPHcLSYK
T12(Phospho) C15(Carbamidomethyl)	WIQVDGEDADKtGGcVTQ
T12(Phospho) C15(Farnesyl)	WIQVDGEDADKtGGcVTQ
Y19(Phospho)	IDRLPDKNSSLDHPHCLSyK
Y6(Phospho)	VEHVSySEK

Peptides found with high confidence with by AspN digestion

S10(Phospho)	DFYFSPGPPsNSPLSTPTK
S10(Phospho)	DSLASRKPFsPK
S10(Phospho) C26(Carbamidomethyl)	DSLASRKPFsPKDKEVPIGHKSLTQcSL
S12(Phospho)	DFYFSPGPPSNsPLSTPTK
S12(Phospho)	DEGSASPFPLDsLASRKPFSPK
S15(Phospho)	DEGSASPFPLDSLAsRKPFSPK
S20(Phospho)	DEGSASPFPLDSLASRKPFsPK
S34 S35 S43 (Phospho)	GLKLTLPTLRDPPSTPSSASSTPLssPmVDFYFsPGPPSNSPLSTPTK
S6(Phospho)	DEGSAsPFPLDSLASRKPFSPK
S7(Phospho)	DPLGDLsMQDPYAG
S7(Phospho)	DPPSTPsSASSTPLSSPMV
S8(Phospho)	DPPSTPSsASSTPLSSPMV

Trypsin-digestion:

Stonin-1 OS=Mus musculus

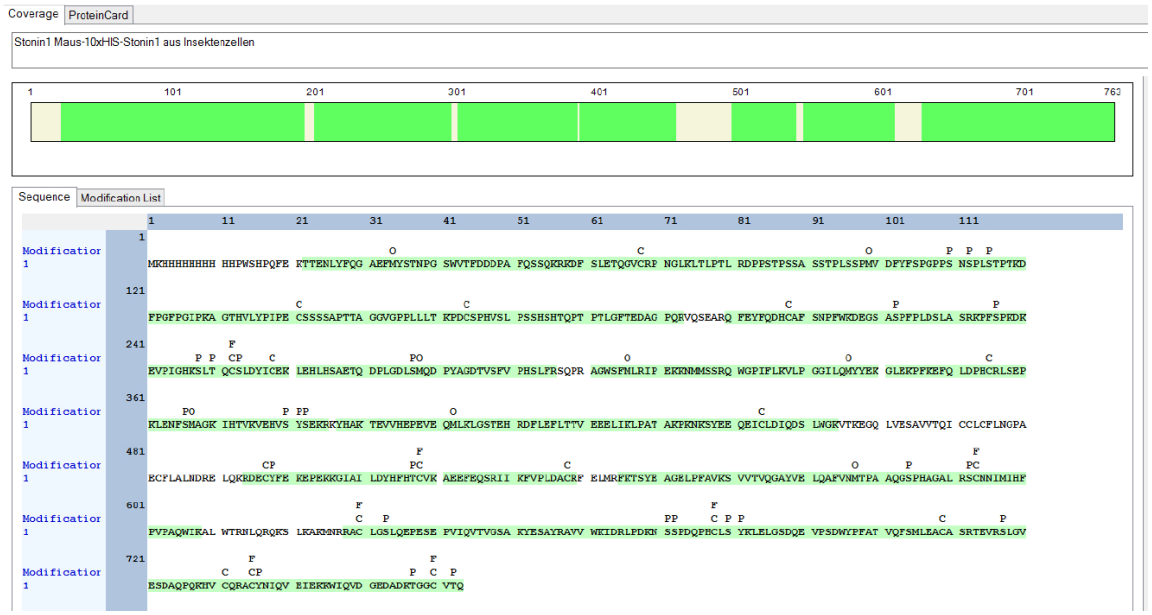

AspN-digestion:

Stonin-1 OS=Mus musculus

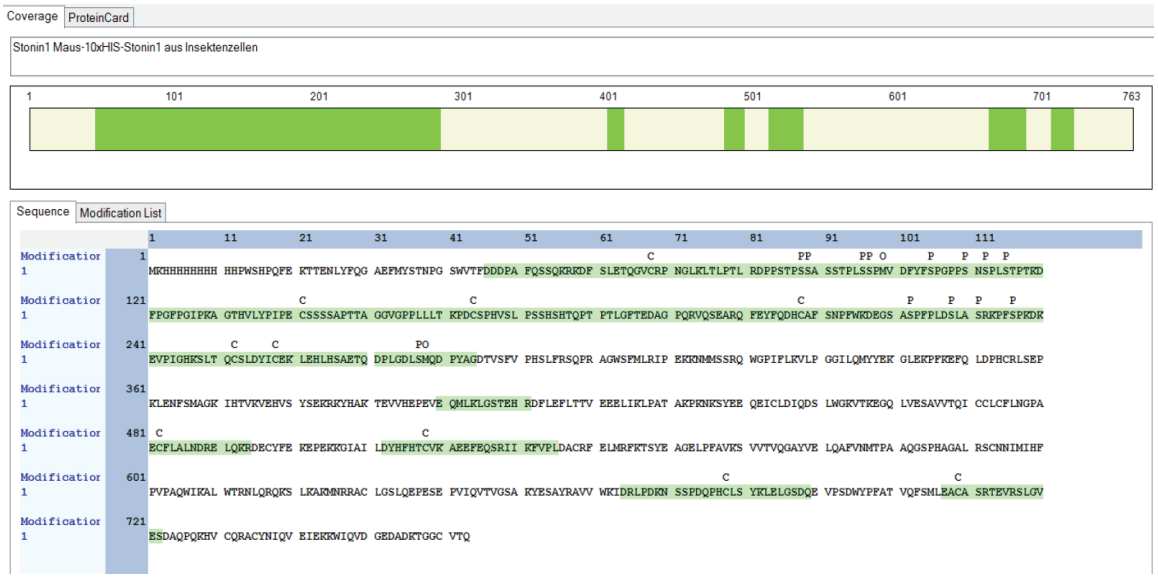

C. Kinase screen data

1. Project

Aim of the study was to identify protein kinase(s) which accept a given sample peptide as a substrate.

To that end, the phosphorylation profile of the biotinylated sample peptide “A2” was determined at 1 µM in singlicate in a radiometric assay (^{33}PanQinase ® Activity Assay) on a panel of 245 Ser/Thr kinases (see section 3), using streptavidin-coated FlashPlate® HTS PLUS plates.

Please note:The KinaseFinder service is a standardized screening assay, suitable to economically identify kinases in respect to their ability to phosphorylate a given substrate. However, due to inherently variable specific activities of the tested kinases, it is not suitable to determine kinetic parameters or get quantitative, comparative results.

As the primary KinaseFinder assay is performed at one substrate concentration in singlicate, it is mandatory to verify selected hits from the primary screening in a follow-up verification assay (e.g. ProQinase´s KinaseFinder verification service).

2. Test Sample

Peptide “A2” was provided as a 2 x 10^{-04} M stock solution in 50 mM Hepes, pH 7.5, 1000 µl in a vial.

The vial safely arrived at ProQinase on November 27, 2018.

The biotinylated sample peptide was tested at 1 µM final assay concentration.

Please note: The sample may be returned at customer´s expense. From the date of report, the sample will be stored at -20° Celsius for 6 months and will then be discarded without further notice.

3. Protein Kinase Assay

A radiometric protein kinase assay (^{33}PanQinase® Activity Assay), based on streptavidin-coated FlashPlate® PLUS plates (PerkinElmer, Boston, MA, USA) was used for measuring the kinase activity of the 245 Ser/Thr kinases. The reaction cocktails were pipetted into 96 well, V-shaped polypropylene microtiter plates (“assay plates”) in the following order:

• 10 µl of kinase solution
• 40 µl of buffer/ ATP/ test sample mixture

The reaction cocktails contained 60 mM HEPES-NaOH, pH 7.5, 3 mM $MgCl_2$, 3 mM $MnCl_2$, 3 µM Na-orthovanadate, 1.2 mM DTT, 1 µM ATP/[γ-^{33}P]-ATP (8.0 x 10^{05} cpm per well), protein kinase (1-400 ng/50µl) and sample peptide (1 µM). *Please note: Components of the sample buffer are not included in this specification.*

All PKC assays (except the PKC-mu and the PKC-nu assay) additionally contained 1 mM $CaCl_2$, 4 mM EDTA, 5 µg/ml Phosphatidylserine and 1 µg/ml 1.2-Dioleyl-glycerol. The MYLK2, CAMK1D, CAMK2A, CAMK2B, CAMK2D, CAMK4, CAMKK2 and DAPK2 assays additionally contained 1 µg/ml Calmodulin and 0.5 mM $CaCl_2$. The PRKG1 and PRKG2 assays additionally contained 1 µM cGMP.

Each assay plate maximally comprised 95 kinase reaction cocktails, one well of each assay plate was used for a buffer/substrate control containing no enzyme. The assay plates were incubated at 30° C for 60 minutes. Subsequently, the reaction cocktails were stopped with 20 µl of 4.7 M NaCl/35 mM EDTA. The reaction cocktails were transferred into 96-well streptavidin-coated FlashPlate® HTS PLUS plates, followed by 30 min incubation at room temperature on a shaker to allow for binding of the biotinylated peptides to the streptavidin-coated plate surface. Subsequently, the plates were aspirated and washed three times with 250 µl of 0.9% NaCl. Incorporation of radioactive ^{33}Pi was determined with a microplate scintillation counter (Microbeta, Perkin Elmer).

Under the chosen conditions, proteins are unspecifically binding to the streptavidin-coated FlashPlate® PLUS plates only to low extent. For evaluation of the results of the FlashPlate® PLUS - based assays, the background signal of each kinase (w/o biotinylated peptide) was determined in parallel. The background signal of the streptavidine-coated FlashPlate® PLUS plates (w/o enzyme, w/o peptide) had previously been determined at an input of 8.0 x 10^{05} cpm per well to be 32 cpm ± 16 cpm (n = 96).

4. Results

For each kinase, the activity value (raw counts of the kinase assay plus sample peptide as measured in the FlashPlate® HTS PLUS plate assay), the kinase background value (kinase w/o sample peptide), the median of three background values of the sample peptide and the corrected activity value (raw activity value minus sample peptide background) are compiled in the attached Excel file **"14711_FMP_RESULTS"**.

Additionally, the activity ratio value for each kinase is given, describing the ratio between the activity of the particular kinase with sample peptide (corrected for peptide background) and the raw kinase activity value without sample peptide. If the corrected activity of the particular kinase plus sample peptide is at least 5 fold above the FlashPlate® HTS PLUS plate background (her e: (5 x 32) + (5 x 16) = 240 cpm; see section 3), a ratio value > 3 may be considered as significant.

Please note, however, that these are only statistical recommendations. It is therefor mandatory to verify the selected "hits" in a follow-up hit verification assay, e.g. ProQinase´s KinaseFinder verification service.

Barcharts of the kinase activity values (corrected for sample peptide background) and the activity values of each kinase (w/o sample peptide) are compiled in **Fig. 1a-1f** at the end of this report.

November 29, 2018

Dr. Frank Totzke
Biochemical Screening Systems

Phosphorylation profile of peptide "biotin-DFYFSPGPPSNSPLSTPTKDFPGF" in 245 Ser/Thr kinase assays; Sample peptide concentration: 1 µM; All values in cpm

Kinase (ProQinase Lot #)	Enzyme, ng/well	Kinase activity with peptid	Kinase activity w/o peptide	Kinase activity with peptide, corrected (A-C)	Activity Ratio (D/B)
ACV-R1 (Lot001)	20	19	46	-21	-0.46
ACV-R1B (Lot003)	10	37	37	-3	-0.08
ACV-R2A (Lot001)	50	91	118	51	0.43
ACV-R2B (Lot001)	25	76	94	36	0.38
ACV-RL1 (Lot002)	20	70	54	30	0.56
AKT1 aa106-480 (Lot007)	25	55	97	15	0.15
AKT2 aa107-481 (Lot003)	200	76	103	36	0.35
AKT3 aa106-479 (Lot004)	10	67	307	27	0.09
AMPK-alpha1 aa1-550 (Lot001)	200	126	175	86	0.49
ARK5 (Lot002)	100	119	83	79	0.95
ASK1 (Lot002)	5	31	70	-9	-0.13
Aurora-A (Lot004)	50	217	191	177	0.93
Aurora-B (Lot008)	100	106	98	66	0.67
Aurora-C (Lot009)	100	85	37	45	1.22
BMPR1A (Lot002)	50	61	37	21	0.57
B-RAF VE (Lot002)	25	70	16	30	1.88
B-RAF wt (Lot001)	25	46	73	6	0.08
BRSK1 (Lot001)	10	37	60	-3	-0.05
BRSK2 (Lot002)	30	96	86	56	0.65
BUB1B (Lot002)	35	77	83	37	0.45
CAMK1D (Lot002)	100	106	109	66	0.61
CAMK2A (Lot001)	5	24	21	-16	-0.76
CAMK2B (Lot002)	100	63	77	23	0.30
CAMK2D (Lot001)	1	63	40	23	0.58
CAMK2G (Lot001)	1	99	237	59	0.25
CAMK4 (Lot001)	75	57	132	17	0.13
CAMKK1 (Lot002)	40	345	172	305	1.77
CAMKK2 (Lot001)	10	73	94	33	0.35
CDC42BPA (Lot001)	10	61	48	21	0.44
CDC42BPB (Lot001)	25	14	41	-26	-0.63
CDC7/DBF4 (Lot006)	25	34	106	-6	-0.06
CDK1/CycA (Lot005)	15	430	44	390	8.86
CDK1/CycE (Lot001)	50	2183	103	2143	20.81
CDK16/CycY (Lot001)	20	28	34	-12	-0.35
CDK1CycB1 (Lot025)	25	414	614	374	0.61
CDK2/CycA (Lot005)	50	1956	55	1916	34.84
CDK2/CycE (Lot010)	10	401	37	361	9.76
CDK3/CycE (Lot001)	10	94	85	54	0.64

CDK4/CycD1 (Lot007)	25	31	41	-9	-0.22
CDK4/CycD3 (Lot001)	10	57	60	17	0.28
CDK5/p25NCK (Lot001)	15	50	37	10	0.27
CDK5/p35NCK (Lot001)	5	90	139	50	0.36
CDK6/CycD1 (Lot006)	20	64	46	24	0.52
CDK6/CycD3 (Lot004)	100	31	57	-9	-0.16
CDK7/CycH/MAT1 (Lot002)	25	70	58	30	0.52
CDK8/CycC (Lot002)	50	31	37	-9	-0.24
CDK9/CycK (Lot004)	15	70	63	30	0.48
CDK9/CycT (Lot003)	25	58	40	18	0.45
CHK1 (Lot002)	50	37	34	-3	-0.09
CHK2 (Lot002)	10	51	51	11	0.22
CK1-alpha1 (Lot001)	100	155	139	115	0.83
CK1-delta (Lot002)	5	31	8	-9	-1.13
CK1-epsilon (Lot002)	5	34	44	-6	-0.14
CK1-gamma1 (Lot001)	5	16	10	-24	-2.40
CK1-gamma2 (Lot001)	10	39	58	-1	-0.02
CK1-gamma3 (Lot001)	5	23	71	-17	-0.24
CK2-alpha1 (Lot003)	20	44	47	4	0.09
CK2-alpha2 (Lot001)	50	73	73	33	0.45
CLK1 (Lot001)	400	101	88	61	0.69
CLK2 (Lot001)	2	35	55	-5	-0.09
CLK3 (Lot002)	10	31	5	-9	-1.80
CLK4 (Lot002)	50	273	178	233	1.31
COT (Lot018)	300	48	108	8	0.07
DAPK1 (Lot002)	40	51	35	11	0.31
DAPK2 (Lot001)	10	76	76	36	0.47
DAPK3 (Lot002)	10	64	61	24	0.39
DCAMKL2 (Lot001)	20	34	31	-6	-0.19
DMPK (Lot001)	80	4	11	-36	-3.27
DNA-PK (Lot002)	3	37	73	-3	-0.04
DYRK1A (Lot002)	10	108	58	68	1.17
DYRK1B (Lot003)	5	32	48	-8	-0.17
DYRK2 (Lot001)	2	31	82	-9	-0.11
DYRK3 (Lot001)	3	55	39	15	0.38
DYRK4 (Lot002)	10	85	70	45	0.64
EEF2K (Lot001)	2	58	49	18	0.37
EIF2AK2 (Lot003)	10	23	45	-17	-0.38
EIF2AK3 (Lot002)	20	42	138	2	0.01
ERK1 (Lot002)	20	71	19	31	1.63
ERK2 (Lot008)	10	26	39	-14	-0.36
ERK7 (Lot002)	25	155	106	115	1.08
GRK2 (Lot001)	50	24	18	-16	-0.89
GRK3 (Lot002)	10	1	58	-39	-0.67
GRK4 (Lot003)	5	24	14	-16	-1.14
GRK5 (Lot002)	5	24	38	-16	-0.42
GRK6 (Lot002)	15	26	48	-14	-0.29
GRK7 (Lot001)	5	19	32	-21	-0.66
GSG2 (Lot005)	1	57	57	17	0.30
GSK3-alpha (Lot001)	50	142	64	102	1.59
GSK3-beta (Lot003)	50	13	48	-27	-0.56

HIPK1 (Lot001)	20	51	68	11	0.16
HIPK2 (Lot001)	20	375	129	335	2.60
HIPK3 (Lot004)	20	39	29	-1	-0.03
HIPK4 (Lot001)	5	37	136	-3	-0.02
HRI (Lot001)	80	34	58	-6	-0.10
IKK-alpha (Lot005)	50	54	111	14	0.13
IKK-beta (Lot008)	100	61	78	21	0.27
IKK-epsilon (Lot007)	20	38	48	-2	-0.04
IRAK1 (Lot002)	20	24	48	-16	-0.33
IRAK4 (untagged) (Lot006)	10	24	44	-16	-0.36
JNK1 (Lot005)	5	71	45	31	0.69
JNK2 (Lot003)	5	6	23	-34	-1.48
JNK3 (Lot004)	5	90	10	50	5.00
LIMK1 (Lot002)	50	64	24	24	1.00
LIMK2 (Lot002)	200	97	55	57	1.04
LRRK G2019S (Lot003)	5	4	11	-36	-3.27
LRRK2 I2020T (Lot002)	25	46	43	6	0.14
LRRK2 R1441C (Lot002)	25	55	61	15	0.25
LRRK2 wt (Lot005)	30	34	44	-6	-0.14
MAP3K1 (Lot001)	5	109	47	69	1.47
MAP3K10 (Lot001)	15	80	73	40	0.55
MAP3K11 (Lot001)	30	260	194	220	1.13
MAP3K7/MAP3K7IP1 (Lot002)	5	51	84	11	0.13
MAP3K9 (Lot002)	15	38	91	-2	-0.02
MAP4K2 (Lot003)	4	3	48	-37	-0.77
MAP4K4 (Lot008)	50	142	126	102	0.81
MAP4K5 (Lot001)	3	48	42	8	0.19
MAPKAPK2 (Lot004)	5	24	54	-16	-0.30
MAPKAPK3 (Lot001)	10	14	15	-26	-1.73
MAPKAPK5 (Lot005)	20	24	15	-16	-1.07
MARK1 (Lot001)	100	104	101	64	0.63
MARK2 (Lot003)	5	35	32	-5	-0.16
MARK3 (Lot001)	100	101	558	61	0.11
MARK4 (Lot002)	5	38	14	-2	-0.14
MEK1 wt (Lot002)	50	16	39	-24	-0.62
MEK2 (Lot002)	100	77	39	37	0.95
MEK5 (Lot005)	100	48	52	8	0.15
MEKK2 (Lot005)	100	77	29	37	1.28
MEKK3 (Lot004)	50	219	135	179	1.33
MELK (Lot001)	100	48	39	8	0.21
MINK1 (Lot002)	10	71	26	31	1.19
MKK4 (Lot001)	25	14	41	-26	-0.63
MKK6SDTD (Lot001)	50	68	55	28	0.51
MKK7 (Lot002)	150	34	41	-6	-0.15
MKNK1 (Lot001)	30	34	34	-6	-0.18
MKNK2 (Lot002)	5	8	31	-32	-1.03
MLK4 (Lot002)	50	23	35	-17	-0.49
MST1 (Lot002)	5	71	45	31	0.69
MST2 (Lot003)	10	11	31	-29	-0.94

MST3 (Lot001)	20	29	45	-11	-0.24
MST4 (Lot001)	100	44	81	4	0.05
mTOR (Lot012)	20	46	27	6	0.22
MYLK (Lot001)	10	58	19	18	0.95
MYLK2 (Lot001)	5	19	73	-21	-0.29
MYLK3 (Lot001)	25	55	29	15	0.52
NEK1 (Lot003)	5	49	96	9	0.09
NEK11 (Lot001)	25	33	84	-7	-0.08
NEK2 (Lot002)	50	151	191	111	0.58
NEK3 (Lot001)	10	11	33	-29	-0.88
NEK4 (Lot002)	4	29	42	-11	-0.26
NEK6 (Lot001)	20	39	29	-1	-0.03
NEK7 (Lot002)	25	26	32	-14	-0.44
NEK9 (Lot001)	5	36	73	-4	-0.05
NIK (Lot027)	350	80	113	40	0.35
NLK (Lot002)	10	55	29	15	0.52
p38-alpha (Lot005)	10	71	33	31	0.94
p38-beta (Lot004)	3	42	1	2	2.00
p38-delta (Lot001)	2	23	7	-17	-2.43
p38-gamma (Lot002)	10	611	39	571	14.64
PAK1 (Lot002)	15	42	36	2	0.06
PAK2 (Lot001)	25	29	53	-11	-0.21
PAK3 (Lot001)	20	53	29	13	0.45
PAK4 (Lot003)	50	59	73	19	0.26
PAK6 (Lot001)	25	49	39	9	0.23
PAK7 (Lot001)	15	27	52	-13	-0.25
PASK (Lot001)	50	76	96	36	0.38
PBK (Lot003)	200	27	30	-13	-0.43
PDK1 (Lot002)	20	7	52	-33	-0.63
PHKG1 (Lot002)	5	26	46	-14	-0.30
PHKG2 (Lot001)	10	65	87	25	0.29
PIM1 (Lot003)	2	56	0	16	#DIV/0!
PIM2 (Lot002)	50	46	63	6	0.10
PIM3 (Lot007)	25	66	16	26	1.63
PKA (Lot002)	5	33	74	-7	-0.09
PKC-alpha (Lot005)	5	79	79	39	0.49
PKC-beta1 (Lot004)	5	36	84	-4	-0.05
PKC-beta2 (Lot003)	5	39	11	-1	-0.09
PKC-delta (Lot004)	25	103	49	63	1.29
PKC-epsilon (Lot006)	10	14	4	-26	-6.50
PKC-eta (Lot005)	10	63	76	23	0.30
PKC-gamma (Lot007)	10	12	29	-28	-0.97
PKC-iota (Lot006)	50	32	46	-8	-0.17
PKC-mu (Lot004)	20	59	140	19	0.14
PKC-nu (Lot003)	20	192	58	152	2.62
PKC-theta (Lot008)	5	27	52	-13	-0.25
PKC-zeta (Lot005)	50	198	147	158	1.07
PKC-zeta wt aa184-592 (PKM-zeta) (Lot001)	10	328	84	288	3.43
PKMYT1 (Lot005)	100	81	81	41	0.51
PKN3 (Lot002)	20	98	54	58	1.07

PLK1 (Lot013)	50	90	112	50	0.45
PLK3 (Lot001)	30	66	79	26	0.33
PRK1 (Lot004)	25	59	46	19	0.41
PRK2 (Lot002)	20	17	27	-23	-0.85
PRKD2 (Lot001)	5	23	42	-17	-0.40
PRKG1 (Lot002)	10	31	73	-9	-0.12
PRKG2 (Lot001)	1	55	76	15	0.20
PRKX (Lot001)	10	22	22	-18	-0.82
RAF1 DYDY untagged (Lot002)	10	29	19	-11	-0.58
RIPK2 (Lot003)	50	31	130	-9	-0.07
RIPK5 (Lot001)	5	28	48	-12	-0.25
ROCK1 (Lot002)	5	19	26	-21	-0.81
ROCK2 (Lot002)	5	34	121	-6	-0.05
RPS6KA1 (Lot002)	10	39	26	-1	-0.04
RPS6KA2 (Lot001)	10	56	63	16	0.25
RPS6KA3 (Lot003)	5	11	14	-29	-2.07
RPS6KA4 (Lot001)	50	74	36	34	0.94
RPS6KA5 (Lot001)	25	26	61	-14	-0.23
RPS6KA6 (Lot001)	5	36	17	-4	-0.24
S6K (Lot006)	50	79	79	39	0.49
S6K-beta (RPS6KB2) (Lot002)	100	56	6	16	2.67
SAK (Lot007)	100	99	535	59	0.11
SGK1 (Lot005)	50	57	63	17	0.27
SGK2 (Lot001)	20	0	53	-40	-0.75
SGK3 (Lot004)	50	50	254	10	0.04
SIK1 (Lot003)	50	61	38	21	0.55
SIK2 (Lot001)	2	32	35	-8	-0.23
SLK (Lot002)	25	39	29	-1	-0.03
SNARK (Lot001)	200	234	424	194	0.46
SNK (Lot005)	50	58	154	18	0.12
SRPK1 (Lot001)	25	49	79	9	0.11
SRPK2 (Lot001)	20	55	43	15	0.35
STK17A (Lot001)	25	29	26	-11	-0.42
STK23 (Lot002)	25	79	123	39	0.32
STK25 (Lot001)	10	193	68	153	2.25
STK33 (Lot001)	50	93	90	53	0.59
STK39 (Lot002)	50	34	54	-6	-0.11
TAOK2 (Lot004)	20	49	14	9	0.64
TAOK3 (Lot005)	50	46	55	6	0.11
TBK1 (Lot006)	5	80	86	40	0.47
TGFB-R1 (Lot003)	10	50	70	10	0.14
TGFB-R2 (Lot003)	10	17	20	-23	-1.15
TLK1 (Lot002)	10	28	41	-12	-0.29
TLK2 (Lot002)	5	28	24	-12	-0.50
TSF1 (Lot002)	25	57	83	17	0.20
TSK2 (Lot002)	25	93	116	53	0.46
TSSK1 (STK22B) (Lot002)	5	0	49	-40	-0.82
TTBK1 (Lot004)	5	24	14	-16	-1.14

TTBK2 (Lot007)	20	58	35	18	0.51
TTK (Lot003)	100	112	178	72	0.40
VRK1 (Lot001)	50	109	88	69	0.78
VRK2 (Lot002)	200	93	39	53	1.36
WEE1 (Lot005)	200	61	84	21	0.25
WNK1 (Lot001)	50	174	61	134	2.20
WNK2 (Lot001)	40	22	12	-18	-1.50
WNK3 (Lot001)	10	36	16	-4	-0.25
ZAK (Lot001)	5	59	29	19	0.66